Order Number 9315461

Quantitative neurochemical analysis of the macaque hypothalamic paraventricular nucleus

Ginsberg, Stephen David, Ph.D.

City University of New York, 1993

U·M·I

300 N. Zeeb Rd.
Ann Arbor, MI 48106

QUANTITATIVE NEUROCHEMICAL ANALYSIS OF THE MACAQUE HYPOTHALAMIC PARAVENTRICULAR NUCLEUS

by

STEPHEN D. GINSBERG

A dissertation submitted to the Graduate Faculty in Biomedical Sciences in partial fulfillment of the requirements of the degree of Doctor of Philosophy, The City University of New York

1993

This manuscript has been read and accepted for the Graduate Faculty in Biomedical Sciences in satisfaction of the dissertation requirement for the degree of Doctor of Philosophy.

1/4/93
Date

Chair of Examining Committee

1/6/93
Date

Executive Officer

Supervisory Committee

THE CITY UNIVERSITY OF NEW YORK

ABSTRACT

QUANTITATIVE NEUROCHEMICAL ANALYSIS OF THE MACAQUE HYPOTHALAMIC PARAVENTRICULAR NUCLEUS

by

Stephen D. Ginsberg

Adviser: Professor John H. Morrison, Ph.D.

In an attempt to correlate morphologic organization with defined physiologic responses, a series of six specific aims were performed to assess the chemoarchitecture of the macaque hypothalamic paraventricular nucleus. Specific aim 1 examined the regional distribution of noradrenergic-containing structures throughout the rostrocaudal extent of the monkey hypothalamus using dopamine-ß-hydroxylase immunohistochemistry. In specific aim 2, quantification of dopamine-ß-hydroxylase-immunoreactive varicosities was performed within both magnocellular and parvicellular regions of the monkey hypothalamic paraventricular nucleus. Quantification of noradrenergic varicosities in apposition to immunohistochemically-identified magnocellular neurons within the hypothalamic paraventricular nucleus was performed in specific aim 3 using confocal laser scanning microscopy combined with double label immunofluorescence. Specific aims 4 - 6 assessed the potential affects of the early environmental insult of social deprivation on three neurotransmitter systems within the monkey hypothalamus. In specific aim 4, quantitative analysis of dopamine-ß-hydroxylase-immunoreactive varicosities was performed within the hypothalamic paraventricular nucleus in both socially reared and socially deprived rhesus monkeys. In specific aim

5, a quantitative assessment of the tuberoinfundibular dopaminergic neurons within the hypothalamic paraventricular nucleus and arcuate nucleus using tyrosine hydroxylase immunohistochemistry was performed in socially reared and socially deprived monkeys. Additionally, an assessment of the potential affects of rearing condition on corticotropin-releasing factor-immunoreactive neurons was performed in specific aim 6. These experiments give insight into the noradrenergic input to the hypothalamus with subsequent quantitative analyses within a restricted region, as well as assessing the potential affects of an experimental manipulation on neurotransmitter-specified systems. Taken together, the aims of this project also yielded an assessment of the overall morphologic organization of the hypothalamic paraventricular nucleus in relation to several physiologically functional circuits.

ACKNOWLEDGEMENTS

I gratefully acknowledge the assistance of my mentor, Dr. John H. Morrison. I would also like to thank Dr. Patrick R. Hof, Dr. James L. Roberts, and my examining committee, notably Dr. Paul C. Goldsmith. Finally, I would like to dedicate this thesis to my loving wife, Dr. Jill P. Ginsberg, whose constant support and love throughout the good times and bad times I will never forget.

TABLE OF CONTENTS

LIST OF FIGURES

LIST OF TABLES

ABBREVIATIONS

ACTH	.....	adrenocorticotropin
AHA	.....	anterior hypothalamic area
ANOVA	.....	analysis of variance
ARC	.....	arcuate nucleus
AV3V	.....	anteroventral third ventricle area
CCK	.....	cholecystokinin
CRF	.....	corticotropin-releasing factor
DAB	.....	3,3-diaminobenzidine
DßH	.....	dopamine-beta-hydroxylase
DMH	.....	dorsomedial nucleus
E	.....	embryonic day
GABA	.....	g-aminobutyric acid
GAD	.....	glutamate decarboxylase
GnRH	.....	gonadotropin hormone-releasing hormone
HPA	.....	hypothalamic-pituitary-adrenal
HPG	.....	hypothalamic-pituitary-gonadal
IACUC	.....	Institutional Animal Care and Use Committee
LHA	.....	lateral hypothalamic area
LSM	.....	laser scanning microscope
LY	.....	Lucifer Yellow
MC	.....	magnocellular
MPA	.....	medial preoptic area
NPY	.....	neuropeptide Y
OVLT	.....	organum vasculosum of the lamina terminalis
PBS	.....	phosphate buffered saline
PC	.....	parvicellular
PHA-L	.....	*Phaseolus vulgaris* leucoagglutinin
PNMT	.....	phenylethanolamine-N-methyltransferase
PNZ	.....	perinuclear zone
PVH	.....	hypothalamic paraventricular nucleus
SCN	.....	suprachiasmatic nucleus
SON	.....	supraoptic nucleus
TH	.....	tyrosine hydroxylase
TIDA	.....	tuberoinfundibular dopaminergic
VMH	.....	ventromedial nucleus

Chapter One

Experimental Goals

The hypothalamus has been well characterized neuroanatomically and physiologically in the rat, where a plethora of neurotransmitters, including monoamines and neuropeptides have been described in neuronal perikarya, fibers, and terminals within discrete nuclear masses, and have been implicated in the physiology of functional circuits. In contrast, less literature is presently available on the neurochemistry and morphological organization of the non-human primate hypothalamus. Macaques, including rhesus (*Macaca mulatta*) and cynomolgus (*Macaca fascicularis*) monkeys display a wide variety of complex behaviors that can be carefully assessed behaviorally (e.g. play, social rank, cognitive processing) and physiologically (e.g. neurotransmitter effects, gonadal hormone cyclicity) in controlled laboratory settings. In addition, it is clear that species differences exist within the neuroendocrine axis. For example, the major glucocorticoid secreted from the adrenal cortex in response to hypothalamic-pituitary-adrenal (HPA) activation in rats is corticosterone, whereas in primates the predominant secretagogue is cortisol. The identification of structural differences in the hypothalamus may underscore functional changes observed between species and throughout phylogeny. Similarly, the development of qualitative as well as precise and accurate quantitative data on the neurochemical organization of discrete hypothalamic nuclei is crucial for a better understanding of the functions that these regions subserve. Specifically, the generation of a quantitative, normative database in monkeys of known and controlled

rearing conditions allows for the assessment of potential changes in morphology and/or neurotransmitter content in structures that are experimentally manipulated, developmentally regulated, or vulnerable to neurodegeneration. In addition, normative and experimental data collected in non-human primates have broader implications for the better understanding of human functions. Biologic similarity to humans does not solely justify detailed neuroanatomic studies within monkey species. However, research on fairly long-lived, socially interactive animals such as non-human primates advances basic scientific knowledge on anatomically and physiologically defined circuits, augmenting information gleaned from human clinical studies for the comparative assessment of structure-function relationships. Furthermore, the use of non-human primates in neurobiological research allows for invasive methodologies to further define connectivity and chemical characteristics of neuronal pathways (which may not physically exist in rodents) that are not possible using human subjects.

Within this contextual framework, early studies in the rat central nervous system using monoamine fluorescence histochemistry, which labels catecholamine-containing structures, but does not discriminate between the specific neurotransmitters, led to the observation that the hypothalamus receives an extremely dense monoaminergic innervation (Carlsson et al., '62; Fuxe, '65; Ungerstedt, '71; Björklund et al., '73), notably within the hypothalamic paraventricular nucleus (PVH) and supraoptic nucleus (SON). With the development of antibodies directed against enzymes in the catecholamine biosynthetic pathway, the assessment of specific monoamines was possible. For example, an antibody directed against rat dopamine-ß-hydroxylase (DßH), the enzyme which converts dopamine into

norepinephrine, was employed in a radioimmunoassay experiment using frozen hypothalamic tissue as well as in an immunohistochemical preparation using fixed hypothalamic tissue, allowing for the neurochemical and morphologic characterization of the noradrenergic innervation of the rat hypothalamus (Palkovits et al., '74; Swanson and Hartman, '75). The development of antibodies against tyrosine hydroxylase (TH), the rate limiting enzyme for catecholamine biosynthesis, and phenylethanolamine-N-methyltransferase (PNMT), the enzyme which converts norepinephrine into epinephrine, further allowed for the discrimination of dopaminergic, noradrenergic, and adrenergic processes (van der Gugten et al., '76; Versteeg et al., '76; Swanson et al., '81; Liposits et al., '86b). The results of these experiments suggested that the predominant monoaminergic neurotransmitter within the rat hypothalamus is norepinephrine, localized to fibers and punctate (approximately 1 μm in diameter) terminal varicosities, which paralleled the electrophysiologic and neuropharmacologic data that was concomitantly being generated on the effects of noradrenaline on discrete hypothalamic nuclei (see Sawchenko and Swanson, '83a and Felten et al., '85 for reviews).

Monoamine fluorescence histochemistry has also been used to assess the catecholaminergic innervation of the macaque brain (Schofield and Everitt, '81; Tanaka et al., '82; Felten and Sladek, '83), notably within the hypothalamus (Hoffman et al., '76; Ishikawa and Tanaka, '77). However, no literature in monkey hypothalamus exists on the specific monoamine(s) which comprise this catecholaminergic innervation pattern. Therefore, a specific aim of the present work was devised to assess the noradrenergic innervation of the monkey hypothalamus and adjacent midline thalamic

nuclei and subthalamic area using an antibody directed against DßH derived from a human pheochromocytoma tumor cell line as an immunohistochemical marker. The hypothesis was that DßH immunohistochemistry in the macaque hypothalamus was a more specific marker for noradrenergic (and adrenergic) innervation than monoamine histofluorescence, and would provide a more direct comparison of the noradrenergic innervation between rat and monkey. The results of this qualitative survey demonstrated that a differential distribution of DßH-immunoreactive processes exists within the macaque hypothalamus.

Accordingly, a second aim of this project was developed to assess the density and distribution of DßH-immunoreactive varicosities within a restricted region of the hypothalamus in order to create a quantitative indicator of terminal innervation density. Previous semi-quantitative assessments of noradrenergic innervation relied on subjective terminology in the form of density gradients, or rated innervation density on a scale of 1 - 4, which made comparisons across subjects, species, and even immunohistochemical trials difficult. Therefore, a reproducible, highly accurate method for quantifying afferent inputs within a restricted region was desired for the assessment of DßH immunoreactivity within monkey hypothalamic nuclei. Since varicosity quantification is notoriously inaccurate using conventional light microscopy, particularly in areas of dense terminal fields with several focal planes, a technique was designed using a laser scanning microscope to evaluate the density of DßH-immunoreactive input. In association with the qualitative observations, the PVH was chosen for regional quantitative analysis because of a high density of DßH-immunoreactive varicosities observed throughout the rostrocaudal extent of

the nucleus. The PVH contains at least two distinct neuronal subpopulations, magnocellular (MC) and parvicellular (PC) neurons, which are differentiated primarily by size and efferent projections (Swanson and Kuypers, '80; Swanson and Sawchenko, '83). A hypothesis was designed to test whether the dense noradrenergic input qualitatively observed in regions of the monkey PVH known to contain either MC or PC neurons differed quantitatively in terms of varicosity innervation density. The results of the qualitative survey of DßH immunoreactivity within the macaque hypothalamus and subsequent quantitative analysis within the PVH are presented in Chapter Three.

Dopamine-ß-hydroxylase-immunoreactive varicosity quantification in regions containing either MC or PC PVH neurons allowed for the assessment of noradrenergic input within a circumscribed volume of tissue, but could not assess the potential postsynaptic targets receiving this innervation. Previous morphologic, pharmacologic, and physiologic experiments in rat PVH have suggested that MC neurons containing either vasopressin or oxytocin are innervated by noradrenergic afferents (Sawchenko and Swanson, '81b; Swanson et al., '81; Day et al., '84). In accordance, a third specific aim was constructed to assess the density and distribution of noradrenergic varicosities which contacted vasopressin- and oxytocin-containing neurons. A double label immunofluorescence preparation with antibodies directed against DßH and vasopressin or DßH and oxytocin was employed in combination with confocal laser scanning microscopy to map these interactions. Previous qualitative observations in rat and monkey PVH suggested that the density of noradrenergic innervation was greater in regions containing vasopressinergic neurons than oxytocinergic neurons (McNeill and Sladek, '80; Sladek and Zimmerman, '82). Therefore, a

hypothesis was tested in monkey PVH to determine if quantitative differences exist between the density and/or distribution of DßH-immunoreactive varicosities in apposition to vasopressin-immunoreactive neurons versus oxytocin-immunoreactive neurons. The results of this experiment are presented in Chapter Four.

Taken as a whole, these three specific aims form a cohesive rationale for the investigation of the noradrenergic input to the monkey hypothalamus. The normative data provided by the broad qualitative assessment and regional quantitative analyses are pertinent in regard to future investigations assessing the affects of experimental manipulations on hypothalamic noradrenergic input and related functional interactions within the PVH.

A related field involving the correlation of anatomic structure with physiologic function is the assessment of the biological determinants of behavioral responses. In particular, a multidisciplinary research project has been designed to define the role played by social rearing environment on the development of the central nervous system, notably within a species such as the rhesus monkey, which depends on maternal and peer interactions (with conspecifics) for proper behavioral maturation. A model system used to test the affects of social rearing environment on subsequent development was devised by Harlow, whereby experimental rhesus monkeys were removed from all social contact shortly after birth and behaviorally characterized throughout their lifespan in controlled laboratory conditions (Harlow, '58; Cross and Harlow, '65; Mitchell et al., '66; Harlow et al., '71). This "isolation syndrome" that was created by the lack of social contact was characterized by a variety of behavioral, cognitive, and physical abnormalities. Of particular interest, socially deprived monkeys displayed inappropriate and exaggerated

responses to stress, alternating hypo- and hyper-aggression, appetitive disorders, and sexual dysfunction that are suggestive of severe neuroendocrine abnormalities, notably within the HPA and hypothalamic-pituitary-gonadal (HPG) axes (Kraemer, '91, '92). Since distinct hypothalamic nuclei, including the PVH, are known to be integral central components of the HPA and HPG axes (Plant et al., '78; Swanson, '87), a series of neuroanatomical analyses were designed to assess potential neuropathological changes within discrete neurotransmitter-identified subpopulations in a group of maternal and peer deprived rhesus monkeys relative to a group of monkeys raised in a social colony. In terms of neuropathological examinations, varicosity density assessments and cell counts are two of several quantitative measures that can be used to assess changes in brain structure. Ideally, hypothalamic neurochemistry and receptor density analyses in combination with varicosity density and/or cell counts would provide a more extensive assessment of the affects of social deprivation. However, the brains of these subjects were prepared for regional light microscopic evaluations, including the evaluation of the amygdala, brainstem, hippocampus, and neocortex (see Morrison et al., '90; Ginsberg et al., '92b, '93b; Siegel et al., '92), excluding the possibility for neurochemical measurements.

Within the context of social deprivation and specific aims 1 - 3, a fourth specific aim was designed to assess the distribution and density of DßH-immunoreactive varicosities in MC and PC PVH regions of monkeys raised in differential rearing conditions. The hypothesis being tested was to see if the noradrenergic innervation of the PVH varied as a function of rearing history, since norepinephrine has physiologically-defined effects within the PVH,

notably the stimulation of feeding behaviors, the release of vasopressin from MC PVH neurons and CRF from PC PVH neurons (Leibowitz, '78, '88; Day et al., '84; Day and Renaud, '84; Plotsky, '87; Szafarczyk et al., '87). The results of this experiment are reported in Chapter Five.

An additional objective related to the previous specific aims of this project was to further characterize the neurochemical organization of the monkey PVH by conducting detailed quantitative assessments on transmitter-identified neurons localized within the nucleus. In the light of these parameters, a quantitative analysis of dopamine-containing neurons within discrete hypothalamic regions of socially reared and socially deprived rhesus monkeys, using TH as an immunohistochemical marker was performed as a fifth specific aim. Dopaminergic neurons within the hypothalamus of rat and monkey have been characterized by monoamine histofluorescence and TH immunohistochemistry into four cell groups (A11- A14), principally based upon their location (Dahlström and Fuxe, '64; Felten and Sladek, '83; Chan-Palay et al., '84; van den Pol et al., '84). Of particular interest are the tuberoinfundibular dopaminergic (TIDA) neurons, mainly localized to the PVH and arcuate (ARC) nuclei. Tuberoinfundibular dopaminergic neurons have been demonstrated in rat and monkey to affect anterior pituitary secretion via a projection through the external lamina of the median eminence to the portal capillary plexus, notably to inhibit prolactin release from lactotroph cells (Neill et al., '81; Kawano and Daikoku, '87; Moore et al., '87; Goldsmith et al., '90). Additionally, dopaminergic neurons in the PVH are particularly sensitive to osmotic challenges, and are believed to be central regulators for this stressor (Kiss and Mezey, '86; Young et al., '87; Watts, '92). Socially deprived monkeys have aberrant sexual behaviors (psychosocial and

physical abnormalities) as well as being profoundly polydipsic (Miller et al., '69, '71; Harlow, '74; Kraemer, '92), suggesting that these behavioral deficits are related, at least in part, to the TIDA system. In a similar study of TH-immunoreactive neurons within the substantia nigra and ventral tegmental area, the major source of striatal and cortical dopamine, (Martin et al., '91) reported a 40% reduction in the number of cells immunoreactive for TH, although these cell bodies appeared normal in Nissl preparations. In accordance with the behavioral and neuroanatomical studies, a specific aim was created to assess the distribution and density of TIDA neurons using TH immunohistochemistry within the PVH and ARC of a group of socially deprived monkeys relative to a group of socially reared monkeys. The hypothesis being tested was to see if TIDA neurons would differ in terms of overall number and distribution in the PVH and/or ARC between the two groups as a function of rearing history.

A similar rationale was applied for the quantitative analysis of PVH neurons immunoreactive for corticotropin-releasing factor (CRF). This 41 amino acid peptide, originally isolated from ovine hypothalamus by Vale et al. ('81), has been demonstrated to be one of the most potent secretagogues for adrenocorticotropin (ACTH) and the resultant stress cascade (Rivier and Vale, '83; Rivier and Plotsky, '86; Negro-Vilar et al., '87). Additionally, CRF administration has been reported in a dose- and environment-dependent fashion, to increase arousal, specifically eliciting anorexigenic, anxiety-like, and self-directed (e.g. huddling, digit sucking, and head banging) responses in rhesus monkeys (Kalin, '85; Glowa and Gold, '91). Corticotropin-releasing factor-immunoreactive neurons have been localized in rat and monkey to a subset of PC neurons found within medial regions of the PVH (Swanson et

al., '83; Foote and Cha, '88). Since socially deprived monkeys demonstrate a severe inability to regulate stress responses and display a variety of self-directed behaviors, a specific aim was generated to assess the density and distribution of CRF-immunoreactive neurons within the PVH of socially reared and socially deprived rhesus monkeys. Similar to specific aim 5, the hypothesis being tested in this sixth specific aim was that CRF-immunoreactive neurons would be significantly different between the two groups as a function of rearing history.

Therefore, the goals of specific aims 5 and 6 are twofold. First, to assess potential morphologic changes in regional studies of the TIDA and CRF-containing systems in the brains of maternal and peer deprived rhesus monkeys relative to a group of colony reared subjects. Secondly, to relate the normative data generated on the density and distribution of TH- and CRF-immunoreactive neurons to the previous aims, in an attempt to further characterize the neurochemical and morphologic organization of the non-human primate PVH. The results of the experiments described in specific aims 4 and 5 are reported in Chapter Six.

Background

The hypothalamus is a highly ordered complex of nuclear groups and fiber systems with a myriad of afferent, efferent, and intrinsic circuits. Through these connections and various feedback loops, the regulation and integration of many homeostatic behaviors is achieved, collectively controlling the "internal milieu" of the vertebrate (Stellar, '54). For example, the hypothalamus is involved in such varied responses as appetitive behaviors, circadian rhythms, emotional integration, reproduction, stress, sympathetic (notably cardiovascular) outflow, and thermal regulation

(Ranson, '40; Luiten et al., '87; Swanson, '87). Along with the epithalamus, dorsal thalamus, and ventral thalamus, the hypothalamus is a diencephalic structure (Christ, '69). The hypothalamus is bounded anteriorly by the lamina terminalis, posteriorly by an ill-defined plane between the posterior commissure and the caudal aspect of the mammillary bodies, dorsally by the hypothalamic sulcus, ventrally by the infundibulum, and laterally by the globus pallidus and internal capsule at rostral levels and the subthalamus and crus cerebri at caudal levels (Christ, '69; Nauta and Haymaker, '69). The hypothalamus has traditionally been subdivided into 6 zones, including the periventricular, preoptic, middle (which includes the PVH), lateral, tuberal, and caudal regions (Papez and Aronson, '34; Ingram, '40; Rioch et al., '40). The following review of hypothalamic circuitry (including an extensive description of the structure and function of the PVH) will proceed in a rostrocaudal direction in accordance with the 6 hypothalamic zones.

Periventricular region

The periventricular region includes the periventricular fiber bundle, a subset of which has been shown to be noradrenergic (see Chapter Three), as well as fibers arising from autonomic brainstem nuclei, including the nucleus of the solitary tract, as well as intrahypothalamic fibers, such as efferents from the dorsomedial nucleus (DMH) which project rostrally to the PVH and medial preoptic area (MPA) (Ricardo and Koh, '78; Ter Horst and Luiten, '87; Ter Horst et al., '89). Surrounding the preoptic recess of the third ventricle in the periventricular region is the anteroventral third ventricle area (AV3V). The AV3V contains the median preoptic nucleus and the circumventricular organum vasculosum of the lamina terminalis (OVLT). These structures, along with the subfornical organ, are sensitive to plasma and cerebrospinal

fluid levels of angiotensin II and are believed to mediate vasopressin release in response to dehydration via a direct projection to the PVH and SON (Sawchenko and Swanson, '83b; Gardiner et al., '85; Lind, '88). The OVLT in rat and hamster also contains a dense plexus of fibers that are immunoreactive for gonadotropin hormone-releasing hormone (GnRH) (Piekut, '83; Lehman and Silverman, '88). Whether GnRH is released into the third ventricle through the OVLT has not been clarified. The ARC, which lies in the periventricular zone surrounding the third ventricle, ranging from the median eminence at mid hypothalamic levels to the mammillary recess of the third ventricle at caudal levels, is also considered part of the periventricular region. The ARC is a complex aggregate of parvicellular (small, bipolar) cells, a significant portion of which form the tuberoinfundibular system which projects through the external lamina of the median eminence to the portal capillary plexus, affecting anterior pituitary function (Weigand and Price, '80; Lechan et al., '82). Several neurotransmitter-identified substances have been localized to rat ARC neurons, including ACTH, g-aminobutyric acid (GABA), neuropeptide Y (NPY), proopiomelanocortin-derived peptides, somatostatin, and TH (Sawchenko et al., '82; Bai et al., '85; Everitt et al., '86; see Chapter Six).

Preoptic region

The preoptic region, classically defined as containing the MPA and lateral preoptic area, is believed to be the rostralmost extension of the hypothalamus (Papez and Aronson, '34; Christ, '69). The MPA contains several diffuse cellular masses, and is contiguous with the rostral regions of the periventricular division. Thus, whether a structure is considered in the preoptic or periventricular region at the most rostral hypothalamic levels is arbitrary. The rat MPA contains a sexually dimorphic nucleus with several

cytoarchitectonic subdivisions, notably within the medial preoptic nucleus-central division, which in the male is approximately twice the volume than in the female (Bloch and Gorski, '88). Several neurotransmitter systems have been identified in the medial preoptic nucleus-central division, including DßH- and NPY-immunoreactive fibers, and cholecystokinin (CCK)-immunoreactive neurons (Simerly et al., '86). Sexually dimorphic nuclei have also been located within the human MPA (Swaab and Fliers, '85; LeVay, '91). Interestingly, LeVay ('91) has recently demonstrated that a small preoptic nuclear group varies in volume relative to the sexual orientation of a male subject. However, the function(s) of these sexually dimorphic nuclei need to be further characterized. Additionally, estradiol-concentrating cells and estrogen receptor- and progesterone receptor-immunoreactive neurons have been found in the MPA of female rats and monkeys, indicating that this region is most likely involved in the central limb of the HPG axis (Pfaff and Keiner, '73; Pfaff et al., '76; Bethea et al., '92; Blaustein, '92; Leranth et al., '92). The lateral preoptic area, which has not been as well characterized as the MPA, has been demonstrated in early lesion studies to be involved in the maintenance of temperature, notably regulating the dissipation of heat (Ranson, '40; Stellar, '54).

Middle region

The middle region of the hypothalamus contains several nuclei, including the suprachiasmatic nucleus (SCN), which is located bilaterally in the subventricular region between the optic chiasm and the floor of the third ventricle, and is believed to be the central pacemaker for circadian rhythms (for a review see Turek and Van Cauter, '88). The SCN receives visual information via connections from the retina and the intergeniculate leaflet in

rat as assessed by anterograde tract tracing techniques (Moore and Lenn, '72; Moore, '89). The SCN contains a parvicellular population of neurons, a subset of which express vasopressin, but not oxytocin (Sofroniew and Weindl, '80). These vasopressinergic neurons have been demonstrated in rat to project to several basal forebrain and hypothalamic nuclei, including the lateral septum, nucleus of the diagonal band, ARC, PVH, and SON (Sofroniew and Weindl, '78; Stephan et al., '81). A population of glutamate decarboxylase (GAD)- and GABA-immunoreactive perikarya are also localized to the SCN, and are thought to be interneurons (Schimchowitsch et al., '91).

The anterior hypothalamic area (AHA) contains a loose association of cell bodies and fibers of passage in addition to the PVH, SCN, and SON. The stria terminalis also terminates diffusely in this region (Nauta and Haymaker, '69). Autoradiographic and retrograde tracing studies within the AHA have revealed ascending efferents through the MPA to the lateral septum and nucleus of the diagonal band, and descending efferents to the PVH and DMH, as well as projections to the brainstem and the periaqueductal grey (Conrad and Pfaff, '76; Semenenko and Lumb, '92). The exact functions that the AHA subserve are not well defined.

Cytoarchitectonics of the PVH

The PVH (of Malone) corresponds to the filiform nucleus (of Fortuyn) and the subventricular nucleus (of Cajal) (Ingram, '40; Swanson and Sawchenko, '83). The PVH is a densely packed column of neurons which is bounded medially by the ependymal cells of the third ventricle and laterally extends past the columns of the fornix. In monkey, the PVH extends 5 - 6 mm in the rostrocaudal plane, emerging as a distinct nuclear mass caudal and slightly ventral to the MPA, abutting the subependymal layer of the third

ventricle. The PVH shifts to a more dorsal and lateral position, abutting the fornix at its caudal extent, and terminates at the level of the DMH.

The PVH contains at least two distinct neuronal populations, MC neurons, which in the monkey have a long axis cross sectional length of approximately 40 - 50 μm, and PC neurons, which are approximately 15 - 25 μm in diameter in the long axis (Rafols et al., '87). Magnocellular neurons are localized primarily to the PVH and SON as well as a few accessory magnocellular nuclei and synthesize the nonapeptide hormones vasopressin, oxytocin, and their respective neurophysin carrier proteins. These hormones are derived from a larger prohormone molecule that undergoes post-translational cleavage within neurosecretory granules during fast axonal transport (Gainer et al., '77). Parvicellular neurons are localized to medial and periventricular regions of the PVH and contain a variety of neurotransmitters and neuropeptides including CRF, dopamine, enkephalin, somatostatin, and thyrotropin-releasing hormone (Swanson and Sawchenko, '83).

In the rat, the PVH has been divided into subnuclei, which have been differentiated primarily on the basis of their size and efferent projections. Swanson and Kuypers ('80) divided the PVH into at least 8 subdivisions (3 MC groups and 5 PC groups), which is similar to the parcellation of the PVH performed by Armstrong et al. ('80). Extensive anterograde and retrograde tract tracing studies are necessary before subnuclei can be ascribed in monkey PVH. Clearly MC and PC regions exist, but they do not appear to be as discretely organized as in the rat.

In terms of development, MC PVH neurons in rat become post mitotic between embryonic days (E) 13 and 15 (Altman and Bayer, '78). These neurons then migrate from the ependymal region of the third ventricle

laterally to where the PVH will eventually be located and begin to express vasopressin and oxytocin mRNA (as assessed by *in situ* hybridization) and neurophysin immunoreactivity by E 16 (Whitnall et al., '85a; Laurent et al., '89). By E 17 and 18, vasopressin-immunoreactive neurons are detectable whereas oxytocin-immunoreactive neurons are not visualized until E 20 (Boer et al., '80; Buijs et al., '80). The time course of hormonal expression may relate to a differential activation of the synthetic machinery (e.g. enzymes and neurosecretory vesicles) within vasopressinergic and oxytocinergic neurons (Whitnall et al., '85a). Furthermore, the catecholaminergic input to rat neurophysin-immunoreactive neurosecretory neurons is not observed until E 21 (Khachaturian and Sladek, '80). Although the nonapeptides are detectable prior to birth, fully developed connections, as assessed by axonal growth, dendritic arborization, and synapse formation, are not complete until after post natal day 15 in mouse PVH (Silverman et al., '80).

In the adult rat hypothalamus, there are approximately 2000 MC neurons per PVH (with equivalent numbers of vasopressin- and oxytocin-immunoreactive neurons) and approximately 7000 PC neurons per PVH (Bodian and Maren, '51; Rhodes et al., '81; Sawchenko and Swanson, '81b; Kiss et al., '83, '91). Morphologically, MC neurons tend to have a multipolar, or pyramidal shape, whereas PC neurons tend to be bipolar in nature as assessed immunohistochemically and by intracellular filling (Hoffman et al., '91; see Chapter Four). Both MC and PC neurons tend to have 2 - 3 aspiny, primary dendrites which align in the dorsoventral plane and remain within the morphological boundaries of the PVH (van den Pol, '82; Rafols et al., '87). Additionally, a clear perinuclear zone (PNZ) between the border of the PVH and the surrounding neuropil has been described in rat (Sawchenko et al., '83;

Oldfield and Silverman, '85). In terms of inter PVH connectivity, dye-coupling and gap junctions have been found between MC neurons in rat which may explain the coordinated firing of oxytocin neurons during suckling and the dynamic vasopressinergic neuron-glia interactions during osmotic challenges (Lincoln and Wakerley, '75; Andrew et al., '81; Hatton et al., '84). In addition, MC and PC dendrites have been observed to form synaptic contacts, potentially coordinating firing responses and overall neuroendocrine output (van den Pol, '82; Sawchenko and Swanson, '83a).

Physiology of PVH neurons

Magnocellular neurosecretory neurons have also been extensively characterized electrophysiologically. Specifically, PVH neurons that have their terminals in the posterior pituitary can be antidromically activated to study their firing properties in response to a variety of stimuli, such as suckling, salt loading, hemorrhage, and psychogenic stressors (Renaud, '87). Magnocellular neurons have been characterized as being vasopressin- or oxytocin-secreting by their differential firing patterns to various stimuli (e.g. oxytocin-containing neurons fire after a suckling stimulus, whereas vasopressin-containing neurons do not) (Lincoln and Wakerley, '75). Additionally, vasopressinergic neurons display a phasic bursting response when stimulated, whereas oxytocinergic neurons display a fast, synchronous response when activated (Cobbett et al., '86; Hoffman et al., '91; Renaud and Bourque, '91). The phasic activity of vasopressin-containing MC neurons is not discernible when these cells are at rest. Only when the appropriate stimuli, such as cardiovascular or osmotic challenges are applied does the phasic bursting take place, effectively releasing a greater amount of the hormone into the plasma per action potential than if there was a continuous

discharge of spikes (Legendre and Poulain, '92). Parvicellular neurons can also be antidromically activated by stimulating the median eminence with an electrode. As would be predicted by the multiplicity of neurotransmitter-identified substances in PC neurons, the electrophysiologic properties of these neurons vary. However, MC and PC neurons can be discriminated from each other electrophysiologically because PC neurons display low threshold Na^+ spikes and higher membrane time constants than MC neurons (Hoffman et al., '91; Tasker and Dudek, '91).

Afferent connections to the PVH

The PVH receives several different afferents from brainstem nuclei, circumventricular organs, hypothalamic nuclei, and limbic structures. Brainstem nuclei contribute several projections to discrete regions of the PVH utilizing several neurotransmitter-identified substances including norepinephrine, epinephrine, serotonin, and NPY. The noradrenergic innervation derives from three brainstem nuclei, as assessed by retrograde tract tracing combined with DßH immunohistochemistry, and by electrophysiology. Specifically, the A1 cell group (dorsal to the lateral reticular nucleus in the caudal ventrolateral medulla) projects preferentially to vasopressinergic MC neurons, and the A2 cell group (within the nucleus of the solitary tract) projects to MC and PC PVH regions, whereas the locus coeruleus (A6) projects to a restricted region of the PC PVH, notably within the periventricular region (Cunningham and Sawchenko, '88; Day, '89). Noradrenergic afferents have been demonstrated by several investigators in rat to form axodendritic and axosomatic asymmetric synapses onto neurophysin- and vasopressin-containing perikarya (Silverman et al., '83, '85; Nakada and Nakai, '85; Nakai et al., '85, '86; Ochiai et al., '88; Ochiai and

Nakai, '90; Shioda and Nakai, '92). Although earlier pharmacologic experiments suggested an inhibitory role for hypothalamic norepinephrine (Moss et al., '71, '72), the noradrenergic innervation of the PVH is presently believed to be excitatory at physiologic doses. For example, noradrenergic activation by application of agonists and/or stimulation of noradrenergic cell groups/ascending noradrenergic fibers stimulates vasopressin release through alpha-1 adrenergic receptors from MC neurons and CRF from PC neurons in a variety of *in vivo* and *in vitro* preparations (Day et al., '84, '85; Blessing and Willoughby, '85; Randle et al., '86b; Plotsky, '87; Szafarczyk et al., '87; Willoughby et al., '87; Saphier, '89; Saphier and Feldman, '89).

In terms of adrenergic input, the C1, C2, and locus coeruleus cell groups (which correlate anatomically with the noradrenergic cell groups) supply epinephrine to PC regions of the PVH, notably to CRF-immunoreactive neurons, where synaptic contacts have been demonstrated at the ultrastructural level (Liposits et al., '86a; Cunningham et al., '90). The restricted innervation by adrenergic fibers to the PC PVH is relevant to the present work, indicating that the majority of DßH-immunoreactive processes, notably within MC regions, are likely to be noradrenergic. Serotoninergic projections to the PVH have been demonstrated in rat to derive from the medial raphe nucleus, with both dorsal and pontine raphe subdivisions supplying a smaller proportion of this innervation (Sawchenko et al., '83). Serotonin immunoreactivity is relatively sparse within the morphological boundaries of the PVH, but more dense within the PNZ (Sawchenko et al., '83), indicating that the effects of serotonin on PVH neurons may be mediated by the processes of interneurons. Neuropeptide Y, which stimulates nutrient (notably carbohydrate) intake at the level of the rat PVH (Stanley and

Leibowitz, '85; Leibowitz, '91), is colocalized within the A1, C1, and C2 catecholaminergic brainstem cell groups, and is therefore likely to project to both MC and PC PVH regions (Everitt et al., '84a; Sawchenko et al., '85). The parabrachial nucleus, located in the pons lateral to the locus coeruleus, is likely to convey gustatory information to the PVH (Norgren, '77). Electrophysiologic and anatomic evidence suggests that the parabrachial input is excitatory, and the density of innervation is greater in PC regions (Jhamandas et al., '92).

Inputs from circumventricular organs, which are on the peripheral side of the blood-brain barrier, to the PVH have been reported in rat. Specifically, tract tracing studies have identified inputs from the subfornical organ and the OVLT to the PVH, which are responsive to circulating levels of angiotensin II (Lind, '88). These structures are thought to modulate fluid homeostasis through their respective projections to the PVH (for a review see McKinley et al., '90). In addition, a reciprocal projection from medial and periventricular PC PVH neurons has been identified in rat using the anterograde tracer *Phaseolus vulgaris* leucoagglutinin (PHA-L) (Larsen et al., '91), indicating a possible feedback loop for fluid regulation.

The majority of limbic input to the PVH terminates in the PNZ surrounding the nucleus, rather than a direct innervation pattern, suggesting the interaction of interneuronal processes in the integration of limbic input with the neurosecretory system. In rat, retrogradely labeled fibers from the cortico-medial amygdala, lateral septum, and ventral subiculum have been demonstrated to project to the PNZ (Oldfield et al., '85; Oldfield and Silverman, '85). The PNZ in rat also receives an acetylcholine-containing projection likely to originate from choline acetyltransferase-immunoreactive

neurons located in the lateral septal nucleus as well as in the PNZ dorsal to the SON (Mason et al., '83; Meeker et al., '88). Additionally, the bed nucleus of the stria terminalis projects in rat and monkey to the PNZ as well as to PC regions of the PVH, with MC regions fairly devoid of this input (Sawchenko and Swanson, '83b; Rafols et al., '87).

The intrinsic afferent connections of the hypothalamus to the PVH have been extremely difficult to isolate, partly due to the sheer number of fiber systems coursing through this relatively small amount of space. In addition, most of these short connections are of a very fine caliber, and are difficult to inject with tracer substances without inadvertently labeling fibers of passage. Therefore, this description may actually underestimate the extent of intrahypothalamic connectivity due to the technical restrictions at the present time. To date in rat, the ARC, DMH, and the MPA furnish the majority of interhypothalamic projections to the PVH, with the ventromedial nucleus (VMH), SCN and AHA and lateral hypothalamic area (LHA) also contributing fibers (Ter Horst and Luiten, '87). Specifically, the ARC projection in rat includes NPY and ACTH as neurotransmitter-identified candidates to oxytocinergic MC neurons and CRF-immunoreactive PC neurons (Liposits et al., '88), whereas galanin- and NPY-immunoreactive projections from the DMH form synaptic contacts with PC PVH neurons (Bai et al., '85; Sawchenko and Pfeiffer, '88). Other potential transmitter candidates for these interhypothalamic connections include interneuronal processes containing GABA and glutamate, which have been demonstrated to form synapses onto neurophysin- and vasopressin-immunoreactive neurons within the rat PVH (van den Pol, '85, '91; Decavel et al., '89; Decavel and van den Pol, '92). The functional significance of these inputs to the PVH has not been

completely characterized, yet it appears that these interconnections assist in the coordination of neuroendocrine responses.

Efferent output of the PVH

The efferent projections of the PVH (and SON) comprise the major outflow pathways for neuroendocrine release (see Harris, '48; Bargmann and Scharrer, '51; Bodian and Maren, '51 for a historical perspective). The axons of PVH MC neurons arch laterally past the fornix and join axons exiting from the SON to form the hypothalamo-neurohypophysial tract, which terminates in the perivascular spaces within the posterior pituitary and delivers vasopressin and oxytocin to the systemic circulation (Antunes et al., '77; Antunes and Zimmerman, '78). The axons of PC neurons either course through the external lamina of the median eminence to the portal capillary plexus and affect either anterior pituitary function, or terminate in the brainstem and/or upper spinal cord (Swanson and Kuypers, '80; Sawchenko and Swanson, '82). An example of the former are the approximately 2000 CRF-containing neurons located in the medial PC region per rat PVH which, when activated, secrete CRF into the portal capillary plexus (approximately 215 ± 49 pg/ml at baseline) which, in turn, stimulates anterior pituitary corticotroph cells to release ACTH into the systemic circulation (Swanson et al., '83; Plotsky, '85). Glucocorticoid feedback through Type I (high affinity mineralocorticoid) and Type II (low affinity glucocorticoid) receptors at the level of the hippocampal formation and in CRF-containing neurons of the PVH have been demonstrated in rat (McEwen et al., '86; Liposits et al., '87; Ahima et al., '91; Ahima and Harlan, '91), suggesting multiple sites in the central nervous system for negative feedback upon the HPA axis. The descending population of PC neurons project in rat, cat, and monkey either to

preganglionic sympathetic neurons in the intermediolateral column at thoracic spinal cord levels, or to medullary cell groups including A1, A2, and the parasympathetic neurons of the nucleus of the solitary tract (Saper et al., '76a; Hosoya and Matsushita, '79; Caverson et al., '84; Hosoya et al., '91). Neuroanatomic studies in rat and monkey have demonstrated vasopressin- and oxytocin-immunoreactive fibers and terminals in these regions, implicating these classically-defined hormones as potential neurotransmitter candidates for this hypothalamic-autonomic projection (Swanson and McKellar, '79; Sawchenko and Swanson, '82; Sladek and Sladek, '83; Cechetto and Saper, '88). Similarly, electrophysiological studies demonstrated that both oxytocin and vasopressin inhibit the firing of sympathetic neurons (Gilbey et al., '82; Buijs et al., '90). These experiments suggest that a series of reciprocal connections exist between the autonomic cell groups in the spinal cord/medulla and the PVH for the possible regulation and integration of neuroendocrine release with autonomic outflow.

Supraoptic nucleus

The SON (of Lenhossék), which straddles the optic tract, corresponds to the tangential nucleus (of Cajal) and the basal optic ganglion (of Meynert) (Rioch et al., '40; Swanson and Sawchenko, '83). The neurons within the SON display predominantly MC morphology, and in Nissl preparations can be easily discriminated from the surrounding cell-poor PNZ and AHA by their darkly stained, eccentric nucleoli and abundance of cytoplasmic Nissl substance. The SON and PVH are two of the most vascularized regions within the central nervous system, and MC neurons are routinely observed in close proximity to capillaries (Stellar, '54; van den Pol, '82; Rafols et al., '87). Cell counts conducted in rat estimate between 4400 - 4700 MC neurons reside

within the morphological boundaries of the SON (Leranth et al., '75; Rhodes et al., '81). The neurons of the SON, similar to the MC neurons of the PVH, terminate in the perivascular spaces of the posterior pituitary via the hypothalamo-neurohypophysial tract, which is approximately 5 mm long in the rat (Hatton et al., '84). Axon collaterals have also been described for rat SON neurons which remain within the morphological boundaries of the nucleus (Mason et al., '84), potentially synchronizing firing patterns for coordinated neurotransmitter release. In terms of afferents, the SON receives inputs similar to the PVH, with a few additions, notably within the PNZ immediately dorsal to the nucleus. Specifically, the PNZ, and to a lesser degree the SON, receives a projection from the diagonal band nuclei in rat with GABA as a potential neurotransmitter candidate, that may function as a modulatory input to inhibit baroreflex activation of vasopressinergic neurons (Jhamandas and Renaud, '86a, '86b; Jhamandas et al., '89). The PNZ also contains cholinergic neurons as assessed by choline acetyltransferase immunohistochemistry (Mason et al., '83; Meeker et al., '88).

The accessory magnocellular nuclei, as their name suggests, are small clusters of MC neurons located between the PVH and SON, which express either vasopressin or oxytocin. Little is known about the intrinsic properties of these cells, and whether they differ from the MC neurons of the PVH and SON. Analyses conducted on sagittal sections through the human hypothalamus suggest that the accessory magnocellular nuclei form a thin bridge of neurons between the PVH and SON, possibly functioning to coordinate the firing properties of the two nuclei (Ingram, '40; Braak and Braak, '87).

Lateral region

The lateral region consists mainly of the LHA, ranging from the lateral preoptic area rostrally (these areas are difficult to differentiate), to the subthalamic and midbrain tegmentum area caudally. The LHA is believed to modulate appetitive behaviors, cardiovascular pressor/depressor responses, and metabolism (Luiten et al., '87; Allen and Cechetto, '92). The medial forebrain bundle also courses through the LHA, carrying both ascending and descending fibers and is thought to play a role in the integration of behaviors and emotional responses. The medial forebrain bundle is not a cohesive bundle, but rather a series of related fascicles passing through the central grey of the LHA. The lateral region also contains the tuberomammillary nucleus, located in posterior regions of the hypothalamus, lateral to the mammillary complex and rostral to the midbrain tegmentum. The tuberomammillary nucleus is the only site in the mammalian central nervous system that contains histaminergic neurons, which project diffusely throughout the neuraxis (Inagaki et al., '88). The histamine-containing neurons of the tuberomammillary nucleus have also been demonstrated in several species to colocalize GABA (Airaksinen et al., '92). Histamine has many diverse effects involved in arousal responses such as sleep/wakefulness and nociception, principally acting through H1 and H2 histamine receptors (see Yamatodani et al., '91 for a review).

Tuberal region

The tuberal region of the hypothalamus is composed of the mediobasal region, including the VMH and ARC (which was described in the periventricular region), as well as more dorsally-located regions including the DMH and the perifornical and posterior hypothalamic areas (Papez and

Aronson, '34; Ingram, '40). The VMH, located in the mediobasal hypothalamus dorsal and lateral to the ARC and ventral and lateral to the DMH, consists of a core of densely packed, medium sized neurons embedded in a more loosely packed shell of neurons (Saper et al., '76b; Bleier, '84). The predominant afferent input to the VMH is from the amygdala, which is likely to be conveying olfactory information (Swanson, '87). As demonstrated by autoradiographic methods in rat and cat, the shell and core regions of the VMH receive inputs from discrete subnuclei within the amygdaloid complex. Specifically, the medial and basolateral amygdaloid nuclei project heavily to the core of the VMH via the ventral amygdalofugal pathway, whereas the ventral subiculum and associated amygdalo-hippocampal area project heavily to the shell of the VMH through the stria terminalis (McBride and Sutin, '77; Krettek and Price, '78). Additionally, a CCK-immunoreactive projection from the parabrachial nucleus has also been demonstrated to synapse onto core VMH neurons, possibly conveying gustatory information to the nucleus (McBride and Sutin, '77; Norgren, '77; Inagaki et al., '84; Záborszky et al., '84). The VMH in female rat and monkey has also been demonstrated to concentrate estradiol as well as contain both estrogen receptor- and progesterone receptor-immunoreactive neurons (Pfaff and Keiner, '73; Pfaff et al., '76; Bethea et al., '92; Blaustein, '92; Leranth et al., '92). In addition, gonadal steroids regulate the binding capacity of VMH neurons to concentrate oxytocin, which has recently been demonstrated to facilitate maternal and social behaviors in rodents (for a review see Insel, '92). Efferents from the VMH project to limbic, hypothalamic, and mesencephalic structures, including the bed nucleus of the stria terminalis, medial and lateral septal nuclei, anterior and medial preoptic areas, and the periaqueductal grey (Saper

et al., '76b; Krieger et al., '79). The VMH in rat and monkey also projects to the amygdaloid nuclei, suggesting that a reciprocal connection exists between the two structures (Saper et al., '76b; Amaral et al., '82), possibly integrating olfactory stimuli and reproductive behaviors.

The DMH is a distinct cell group located ventral and medial to the caudal aspect of the PVH. The DMH contains medium sized neurons which have been demonstrated in rat using anterograde tract tracing with PHA-L to project to hypothalamic structures including the ARC, LHA, MPA, and PC PVH, as well as descending projections to autonomic brainstem cell groups including the nucleus of the solitary tract, nucleus ambiguus, and the caudal ventrolateral medulla (Ter Horst and Luiten, '86; Thompson et al., '92). In addition, comparative cytoarchitectonic and DßH immunohistochemistry studies suggest that the DMH and ARC form a continuum in the periventricular region medial to the VMH (Broadwell and Bleier, '76; Bleier, '84; see Chapter Three). In terms of hypothalamic function, the DMH is believed to provide a final common interhypothalamic projection to the PVH, potentially integrating feeding behavior with neuroendocrine output (Luiten et al., '87; Ter Horst and Luiten, '87).

The perifornical area, as its name suggests, surrounds both medial and lateral aspects of the fornix at the level of the DMH, immediately caudal to the PVH. Kawata and Sano ('82) in monkey have identified MC-like neurons in the perifornical area that are immunoreactive for vasopressin and oxytocin. The perifornical area in guinea pig contains the magnocellular dorsal nucleus that projects to the lateral septum with enkephalin as a neurotransmitter candidate (Poulain et al., '84).

The posterior hypothalamic area is a fairly cell poor region that separates the caudal hypothalamus from the zona incerta and midline thalamic nuclei. The region is bounded laterally by the tuberomammillary nucleus and the LHA and caudally by the mammillary complex. Several fiber tracts, including the fornix, inferior thalamic peduncle, and mammillothalamic tract course through the posterior hypothalamic area (Nauta and Haymaker, '69).

Caudal region

The caudal region of the hypothalamus contains the mammillary complex, which has been described by Papez ('37) as connecting the hippocampal formation with the anterior thalamic nuclei, functioning as a circuit to integrate emotional responses. The monkey mammillary complex consists of several subdivisions including the medial, lateral, premammillary, and supramammillary nuclei (see Papez, '37 and Veazey et al., '82 for a more detailed cytoarchitectonic analysis). The connectivity of the mammillary complex is beyond the scope of this review. Briefly, afferent input from the subiculum primarily innervates the medial mammillary nucleus via the postcommissural fornix, whereas septal input primarily innervates the lateral mammillary nucleus via the medial forebrain bundle (Ingram, '40; Nauta and Haymaker, '69). The principal efferent pathway from the mammillary body exits dorsally and splits into the ascending mammillothalamic tract and the descending mammillotegmental tract. The mammillothalamic tract innervates the anterodorsal nucleus bilaterally and the anteroventral and anteromedial nuclei ipsilaterally. The mammillotegmental tract projects topographically to nuclei within the pontine tegmentum (Swanson, '87).

In this review, it becomes apparent that connectivity, neurotransmitter content, and subsequent function varies greatly throughout the six hypothalamic zones, involving several modalities and affecting the neuraxis through both neuronal and endocrine output. The specific aims outlined in this project assess several neurotransmitter-identified substrates mainly within the PVH in an attempt to clarify the neurochemical and morphologic organization of this hypothalamic neuroendocrine nucleus relative to the multiplicity of functions that it subserves within the primate diencephalon.

Chapter Two

Animals

The rhesus monkeys used in these studies (ages 19 - 27 months) were born and raised at the Harlow Primate Center, Madison, Wisconsin, and were either socially reared or socially deprived (see Appendix). Socially reared animals (n = 8) were housed from birth to the age of 6 months with their mother. These animals were separated from their mother after 6 months and housed in peer groups of 4 young monkeys in a 2 cubic meter cage. Socially deprived animals (n = 5) were born and kept with their mother in her home cage prior to separation. Three days after birth, socially deprived animals were removed from their mother and taken to the nursery where they remained for 1 month in small cages (46 cm x 51 cm x 64 cm) and were fed infant formula. After 1 month, socially deprived animals were able to feed themselves, and were transferred to single cages. All socially deprived animals were raised in the same room and had auditory, olfactory, and visual, but not tactile, contact with other subjects. Monkeys had free access to water and were fed a fixed amount of monkey chow based upon age and weight. Juvenile cynomolgus monkeys (n = 5) were feral born and maintained in single cages at the Mount Sinai Medical Center animal facility until sacrificed. Both male and female monkeys were used in these studies. These experiments were conducted within NIH guidelines for animal research and were approved by the Institutional Animal Care and Use Committee (IACUC) of the University of Wisconsin and the Mount Sinai Medical Center.

Tissue preparation

Immunohistochemistry was performed on monkey tissue that was fixed by perfusion using paraformaldehyde, a solid polymer of the gas formaldehyde, which reacts mainly with free amino groups (Sternberger, '86). Fixation confers rigidity to the tissue by cross linking proteins, preserving the morphologic structure of the brain as well as allowing for thin sections to be cut on a cryostat. The process of fixation also preserves the antigenicity of epitopes that can be recognized by specific antibodies.

All of the monkeys in this project were sacrificed by a transcardial perfusion technique, which utilized the subject's vascular system as a route to deliver the paraformaldehyde solution to the brain. Briefly, the left ventricle was canulated and the right atrium was severed. In this manner, perfusate was pumped under pressure through the vascular system, clearing out the blood, and fixing the tissue by capillary diffusion. The descending aorta was also clamped to direct the flow toward the head and avoid perfusing the lower portion of the animal.

Monkeys were sedated with ketamine hydrochloride (25 mg/kg, intramuscular injection) and sodium pentobarbital (30 mg/kg, intraperitoneal injection) and then intubated with an endotracheal tube and ventilated. The monkeys continued to be ventilated during the perfusion to maintain oxygen to the brain in an attempt to avoid anoxia, which can lead to massive neurochemical release and loss of antigenicity. Prior to transcardial perfusion, 1.5 ml of aqueous sodium nitrite was injected into the left ventricle to induce vasodilation, which aids in the flow of fixative. Ice-cold 1% paraformaldehyde in phosphate buffered saline (PBS, 0.12M, pH 7.4) was delivered via a perfusion pump (275 - 325 ml/min flow rate) to flush the

vascular system of blood followed by ice-cold 4% paraformaldehyde in PBS delivered at the same flow rate for an additional 8 - 9 minutes. This protocol has been proven to be effective for the assessment of DßH and TH immunohistochemistry in monkey telencephalon (Morrison et al., '82; Lewis et al., '88). Brains were carefully removed and hypothalamic blocks ranging from the decussation of the anterior commissure anteriorly to the mammillary bodies caudally were cut in the coronal plane and post fixed by immersion in 4% paraformaldehyde for 6 hours. The hypothalamic tissue was also cryoprotected in a series of 12%, 16%, and 18% sucrose solutions in PBS to avoid damage during frozen sectioning.

For this project, sections evenly spaced throughout the rostrocaudal extent of the hypothalamus (notably the PVH) were necessary. A 1 in 13 series of 30 µm thick sections were taken, effectively sampling every 390 µm. This allowed for 9 tissue sections throughout the rostrocaudal extent of the PVH per subject to be analyzed for each immunohistochemical procedure. One series was stained with thionin to recognize cellular landmarks in conjunction with Bleier's ('84) atlas of the rhesus monkey hypothalamus. Thionin is an aniline dye that labels stacks of cytosolic rough endoplasmic reticulum, or "Nissl substance", and nucleoli, allowing for the differentiation of neurons based upon size and cytoplasmic morphology as well as the identification of glial and ependymal cells.

Immunohistochemical procedure

Several high affinity antibodies were employed in this project to localize specific epitopes within the confines of a tissue section, allowing for the subsequent morphologic characterization of discretely localized antigenic sites in conjunction with microscopic techniques. The specific antibodies

directed against CRF, DßH, oxytocin, TH, and vasopressin have been fully characterized previously (O'Connor et al., '79; Markey et al., '80; Frigon et al., '81; Hou-Yu et al., '82, '86; Vale et al., '83). Briefly, the antibodies used to detect noradrenergic- and dopaminergic-containing structures were directed against enzymes in the catecholamine biosynthetic pathway, since the catecholamines themselves are not highly antigenic. The antisera for DßH and TH were derived from purified preparations of human pheochromocytoma tumors, which secrete large amounts of catecholamines. In contrast, the CRF, oxytocin, and vasopressin antibodies were raised against an antigenic epitope within each of the respective peptides. The CRF, DßH, and TH antibodies were polyclonal and raised in rabbit, indicating that the antigen was not isolated from a single clone, whereas the oxytocin and vasopressin antisera were developed in mouse from a single clone (monoclonal) directed against synthetic forms of each nonapeptide.

Once an antigen-antibody complex is formed *in situ*, a histochemical method of visualizing the reaction is necessary. The experiments performed in specific aims 1, 2, 4, 5, and 6 utilized an immunoperoxidase protocol to generate a reaction product that was suitable for qualitative and quantitative analyses. In this method, a biotinylated secondary antibody was conjugated to the antibody-antigen complex followed by an avidin-horseradish peroxidase tertiary antibody step. A punctate, dark brown, electron dense reaction product was precipitated by adding nickel-cobalt intensified 3,3-diaminobenzidine (DAB) and hydrogen peroxide to the avidin-biotin-horseradish peroxidase bridge. The nickel-cobalt DAB reaction product was permanent, and displayed a high signal-to-noise ratio suitable for detailed morphologic analysis using light microscopy and laser scanning microscopy.

Since quantitative analyses were performed, all of the histochemical procedures were tightly monitored to maintain consistent precipitation of the DAB reaction product. Of particular importance in specific aims 2 - 4 was to insure that tissue sections were completely immunolabeled throughout their axial depth in order to fully assess the number of DßH-immunoreactive varicosities through the three dimensions of the tissue section (see Chapters 3 - 5).

Tissue sections were incubated overnight in a PBS solution containing the primary antiserum (at its proper dilution), 0.3% Triton X-100, and 0.5 mg/ml bovine serum albumin at 4°C. Triton X-100 is a nonpolar detergent which was used to slightly damage cell membranes, allowing for better penetration of the immunoreagents into the tissue section. Bovine serum albumin is a high molecular weight protein which blocks the labeling of non-antigenic elements within a tissue section. The secondary and tertiary steps were performed using the Vectastain ABC kit (Vector Laboratories, Burlingame, CA) with DAB (Sigma, St. Louis, MO, 5 mg/ml) intensified with 0.05% nickel ammonium sulfate and 0.05% cobalt chloride as a chromogen and 0.003% hydrogen peroxide as a catalyst. The tissue sections were mounted on chrome-alum coated slides, dehydrated through an ascending ethanol series and coverslipped with DPX (Fluka, Germany) permanent mounting media. If the primary, secondary, or tertiary reagents from the protocol were removed, there was no immunohistochemical labeling of the tissue.

In specific aim 3 a double labeling procedure was used to observe two antigens in the same tissue section for subsequent analysis by confocal laser scanning microscopy. This method differed from the immunoperoxidase-

DAB process in that fluorescent molecules were conjugated to the antibody-antigen complex, which allowed for the visual discrimination of the two antigens using epifluorescence with the appropriate barrier filters, or using lasers with the appropriate wavelength to discriminate the fluorophores. Immunofluorescent preparations generate high intensity signals which are optimal for confocal laser scanning microscopy. However, disadvantages with these preparations include autofluorescence and fading of the fluorophores over time.

In this protocol, anti-DßH and anti-vasopressin/anti-oxytocin were used to label varicosities and perikarya, respectively. Since the polyclonal DßH antibody was raised in rabbit and the monoclonal vasopressin and oxytocin antibodies were raised in mouse, the secondary antibodies were processed simultaneously (all at a working dilution of 1:200), followed by a tertiary step (also at a 1:200 dilution) for the anti-DßH label. The vasopressin and oxytocin antibodies were visualized with horse anti-mouse IgG conjugated to fluorescein isothiocyanate (Vector Laboratories) and the DßH antibody was visualized with a biotinylated goat anti-rabbit IgG (Vector Laboratories) reagent in the same PBS solution for 2 hours, followed by avidin conjugated to Texas Red (Vector Laboratories) in PBS for two hours. Tissue sections were mounted onto chrome-alum coated slides and coverslipped using PermaFluor (Lipshaw, Pittsburgh, PA) mounting media. Control experiments included the omission of the anti-DßH antibody; the omission of the anti- vasopressin or oxytocin antibody; using the same antibody (e.g anti-DßH) twice in the double label procedure; switching the staining sequence (e.g. a secondary and tertiary conjugate for anti-vasopressin); or reversing fluorophores.

In addition, an intracellular filling method was also used in specific aim 3 to assess the morphology of MC cells in the immunohistochemical procedure. Intracellular filling allows for the visualization of cellular processes *in situ* by injecting a dye into the cytosol of a cell. In this preparation, a pipette filled with the fluorescent naphthalimide dye Lucifer Yellow (LY, see Stewart, '78) was used to identify MC neurons. Specifically, the pipette tip was lowered into the PVH within a 200 μm thick tissue section until a cell body was impaled. Lucifer Yellow was then iontophoresed into the cell until all of the processes within the confines of the thick section appeared to be labeled.

Two hypothalamic blocks postfixed for 2 hours in 4% paraformaldehyde were cut on a vibratome in ice-cold PBS at a section thickness of 200 μm. A 2 hour, rather than 6 hour post fixation interval was found to be optimal because over fixation impeded the penetration of the intracellular dye. Since the tissue was lightly fixed and quite fragile, a vibratome was used for tissue sectioning rather than a cryostat. Hypothalamic tissue sections were mounted onto nitrocellulose filter paper (Whatman, 0.45 μm pore size, Maidstone, England), connected to the anode of a current microiontophoresis programmer (World Precision Instruments, New Haven, CT). The cathode was attached to a glass micropipette (outer diameter 0.86 mm, A-M Systems Inc., Everett, WA) pulled to a tip diameter of 0.25 μm with a vertical pipette puller (David Kopf Instruments, Tujunga, CA) and filled with a 5% aqueous solution of the fluorescent dye LY (Sigma, St. Louis, MO). A constant current of 100 nA was applied to iontophorese the LY. In this manner, a negative current was used to inject the LY into the tissue section. The micropipette was lowered into the tissue section by a micromanipulator

(Goodfellow, Cambridge, England) and a fluorescence microscope (Labophot, Nikon, Japan) equipped with a 10x objective and a B2A filter allowed for the visualization of the LY and autofluorescent tissue landmarks. Each cell was filled for approximately 10 - 15 minutes, at which time all of the processes within the confines of the tissue section appeared to be labeled. As previously described by de Lima et al., ('90), cells were considered to be completely filled when no cut off processes were visible and fine axonal and dendritic processes were observed to follow their appropriate trajectories.

Data Analysis

Qualitative analysis was performed on a light microscope (Axiophot, Zeiss, Germany) at magnifications of 100x and 200x for the experiments in specific aims 1, 2, 4, 5, and 6. Darkfield and differential interference contrast optics were also used to photograph DßH-immunoreactive varicosities in specific aim 1. The qualitative analysis in specific aim 3 was performed using epifluorescence optics attached to a laser scanning microscope (LSM, Zeiss, Germany), switching between the appropriate fluorescein and Texas Red barrier filters at 100x and 250x.

A laser provides a focused, high intensity beam of light that will reflect off of fluorescent and/or electron dense materials. In a LSM, a specimen is bombarded with a laser beam, and the reflected light is directed towards a detection surface via a photomultiplier tube for subsequent analysis of the reflected surface (see Inoué, '90 for a more detailed description). In this manner, a high degree of two-point resolution and a low degree of axial depth is obtained, which is optimal for quantification of varicosities throughout several z-axis planes within the confines of a tissue section. In a confocal setting, the reflected light is aimed at a small pinhole in front of the

detector, allowing only the light within a circumscribed axial depth (for example, < 0.5 μm with a 25x oil lens) to reach the detection surface (Inoué, '90).

In specific aims 2 and 4, the LSM was used to quantify DβH-immunoreactive varicosities through a volume of tissue within the PVH. See Chapter 3 for a series of experiments which assessed the precision and accuracy of the LSM varicosity quantification as compared to conventional light microscopy. The LSM used an argon laser (a combination of 488 nm and 514 nm wavelengths) with a 0.1 neutral density filter as an illumination source and was coupled to a computer driven stage (MSP65, Zeiss, Germany) and a computer workstation (DEC 3100, Digital Equipment Corp., Maynard, MA). The LSM allowed for the localization of DβH-immunoreactive varicosities in the *x*-, *y*-, and *z*-axis planes throughout the entire thickness of a tissue section because images which were only in focus in the specific scanning plane (vertical resolution < 3 μm in the nonconfocal mode) were digitized and transmitted to the computer monitor where the actual quantification was performed by software developed in this laboratory. A series of 8 z-axis planes were collected for each tissue section, with 9 sections throughout the rostrocaudal extent of the PVH quantified in 10 monkeys for a total of 90 sections analyzed. A nonconfocal mode was selected because of the size of the varicosities and diminished reflectance of the DAB precipitate compared to fluorescent labels. The nonconfocal optical sections were extremely crisp, and varicosities which were in focus could be readily and reproducibly discriminated from background.

Dopamine-ß-hydroxylase-immunoreactive varicosities were characterized morphologically as the axon traversed through all three planes

of section. Specifically, varicosities were identified within the plane of focus as punctate, spherical structures intensely labeled with DAB reaction product. The varicosities counted in this study were similar to previous electron microscopic reports of DßH-immunoreactive varicosities in the PVH and basal forebrain of rats as being approximately 1 µm in diameter and discontinuous from intervaricose segments < 0.5 µm in diameter (Olschowka et al., '81; Liposits et al., '86b; Chang, '89). Every varicosity had a fixed *x*, *y*, and *z* coordinate attributed to it relative to a 0, 0, 0 (home) point stored in a datafile for each section. In this analysis scheme, the *x* and *y* coordinates remained fixed for each field while the *z* coordinate was moved at a 3 µm step interval to assess innervation density of a volume of tissue. In order to maintain experimental consistency, quantification always began at the top of a section and the *z*-axis plane was stepped down.

A 25x oil objective was used for the LSM analysis, and the area sampled for each field was 260 µm in the *x* plane, 165 µm in the *y* plane, and the section thickness was 24 µm, creating a volume of 1.04×10^{-3} mm^3 per field. At this magnification, the resolution on the computer monitor was 2.4 pixels per µm. The number of varicosities that were quantified for each of the 9 tissue sections per subject was collapsed to yield a final effective volume of 9.27×10^{-3} mm^3 per subject.

In specific aim 3, tissue sections were scanned twice using argon lasers with specific excitation wavelengths, capturing sequential images for subsequent computer-generated overlay and analysis. Confocal analysis was necessary in this series of experiments in order to quantify DßH-immunoreactive varicosities which were < 0.5 µm away from immunohistochemically-identified neurons. A 488 nm argon laser was

employed to detect the fluorescein-conjugated vasopressin or oxytocin signal and a 514 nm argon laser was employed to detect the Texas Red-conjugated DßH signal. In this manner, vasopressin- and oxytocin-immunoreactive neurons were assessed through their total somal volume, along with the corresponding DßH-immunoreactive varicosities in the same volume of tissue, in a series of optical sections 1 µm apart (neurons ranged approximately from 10 - 14 µm thick in the *z*-axis plane) while the *x* and *y* coordinates remained fixed for each field. To maintain experimental consistency, the fluorescein image was scanned first, and the analysis always began at the top of a tissue section and the *z*-axis plane was stepped down. All of the data acquisition procedures were computer automated to insure tightly controlled and accurate scanning parameters for the detection of each signal. Similar to specific aims 2 and 4, a 25x oil objective was selected for the LSM analysis, which allowed for a resolution 2.4 pixels per µm on the computer monitor. The area sampled for each field was 260 µm in the *x* plane, 165 µm in the *y* plane, and the confocal section thickness was < 0.5 µm, creating a volume of 2.15×10^{-5} mm^3 per optical section.

Pairs of confocal optical sections (one fluorescein image and one Texas Red image for each z-axis plane) were scanned on the LSM and digitized to the computer monitor where the images were aligned with respect to the *x*, *y*, and *z* coordinates, and overlaid to yield a resultant image. The scoring of DßH/vasopressin and DßH/oxytocin contacts was characterized morphologically by toggling between the 2 optical sections (Texas Red/DßH and fluorescein/vasopressin or oxytocin) and the resultant overlay image for each z-axis plane using custom designed morphometry software. For the vasopressin- or oxytocin-immunoreactive image, pixels which contained a

fluorescein signal were coded in yellow and in the DßH image, pixels which contained a Texas Red signal were coded in red. Additionally, pixels in the overlay image which contained both a fluorescein and a Texas Red signal were coded in blue, signifying that a DßH-immunoreactive varicosity was in apposition (< 0.5 μm apart, with 2.4 pixels per μm) to a vasopressin- or oxytocin-immunoreactive neuron. An apposition was registered only if both signals were present in the same pixels, thus, even excluding profiles where two signals were in adjacent pixels. A varicosity-to-neuron ratio was based upon data collected for each immunohistochemically-identified cell, which was further characterized morphologically to assess noradrenergic innervation density directly on the soma versus on the proximal dendrites.

In specific aims 5 and 6, quantitative analysis of TH- and CRF-immunoreactive neurons was performed on 9 immunostained sections evenly spaced throughout the rostrocaudal extent on the left PVH (and ARC for TH) of each animal for a total of 90 tissue sections analyzed per antibody series. In these neuron counting experiments, light microscopic analyses were performed because a large field of view was being assessed and precise LSM axial resolution was not necessary for identifying neurons. The analysis was done at a magnification of 200x on the Axiophot light microscope which was coupled to the MSP65 stage controller and the DEC 3100 computer workstation as well as a Macintosh IIci server (Apple Computer Inc., Cupertino, CA) equipped with the morphometry software package. Similar to the LSM analyses, each immunoreactive neuron had a fixed x, y, and z coordinate attributed to it relative to a 0, 0, 0 (home) point recorded in a datafile for each section. The criteria for counting immunoreactive neurons was that one or more processes were immunolabeled and/or the nucleus was

visible by being immuno-negative relative to the stained perikarya. The number of TH- and CRF-immunoreactive neurons for 9 sections per animal was collapsed to yield a total value for comparison across conditions. All investigators were blind to the rearing conditions of the monkeys. A two-tailed Student's *t*-test was used for the statistical analyses in specific aims 1 - 6 and a two-way analysis of variance (ANOVA) was also used in specific aim 4.

Chapter Three

SUMMARY

The distribution of noradrenergic processes within the hypothalamus of rhesus monkeys (*Macaca mulatta*) was examined by immunohistochemistry using an antibody against DßH. The results revealed that the pattern of DßH immunoreactivity varied systematically throughout the rhesus monkey hypothalamus. Extremely high densities of DßH-immunoreactive processes were observed in the PVH and SON, while relatively lower levels were found in the ARC and DMH and in the MPA, perifornical, and suprachiasmatic areas. Moderate levels of DßH immunoreactivity were found throughout the LHA and in the internal lamina of the median eminence. Very few immunoreactive processes were found in the VMH or in the mammillary complex. Other midline diencephalic structures were found to have high densities of DßH immunoreactivity, including the paraventricular nucleus of the thalamus and a discrete subregion of nucleus reuniens, the magnocellular subfascicular nucleus. A moderate density of DßH-immunoreactive processes were found in the rhomboid nucleus and zona incerta whereas little DßH immunoreactivity was found in the fields of Forel, nucleus reuniens, or subthalamic nucleus. The differential distribution of DßH-immunoreactive processes may reflect a potential role of norepinephrine as a regulator of a variety of functions associated with the nuclei that are most heavily innervated, e.g., neuroendocrine release from the PVH and SON, and GnRH release from the MPA and mediobasal hypothalamus. Additionally, quantitative analysis of DßH-immunoreactive varicosities was performed on

a LSM in both MC and PC regions of the PVH. The methodology employed in this study allowed for the high resolution of immunoreactive profiles through the volume of tissue being analyzed, and was more accurate than conventional light microscopy in terms of varicosity quantification. Quantitatively, a significant difference in the density of DßH-immunoreactive varicosities was found between MC and PC regions, suggesting that PC neurons received a denser noradrenergic input. These differential patterns may reflect an important functional role for norepinephrine in the regulation of anterior pituitary secretion through the HPA stress axis.

INTRODUCTION

A substantial body of neuroanatomic research on the hypothalamus has been conducted in the rat, where connectivity and chemical characteristics of several neurotransmitter systems, including monoamines and various neuropeptides, have been described (Swanson and Sawchenko, '83; Swanson, '87; Meister et al., '90). However, minimal information is available on the cellular and neurochemical organization of the hypothalamus in non-human primates. Within this framework, the catecholaminergic innervation of the hypothalamus has been described as particularly dense in rats and monkeys by monoamine fluorescence histochemistry (Fuxe, '65; Hoffman et al., '76; Ishikawa and Tanaka, '77; Felten and Sladek, '83). The majority of this catecholaminergic innervation is noradrenergic, as determined by radioimmunoassay analysis in micropunches of rat hypothalamic tissue (Palkovits et al., '74; Versteeg et al., '76). Additionally, antibodies directed against DßH, an essential enzyme for norepinephrine synthesis, have allowed

for the characterization of noradrenergic (and adrenergic-see Discussion) processes within the rat hypothalamus (Swanson and Hartman, '75).

A morphologic examination of noradrenergic input into the hypothalamus is particularly relevant in respect to the multitude of neuropharmacologic and electrophysiologic studies utilizing noradrenergic agents in a variety of hypothalamic preparations. For example, norepinephrine is believed to influence the HPA axis at the level of the PVH and SON as well as modulate gonadotropin release from the MPA and mediobasal hypothalamus (Day et al., '84; Plotsky, '87; Szafarczyk et al., '87; Terasawa et al., '88; Saphier and Feldman, '89). In addition, both alpha- and beta-adrenoceptors have been localized to discrete hypothalamic nuclei by tritiated ligand binding assays (Leibowitz et al., '82). However, the exact nature of the function(s) of norepinephrine *in situ* remains unclear. By correlating the results of experimental manipulations with neuroanatomic studies, a more comprehensive understanding of the function of the noradrenergic system within the hypothalamus should emerge.

In order to assess the density of DßH-immunoreactive afferent input within a restricted region of the hypothalamus, a method was developed using a LSM which allowed for the accurate localization and quantification of varicosities through the *x*, *y*, and *z* planes of a tissue section. The PVH is a heterogeneous structure that contains at least two distinct neuronal subtypes, MC neurons and PC neurons, which have been differentiated primarily on the basis of their size and efferent projections (Swanson and Kuypers, '80; Swanson and Sawchenko, '83). In regard to the afferents of these cells, the apposition of monoamine histofluorescent varicosities to neurophysin-immunoreactive perikarya has been described at the light microscope level in

the PVH of rat and monkey (McNeill and Sladek, '80; Sladek and Zimmerman, '82), as well as a report in rat that DßH-immunoreactive varicosities are in contact with vasopressin-immunoreactive neurons (Hornby and Piekut, '87). Electron microscopic examination of DßH-immunoreactive profiles in the rat PVH has demonstrated primarily asymmetric, axodendritic and axosomatic synapses onto unlabeled postsynaptic neurons (Olschowka et al., '81; Liposits et al., '86b; Decavel et al., '87). In addition, double label immunoelectron microscopy and immunoelectron microscopy combined with autoradiography have demonstrated in the rat that there are synaptic contacts between noradrenergic varicosities and vasopressinergic perikarya, verifying the light microscopic observations (Silverman et al., '83, '85; Nakada and Nakai, '85; Nakai et al., '86; Ochiai et al., '88; Ochiai and Nakai, '90). By examining the DßH-immunoreactive input to MC and PC regions of the PVH, this study assessed noradrenergic varicosity density on two morphologically and functionally separate neuronal subpopulations that are critically involved in the central regulation of the HPA axis, as well as modulating appetitive behaviors and autonomic (notably sympathetic) outflow (Sawchenko and Swanson, '81a; Luiten et al., '87; Swanson, '87).

To date, no comprehensive DßH immunohistochemical analysis of noradrenergic input to the hypothalamus has been conducted in non-human primates. This report includes a general qualitative description of DßH-immunoreactive innervation of the rhesus monkey hypothalamus and quantitative data on the density of DßH-immunoreactive varicosities within discrete cellular regions throughout the rostrocaudal extent of the PVH. The quantitative data are particularly crucial in regard to the accurate evaluation of terminal field density in the normal monkey hypothalamus. This

normative database may also be used to assess changes that are experimentally induced, neuropathologic, or age-related. Parts of these data have been reported in abstract form (Ginsberg et al., '91).

MATERIALS AND METHODS

Animals

Eight rhesus monkeys (*Macaca mulatta*, ages 19 - 27 months) used in this study were born and raised at the Harlow Primate Center, Madison, Wisconsin. Monkeys had free access to water and were fed a fixed amount of monkey chow based upon age and weight. Both male and female monkeys were used in this study. These experiments were conducted within NIH guidelines for animal research and were approved by the IACUC board of the University of Wisconsin.

Immunohistochemical Procedure

Eight monkeys were sedated with ketamine hydrochloride (25 mg/kg i.m.) and anesthetized with sodium pentobarbital (30 mg/kg i.p.) and were then intubated with an endotracheal tube and ventilated. The chest cavity was opened and the descending aorta was clamped. One and a half milliliters of 1% aqueous sodium nitrite was injected into the left ventricle prior to transcardial perfusion to increase vasodilation. Ice-cold 1% paraformaldehyde in PBS (0.12 M, pH 7.4) was delivered via a perfusion pump (275 - 325 ml/min) as an initial rinse of the vascular system for 45 - 60 seconds followed by ice-cold 4% paraformaldehyde in PBS delivered at the same flow rate for an additional 8 - 9 minutes. Brains were removed and hypothalamic blocks were cut in the coronal plane and postfixed in 4% paraformaldehyde for 6

hours then cryoprotected in a series of 12%, 16%, and 18% sucrose solutions in PBS.

Hypothalamic blocks were removed from 18% sucrose and frozen in dry ice prior to being cut on a cryostat. Immunohistochemical analyses were based on 30 μm thick sections through the extent of the hypothalamus at 390 μm intervals, effectively creating a 1 in 13 series. One series was stained with thionin to assign cytoarchitectonic criteria for the delineation of nuclear boundaries in conjunction with Bleier's ('84) hypothalamic atlas of the rhesus monkey. An adjacent series was processed for immunohistochemistry using a polyclonal rabbit antiserum directed against human DβH at a working dilution of 1:2,000. The primary antibody has been fully characterized immunochemically and immunohistochemically previously and shown to crossreact with monkey DβH (O'Connor et al., '79; Frigon et al., '81; Morrison et al., '82). Other tissue series were set aside and stored for future immunohistochemical analyses.

Tissue sections were incubated overnight in a PBS solution containing the primary antisera, 0.3% Triton X-100, and 0.5 mg/ml bovine serum albumin at 4°C. The secondary and tertiary steps were done according to the Vectastain method (Vector Laboratories, Burlingame, CA) with DAB (Sigma, St. Louis, MO) as a chromogen. The reaction product was intensified with 0.05% cobalt chloride and 0.05% nickel ammonium sulfate added to the DAB solution. The tissue sections were then mounted on chrome-alum coated slides, cleared through an ascending ethanol series and coverslipped with DPX (Fluka, Germany) mounting media. The immunohistochemical procedures were tightly monitored visually and by incubation times in order to maintain consistent precipitation of the DAB reaction product for the

subsequent quantitative analysis. One immunofluorescent series was also prepared for confocal microscopy where tissue sections were placed overnight in the primary antisera solution and then incubated in a secondary antibody preparation of fluorescein horse anti-rabbit IgG (Vector) at a dilution of 1:200 for 2 hours. Tissue sections were mounted on subbed slides and coverslipped using PermaFluor (Lipshaw, Pittsburgh, PA) mounting media. If the primary, secondary, or tertiary reagents from the protocol were removed, there was no immunohistochemical labeling of the tissue.

Data Analysis

Qualitative analysis of DßH-immunoreactive processes throughout the hypothalamus was performed by light microscopy at magnifications of 100x and 200x, beginning at the decussation of the anterior commissure and ending caudal to the mammillary complex. In addition, the evaluation of DßH immunoreactivity present in the subthalamic area and midline thalamic nuclei was included in this study.

Quantitative assessment of DßH-immunoreactive varicosity density within MC and PC regions was performed in 5 rhesus monkeys. Nine immunostained sections evenly spaced throughout the rostrocaudal extent of the PVH were analyzed per animal (a total of 45 sections) on a LSM (Zeiss, Germany). Magnocellular and parvicellular regions were identified on thionin-stained sections and the adjacent immunostained section for DßH-immunoreactive varicosity density. Both MC and PC neurons were observed in homogeneous clusters throughout the PVH and were distinguishable by the size and shape of the somata, with MC clusters tending to be dorsal and lateral to PC clusters.

The LSM used an argon laser with a 0.1 neutral density filter as an illumination source, and was coupled to a computer driven stage (MSP65, Zeiss) and a computer workstation (DEC 3100, Digital Equipment Corp., Maynard, MA). The LSM allowed for the localization of identified structures in the z-axis plane throughout the entire thickness of a tissue section because images which were only in focus in the specific scanning plane were digitized and transmitted to the computer monitor where the actual quantification was performed by software developed in this laboratory. A series of z-axis planes was collected throughout the tissue sections in the nonconfocal mode (see Discussion; 8 different z-axis planes were obtained in each tissue section with a vertical resolution < 3 μm). This precise focus of optical sections in the z-axis plane resulted in a high resolution of DβH-immunoreactive varicosities in each tissue section. Dopamine-ß-hydroxylase-immunoreactive profiles were characterized morphologically as the axon traversed through all 3 planes of section. Specifically, varicosities were identified within the plane of focus as punctate, spherical structures intensely labeled with DAB reaction product, either discontinuous with adjacent labeled profiles or attached to an intervaricose segment. The varicosities counted in this study were similar to previous electron microscopic reports of DβH-immunoreactive varicosities in the PVH and basal forebrain of rats as being approximately 1 μm in diameter and discontinuous from intervaricose segments < 0.5 μm in diameter (Olschowka et al., '81; Liposits et al., '86b; Chang, '89). Every varicosity had a fixed x, y, and z coordinate attributed to it relative to a 0, 0, 0 (home) point stored in a datafile for each section. In this analysis scheme, the x and y coordinates remained fixed for each field (one MC and one PC) while the z coordinate was moved at a constant interval to assess innervation density of a

volume of tissue. Several intervals in the z-axis plane were evaluated, and a 3 μm step interval was found to be optimal. To maintain experimental consistency, quantification always began at the top of a section and the z-axis plane was stepped down. Additionally, tissue shrinkage caused by the immunohistochemical procedure was estimated to be 20% (from 30 μm to 24 μm in the z-axis) by measuring the distance from the top optical section to the bottom optical section. A similar estimation (17%) was reported by investigators who assessed hypothalamic tissue shrinkage linearly (Kiss et al., '91).

A 25x oil objective was used for the LSM analysis, and the area sampled for each field was 260 μm in the *x* plane, 165 μm in the *y* plane, and the section thickness was 24 μm, creating a volume of 1.04×10^{-3} mm^3 per field. The varicosity quantification for each tissue section on the LSM yielded 2 collapsed two-dimensional maps (1 for each of MC and PC regions) which provided a quantitative assessment for the density of DβH innervation within a circumscribed region of monkey PVH. The number of varicosities that were quantified for each of the 9 tissue sections per subject was collapsed to yield a final effective volume of 9.27×10^{-3} mm^3 per subject.

To assess the accuracy of the LSM analysis, varicosity counts on metal-intensified DAB-stained material in 3 μm thick nonconfocal z-axis optical sections were compared to varicosity counts on fluorescent-stained material in 1 μm thick z-axis optical sections in the confocal mode. In addition, varicosity counts on the LSM using a 25x objective were compared to counts performed on a light microscope with a 20x and a 40x objective to assess the accuracy of the LSM system relative to a conventional light microscope. The 20x and 40x objectives were selected for the light microscope analysis because

they encompassed a larger and smaller area for quantification, respectively, than the area analyzed on the LSM. Statistical analyses were performed by a two-tailed Student's *t*-test.

RESULTS

Distribution of DßH-immunoreactive processes within the rhesus monkey hypothalamus

General morphology. Coarse, heavily varicose fibers as well as fine caliber fibers with long intervaricose segments were present throughout the hypothalamus (Fig. 1). Terminal fields with darkly stained, punctate varicosities were also observed in several hypothalamic nuclei, notably within the PVH (Fig. 2). A rostrocaudal gradient in the distribution of DßH-immunoreactive fibers was observed where the rostral two-thirds of the hypothalamus contained a considerable greater density of DßH immunoreactivity than the caudal one-third of the hypothalamus. In addition an apparent mediolateral gradient was also observed in the distribution of DßH-immunoreactive processes where medially-located structures tended to be more densely innervated by noradrenergic fibers than laterally-located structures. No DßH-immunoreactive cell bodies were observed in any of the brain regions investigated.

Preoptic area. A relatively high density of diffusely distributed DßH-immunoreactive processes was observed throughout the MPA, with a particularly heavy concentration of coarse fibers and associated terminal fields in the periventricular region (Fig. 3A). A dense plexus of DßH-immunoreactive fibers was also observed within the medial preoptic nucleus,

located immediately rostral to the adjacent anterior hypothalamic-suprachiasmatic area. Only sparse DßH-immunoreactive fibers were observed in the lateral preoptic area.

Anterior hypothalamic area. The AHA was fairly devoid of DßH immunoreactivity, which was contrasted by the heavier DßH-immunoreactive innervation of the surrounding MPA, suprachiasmatic area, PVH, and SON.

Suprachiasmatic area. A moderate density of DßH-immunoreactive varicose fibers with associated terminal fields was dispersed throughout this area bounded dorsally by the horizontal plane of the floor of the third ventricle and ventrally by the optic chiasm, including both the SCN and subventricular nucleus (Fig. 3B).

Periventricular fiber bundle. This bundle of fibers coursed through the hypothalamus adjacent to the subependymal layer of the third ventricle, and was observed immediately medial to the periventricular regions of the MPA and PVH. Dopamine-ß-hydroxylase-immunoreactive terminal fields, as well as thin caliber fibers of passage, were observed in the subependymal area. These DßH-immunoreactive fibers were most prominent in anterior and middle regions of the hypothalamus and virtually disappeared caudally at the level of the mammillary complex, suggesting a preferential innervation of anteromedial portions of the hypothalamus.

Supraoptic nucleus. The SON contained one of the densest levels of DßH-immunoreactive terminal fields in the hypothalamus. Thick, heavily varicose fibers were observed within the morphological boundaries of the SON, as well as extending into the surrounding AHA (Fig. 3C). Dopamine-ß-hydroxylase-immunoreactive fibers with associated terminal fields were

packed throughout the rostrocaudal extent of the SON, including retrochiasmatic and tuberal regions, with anterior regions having the greatest density of innervation. In thionin-counterstained preparations, DßH-immunoreactive varicosities were observed in close apposition to MC neurons throughout the rostrocaudal extent of the SON. At retrochiasmatic levels, dense DßH-immunoreactive terminal fields were observed immediately dorsal to the optic tract and the intensity of staining was greatest medially at the level of the tuber cinereum. The PC-like neurons of the tuberal and retrochiasmatic regions of the SON clearly received a dense noradrenergic input. Lateral aspects of the retrochiasmatic area (lateral and ventral to the medial forebrain bundle) were not as heavily innervated by DßH-immunoreactive fibers. Occasionally, DßH-immunoreactive fibers within the SON were observed coursing to medial aspects of the internal lamina of the median eminence. In addition, thin nonvaricose DßH-immunoreactive fibers were seen crossing the midline through the dorsal and ventral supraoptic commissures.

Paraventricular nucleus. The PVH contained coarse, highly varicose fibers and dense DßH-immunoreactive terminal fields throughout its rostrocaudal extent (Fig. 2). The pattern of DßH innervation clearly followed the morphologic boundaries of the PVH. In fact, a well-defined delineation between the PVH and surrounding AHA was readily discerned, indicating that DßH-immunoreactive fibers were preferentially innervating cells located in the nucleus. Both MC and PC divisions of the PVH contained extremely dense terminal field input, making any differences in innervation density within the PVH difficult to assess through qualitative observation.

Perifornical region. Surrounding the fornix lateral to the caudal portion of the PVH was a high density of thick, varicose DßH-immunoreactive fibers. A mediolateral gradient in DßH immunoreactivity was observed, with a prominent fiber plexus medial to the fornix, and less intense DßH immunoreactivity in more lateral aspects of the region (Fig. 3D). Examination of thionin-stained sections indicated that the perifornical region contained MC-like neurons similar in morphology to those observed in both the PVH and SON.

Arcuate nucleus. The ARC contained DßH-immunoreactive fibers and associated terminal fields throughout its rostrocaudal extent, with a greater density of immunoreactive processes at anterior levels in close proximity to the median eminence as compared to more caudal regions at the level of the mammillary recess of the third ventricle. At anterior levels, DßH-immunoreactive fibers were observed coursing through the periventricular zone and became continuous with DßH-immunoreactive processes within the DMH (Fig. 4).

Dorsomedial nucleus. The DMH received a dense DßH-immunoreactive fiber plexus as it appeared as a distinct nuclear mass ventral and caudal to the PVH (Fig. 4). The staining intensity and overall distribution of DßH-immunoreactive processes within the DMH was lower than in the PVH. However, the pattern of DßH immunoreactivity was strikingly similar to that in the ARC, with partial overlap in the periventricular zone, suggesting a dorsomedial-arcuate continuum.

Ventromedial nucleus. A low density of DßH-immunoreactive processes was observed in the VMH, which contrasted the relatively high density of DßH-immunoreactive processes in the adjacent ARC and DMH (Fig. 4). The VMH

was effectively demarcated from the surrounding mediobasal hypothalamus by its relative lack of DßH innervation.

Median eminence. A differential distribution of DßH-immunoreactive processes was observed in the median eminence, with coarse fibers and varicosities present in the internal lamina, whereas the external lamina was fairly devoid of DßH immunoreactivity. Within the internal lamina of the median eminence, DßH innervation density was higher in medial regions than in lateral regions.

Lateral hypothalamic area. A moderate density of DßH-immunoreactive processes was observed throughout the LHA, including fibers coursing through the medial forebrain bundle. Pericellular basket-like arrangements between DßH-immunoreactive fibers and unlabeled perikarya were found in medial aspects of the LHA, lateral to the fornix and ventral to the zona incerta (Fig. 1). In addition, medial regions of the LHA tended to be more densely innervated by DßH-immunoreactive processes than lateral regions.

Posterior hypothalamic area. This diffuse region was fairly devoid of DßH-immunoreactive processes.

Mammillary bodies. Overall, the mammillary complex contained little DßH immunoreactivity. A few, very fine, nonvaricose fibers were seen in the supramammillary nucleus. Delicate DßH-immunoreactive fibers were also seen surrounding the mammillothalamic tract as it ascended through the posterior hypothalamus. No appreciable DßH immunoreactivity was observed in the medial or lateral mammillary nuclei.

Distribution of DßH-immunoreactive processes within the subthalamic region and midline thalamic nuclei

Zona incerta. Extremely fine, nonvaricose DßH-immunoreactive fibers of passage were observed in a large bundle coursing in the zona incerta. The majority of these fibers were oriented in the mediolateral plane, and were seen traveling in the midline to the prominently DßH-immunoreactive PVH and DMH.

Subthalamic nucleus. The subthalamic nucleus contained only sparse DßH-immunoreactive fibers.

Fields of Forel. Little, if any, DßH immunoreactivity was detected in any of the fields of Forel. A few thin fibers were observed in close proximity to the zona incerta.

Paraventricular nucleus of the thalamus. Coarse, DßH-immunoreactive fibers with associated terminal fields were observed throughout the rostrocaudal extent of the nucleus. The heaviest innervation was observed in the midline, with less DßH immunoreactivity in dorsal and lateral aspects of the nucleus (Fig. 5A). The density of innervation was comparable to what was observed in the ARC and DMH of the hypothalamus.

Rhomboid nucleus. The rhomboid-like shape of this nuclear mass could be discriminated from the surrounding midline thalamic area by a moderately dense DßH-immunoreactive fiber plexus.

Nucleus Reuniens. Hardly any DßH immunoreactivity was observed throughout the nucleus reuniens, except for a very dense plexus of coarse fibers and associated terminal fields localized to the ventrolateral aspect of the nucleus, which has been described by Papez and Aronson ('34) and Niimi and Kuwahara ('73) as being the magnocellular subfascicular nucleus (Fig.

5B). In thionin preparations, this nucleus contained medium sized, darkly stained neurons with a moderate cell density, and differed slightly from the size and staining intensity of neurons located in the medial aspects of nucleus reuniens. The DßH-immunoreactive processes within the magnocellular subfascicular nucleus clearly delineated this nuclear mass from the surrounding nucleus reuniens.

Intralaminar and medial thalamic nuclei. Little DßH immunoreactivity was observed throughout the intralaminar and medial thalamic area, which contrasted the dense innervation of the paraventricular nucleus of the thalamus, rhomboid nucleus, and magnocellular subfascicular nucleus.

Quantitative assessment of noradrenergic innervation in MC and PC regions of the PVH

A total of 90,782 DßH-immunoreactive varicosities were counted in the PVH of 5 rhesus monkeys. The density of innervation of MC and PC regions was significantly different ($P < 0.003$) indicating that PC neurons received a heavier DßH-immunoreactive input than MC neurons in the same volume of tissue (Fig. 6). A typical MC region of the PVH where structures were quantified using the LSM is shown in Figure 7. The final two-dimensional map of collapsed z-axis planes is a graphic demonstration of the DßH-immunoreactive varicosities counted through the three-dimensional volume of tissue. The number of counts tallied for each successive z-axis step in this specific MC field is presented in Figure 8. A representative computer generated map demonstrating the area of quantification of one MC and one PC region relative to the surrounding anterior hypothalamus is shown in Figure 9.

Quantitative evaluations of varicosity count methodology

To quantify the immunostained varicosities through the thickness of a tissue section, a standard step interval was determined. Since the identified varicosities were approximately 1 μm in diameter (Olschowka et al., '81; Liposits et al., '86b; Chang, '89), a larger step interval was desired for ease of quantification, and to avoid double counting errors. The optimal step thickness was determined experimentally by counting the same region at different intervals (Table 1). Only a 1.7% ± 1.7 (SEM) difference was observed between varicosity counts performed at 2 μm and 3 μm, whereas a 20.9 % ± 2.3 difference was observed between 2 μm and 5 μm, and a 44.2% ± 5.5 difference was observed between 2 μm and 10 μm intervals. Therefore, a 3 μm z-axis step interval was selected overall for ease and accuracy of quantification.

The precision of LSM quantification was found to be extremely high (less than 3% variability) when reliability tests were conducted to evaluate varicosity counts on the same field (Table 2). In order to assess the accuracy of the nonconfocal analysis, varicosity counts of metal-intensified DAB immunohistochemical material in the nonconfocal mode was compared to an immunofluorescent preparation in the confocal mode. The confocal analysis did not appear to offer any increased sensitivity over varicosity counts made in the nonconfocal plane. For example, 6 equivalent fields (volume = 1.04×10^{-3} mm^3) within 300 μm in the rostrocaudal plane were quantified confocally. These fields had a mean density of 708.5 ± 21.3 (SEM), whereas an adjacent field labeled with DAB and counted nonconfocally had a density of 770. In addition, varicosity counts done on the LSM in the nonconfocal mode were compared to those performed on a conventional light microscope.

Varicosity counts were standardized to a 1 mm^3 volume, since the field of analysis differed for each objective (2.92 x 10^{-3} mm^3 at 20x and 7.65 x 10^{-4} mm^3 for 40x on the light microscope and 1.04 x 10^{-3} mm^3 on the LSM at 25x). In addition, the pixel-to-micron ratio for each objective (1.6 at 20x, 3.2 at 40x, and 2.4 at 25x on the LSM) was standardized to a 1:1 ratio to control for the differences in pixel area for each study. A total of 2.95 x 10^5 varicosities/mm^3 was tabulated in a MC PVH region on the LSM, whereas at 20x a total of 1.34 x 10^5 varicosities/mm^3 was found for the equivalent field, a result 46% less than the LSM. At a magnification of 40x, 1.70 x 10^5 varicosities/mm^3 were counted, which was greater than the amount at 20x, but still 58% less than the LSM counts. Therefore, the LSM was determined to be more sensitive in identifying varicosities than the conventional light microscope for quantitative purposes.

DISCUSSION

Antibody specificity

The specificity of the antibody allowed for the discrimination of noradrenergic varicosities from dopaminergic varicosities, however, adrenergic varicosities could not be distinguished from noradrenergic varicosities, since DßH is also located in adrenergic-containing structures. Studies in rat demonstrated both neurochemically and morphologically that the dense noradrenergic innervation of the PVH contains a smaller subset of adrenergic terminals associated with it, mainly in the medial PC region of the PVH known to contain CRF-immunoreactive neurons, whereas MC regions have a sparse adrenergic innervation (Palkovits et al., '74; van der Gugten et

al., '76; Versteeg et al., '76; Swanson et al., '81). Additionally, adrenergic varicosities have been shown to synapse on CRF-immunoreactive perikarya (Liposits et al., '86a). In monkey, no studies have been conducted in the PVH to assess potential adrenergic innervation. Our present assumption is that the majority of DßH-immunoreactive varicosities quantified in this study are noradrenergic, however it is possible that some are adrenergic, especially within PC regions and may have contributed to the significant difference that was observed between MC and PC regions. Experiments using direct antibodies to haptenized norepinephrine or to PNMT (an essential enzyme for the synthesis of epinephrine) are necessary to completely characterize this innervation pattern in the primate, and would be of value to compare this distribution to that observed in the rat PVH.

Noradrenergic innervation of the hypothalamus

Previous descriptions of catecholamine innervation of primate hypothalamus have been performed using monoamine histofluorescent techniques, which do not discriminate between the specific catecholamine neurotransmitters (Hoffman et al., '76; Ishikawa and Tanaka, '77; Sladek and Zimmerman, '82; Felten and Sladek, '83). In this report, the distribution of noradrenergic-containing processes was identified in rhesus monkey hypothalamus with an antibody directed against human DßH. Qualitative observation yielded interregional differences in the DßH innervation of discrete diencephalic areas which are summarized in Table 3. Generally, the findings of this study are in agreement with the previous investigations in primate hypothalamus where the histofluorescent product was attributed to noradrenergic-containing structures as opposed to dopaminergic-containing structures. For example, Ishikawa and Tanaka ('77) suggested that a dense

plexus of histofluorescent fibers in the internal lamina, rather than the external lamina, of the median eminence were noradrenergic, which is consistent with the observations in this report. In terms of comparative neuroanatomy, the hypothalamic distribution of DßH-immunoreactive processes was similar to what has been described in rat, with a few exceptions, notably in the medial preoptic and suprachiasmatic regions. Swanson and Hartman ('75) reported that few DßH-immunoreactive profiles were present in either the MPA or suprachiasmatic area, whereas in the rhesus monkey, these regions are heavily innervated. This structural difference may have functional significance in regard to the complex regulation of the gonadotropin cascade and circadian rhythms which have been attributed to these respective regions within the hypothalamus. A phylogenetic change may have occurred in the noradrenergic input to the suprachiasmatic area, since both cat and rhesus monkey demonstrate this pattern of innervation that is not evident in the rat (Poitras and Parent, '75; Hoffman et al., '76). Another difference in the noradrenergic innervation between rat and rhesus monkey is in the ARC, where the density of fibers appears much greater in primate (Swanson and Hartman, '75; Hoffman et al., '76). This alteration may reflect an important regulatory role for norepinephrine in the control of primate adenohypophysial function, since the ARC contains a large population of neurons which project through the anterior pituitary via the portal capillary plexus of the median eminence (Weigand and Price, '80; Swanson and Sawchenko, '83).

In terms of a neurochemical marker, DßH immunohistochemistry in monkey has revealed a possible continuity of the ARC and DMH that has received little attention using cytoarchitectonic methods. Broadwell and

Bleier ('76) and Bleier ('84) have reported in mouse and rhesus monkey, respectively, on the similarity of cell types in the periventricular zone connecting the ARC and DMH. The overlapping noradrenergic innervation observed in this report may indicate a functional association of these two nuclei (Fig. 4). Tracing studies conducted in rat have demonstrated that cells in both the ARC and DMH project to the PVH, with NPY as a possible neurotransmitter candidate (Bai et al., '85; Ter Horst and Luiten, '87). Therefore, the DßH-immunoreactive pattern may in fact indicate some shared function of these two nuclei, possibly modulating an afferent input into the PVH.

A difference in the rostrocaudal distribution of DßH-immunoreactive fibers was observed, where the rostral two-thirds of the hypothalamus contained a much greater density of DßH immunoreactivity than the caudal one-third. In addition, a mediolateral gradient in the distribution of DßH-immunoreactive processes was also observed within the rhesus monkey hypothalamus, with medial structures tending to have a denser innervation than lateral structures. This pattern of DßH immunoreactivity may reflect the multiple noradrenergic fiber tracts innervating the monkey hypothalamus, with anteromedial regions receiving inputs from at least three different sources, including the dorsal, ventral, and periventricular noradrenergic bundles, which have been characterized in rhesus monkey by monoamine histofluorescence (Schofield and Everitt, '81; Tanaka et al., '82; Felten and Sladek, '83). Similar descriptions of intrahypothalamic DßH innervation patterns have not been characterized in rat *per se*, but Cunningham and Sawchenko ('88) have demonstrated that 3 different noradrenergic-containing cell groups in the caudal medulla (A1 and A2) and pons (locus coeruleus)

contribute to the innervation of the PVH and SON. Further retrograde tracing/DßH immunohistochemistry experiments need to be conducted in the primate to assess the origin of noradrenergic-containing fiber bundles, and whether they project and terminate selectively in a rostrocaudal and mediolateral orientation within the hypothalamus, thus contributing to the dense terminal field distribution observed within the rostral two-thirds of the hypothalamus, ranging from the medial preoptic area to the arcuate-dorsomedial continuum.

Within the midline thalamus, medially-located nuclei also appeared to have a greater noradrenergic innervation than more laterally-located structures. For example, the paraventricular nucleus of the thalamus, rhomboid nucleus, and magnocellular subfascicular nucleus all contained dense DßH-immunoreactive fibers with associated terminal fields whereas the more laterally oriented intralaminar and medial thalamic nuclei were fairly devoid of DßH innervation. The functional relevance of this innervation pattern is difficult to assess at the present time, since the functions of these midline thalamic nuclei have not been well characterized, especially in the primate. Within the subthalamic area, only the zona incerta contained an appreciable amount of DßH innervation in the form of thin, nonvaricose fibers of passage which have been observed in the rat to course to hypothalamic, basal forebrain, and thalamic regions (Swanson and Hartman, '75).

Quantitative assessment of DßH-immunoreactive varicosities in the PVH

In the light of morphologic and physiologic data suggesting that norepinephrine plays a major role in the regulation of the HPA axis, DßH-immunoreactive innervation of rhesus monkey PVH was examined.

Qualitative assessment indicated that noradrenergic varicosities act as a neurochemical marker clearly delimiting the monkey PVH from the surrounding anterior hypothalamic area. Quantitative analysis of DßH-immunoreactive varicosities throughout the rostrocaudal extent of the PVH suggested that a denser noradrenergic input exists in PC regions relative to MC regions. Since in rat PVH there are more PC neurons than MC neurons (Kiss et al., '83, '91; Swanson and Sawchenko, '83), the results of this study may indicate that PC neurons receive a greater DßH-immunoreactive input because there are more per unit volume than MC neurons. Also, by virtue of their smaller size, this increase in density may reflect a tighter cell packing phenomena in PC regions of the PVH. Another possibility is that a single PC neuron receives more DßH-immunoreactive varicosities than a single MC neuron. Furthermore, in rat, noradrenergic-containing neurons in both the A2 and locus coeruleus have been demonstrated to project to primarily PC regions of the PVH, whereas the MC regions are preferentially innervated by A1 afferents (Cunningham and Sawchenko, '88). These differential projections may also effect the overall density of innervation. It is possible that the convergence of noradrenergic inputs on PC neurons is one of the determining factors in terms of the total number of varicosities present.

Methodological considerations

The methodology and instrumentation employed in this study allowed for high resolution analysis of DßH-immunoreactive varicosities in the PVH. Each immunolabeled varicosity presumably contains at least one release site that is likely to be in the form of a functional synapse, although this assumption has not been verified through serial electron microscope sections in primate PVH. In ultrastructural studies of other noradrenergic and

serotoninergic projections, varicosity counts have been determined to be an accurate quantitative indicator of the innervation density of an afferent input (Papadopoulos et al., "87, '89; de Lima et al., '88, '89). While these data demonstrate the overall density of noradrenergic innervation of the PVH, the postsynaptic target(s) of these varicosities could not be assessed. Our assumption is that the vast majority of these varicosities are contacting MC and PC neurons which possess alpha-1 and/or beta-adrenoceptors (Leibowitz et al., '82), but cannot exclude interactions with glia and blood vessels. For example, *in vitro* experiments have demonstrated the presence of both alpha-1 and beta- adrenoceptors on cultured astroglial cells derived from rat cortex (Lerea and McCarthy, '89; Salm and McCarthy, '89). In addition, Swanson et al. ('77) have shown that monoaminergic-containing varicosities innervate blood vessels in rat PVH. Further experiments with a double label immunohistochemical procedure are being conducted to assess the number of DßH-immunoreactive varicosities in apposition to chemically-specified postsynaptic cells, such as vasopressin-immunoreactive MC neurons and CRF-immunoreactive PC neurons, which will restrict the varicosity quantification to these discrete neuronal populations (Ginsberg et al., '93d). In addition, LSM quantification of specific afferent inputs in apposition to target neurons will yield a varicosity-to-neuron ratio which will, in turn, be compared to the present data on overall density of innervation, thereby allowing for a determination of relative innervation density to neurotransmitter-identified neuronal populations within the PVH.

Generally, immunofluorescence is employed in conjunction with LSM analysis because a high intensity signal is desired (Mossberg et al., '90). Disadvantages with fluorescence on the LSM include autofluorescence and

fading of the fluorophore as the laser scans the tissue section. This study employed nickel-cobalt-intensified DAB as a chromogen to visualize the antigen/antibody complex. The DAB precipitate was permanent, displayed a high signal-to-noise ratio, and was not degraded by the laser beam (Deitch et al., '90b), making this procedure conducive to quantitative analysis. Because of the size of the varicosities and diminished reflectance of the DAB precipitate compared to fluorescent labels, a nonconfocal setting was selected to quantify each optical section. Therefore, the resolution in the z-axis plane was approximately 2.5 - 3.0 μm, as opposed to a z-axis resolution of approximately 0.5 μm in the confocal mode with the same objective (Inoué, '90). In a preliminary analysis, no apparent differences were observed between the density of varicosity counts quantified nonconfocally and confocally. Nonconfocal imaging allowed for increased contrast of immunolabeled profiles due to the high intensity and specific wavelength frequencies (a combination of 488 nm and 514 nm) of the laser. The nonconfocal optical sections were extremely crisp, and varicosities which were in focus could be readily and reproducibly discriminated from background. Additionally, optical sections in the nonconfocal mode contained several previously counted varicosities and intervaricose segments brought into the next focal plane, which aided in the localization of new varicosities, as well as allowing the investigator to maintain a tight criteria for quantification (Fig. 7).

Neurobiologists have used LSM systems to generate three-dimensional reconstructions of neuronal profiles and processes (Wallén et al., '88; Deitch et al., '90a). The results of this report along with a study by Mossberg et al. ('90) also give evidence for a new application of the LSM in

neurobiology for the quantification of neurotransmitter-specified terminal fields. Nuclear masses, such as the PVH, as well as laminated structures such as the cerebral cortex can be analyzed in this manner (Morrison et al., '90). Varicosity quantification is a particularly useful application of the LSM, given the notorious difficulty of accurately counting dense terminal fields with a conventional light microscope. Previous quantitative assessment of neurotransmitter-identified varicosity density has been performed using electron microscopy (Papadopoulos et al., '87, '89; de Lima et al., '88, '89). The present technique will be able to augment these analyses by assessing larger volumes of tissue (prepared for light microscopy examination) that would be cumbersome to evaluate by electron microscopy. Similarly, the accurate localization of varicosities through the z-axis plane of a tissue section by LSM analysis has the advantage over conventional light microscopy where the two point resolution is not as high with the same objective and the z-axis plane cannot be precisely monitored to yield reproducible varicosity counts. Thus this LSM method allows for a practical interface between conventional light and electron microscopy that gives a quantitative measurement of innervation density through varicosity counts. Combined with methods which assess receptor distribution and neurotransmitter turnover, changes in varicosity density may be used to evaluate a number of disease-related parameters, effectively becoming a quantitative indicator of potential neuropathologic change(s) associated with a disease state. This procedure will also be useful for the generation of precise data regarding developmental changes in afferent innervation density within specified brain regions.

ACKNOWLEDGMENTS

The authors thank Dr. G.W. Kraemer and Dr. W.T. McKinney for providing the animals used in the study. We also thank Dr. D.T. O'Connor for donating the antiserum, Dr. S.L. Foote and Dr. P. Pasik for helpful discussions, Dr. G.W. Huntley and Dr. J.C. Vickers for critically reviewing the manuscript, and R. Woolley for photographic assistance. This research was supported in part by a pilot research grant from the John D. and Catherine T. MacArthur Foundation Mental Health Research Network I, the Brookdale Foundation, and NIH grant MH45212.

Table 1. Reliability of varicosity counts in different *z*-axis intervals[1]

Magnocellular region Animal	2 μm	3 μm	5 μm	10 μm
W9	275	266	195	93
W7	524	512	463	365
W6	222	232	172	135
Parvicellular region				
W5	577	589	458	367
W6	441	422	351	224
W8	211	197	166	110

[1]Dopamine-ß-hydroxylase-immunoreactive varicosity counts from selected LSM fields at different z intervals is shown. The same field in each animal was counted at the 4 different z-axis step intervals. Note that the counts are similar from the analyses done at 2 μm and 3 μm intervals, whereas the counts drop off precipitously at analyses done with 5 μm and 10 μm steps. Therefore, a 3 μm interval was chosen for the quantitative analyses.

Table 2. Reliability of varicosity field counts through the rostrocaudal extent of MC regions in the PVH of one animal[1]

level	field 1	field 2	% variability
rostral	768	772	0.52
mid	643	663	3.1
mid	610	585	4.3
caudal	998	973	2.6

[1]Dopamine-ß-hydroxylase-immunoreactive varicosities from the same field (volume = 1.04×10^{-3} mm^3) were counted twice on 4 hypothalamic tissue sections through the rostrocaudal extent of the PVH of one animal to assess the reliability of quantified profiles. The mean variability between fields was 2.6% ± 0.8 (SEM), indicating that varicosity counts were highly reproducible.

Table 3. Distribution of DßH-immunoreactive processes in discrete hypothalamic, subthalamic, and midline thalamic regions[1]

DßH innervation	*hypothalamus*
extremely dense	PVHmc, PVHpc, SON
dense	ARC, DMH, MPA, PFA, SCA, SONr,t
moderate	LHA, MEi, SOC
low	AHA, LPA, MB, MEe, PHA, VMH
DßH innervation	*subthalamus/midline thalamus*
dense	PVT, SFNm
moderate	RH, ZI
low	FF, IL, RE, STN

[1]Qualitative description of dopamine-beta-hydroxylase-immunoreactive processes within circumscribed regions of the rhesus monkey diencephalon. Abbreviations: AHA = anterior hypothalamic area; ARC = arcuate nucleus; DMH = dorsomedial nucleus; FF = fields of Forel; IL = intralaminar nuclei; LHA = lateral hypothalamic area; LPA = lateral preoptic area; MB = mammillary bodies; MEe = external lamina of the median eminence; MEi = internal lamina of the median eminence; MPA = medial preoptic area; PFA = perifornical area; PHA = posterior hypothalamic area; PVHmc = paraventricular nucleus of the hypothalamus, magnocellular region; PVHpc = paraventricular nucleus of the hypothalamus, parvicellular region; PVT = paraventricular nucleus of the thalamus; RE = nucleus reuniens; RH = rhomboid nucleus; SCA = suprachiasmatic area; SFNm = magnocellular subfascicular nucleus; SOC = supraoptic commissure; SON = supraoptic nucleus; SONr,t = supraoptic nucleus, retrochiasmatic and tuberal regions; STN = subthalamic nucleus; VMH = ventromedial nucleus; ZI = zona incerta

FIGURE LEGEND

Fig. 1. Differential interference contrast photomicrographs of DßH-immunoreactive fibers in the LHA illustrating the differences observed in fiber caliber and varicosity density. Note the pericellular basket-like arrangement of the thick varicose fiber (curved arrow) on an unlabeled perikarya (asterisk). The arrowheads point to a thin, nonvaricose fiber that can be seen more clearly at higher magnification in B. The boxed area in **A** corresponds to the area shown at higher magnification in **B**. Abbreviation: LHA = lateral hypothalamic area. Scale bar in B = 100 μm.

Fig. 2. Darkfield photomontage of the PVH through rostral (**A**), mid (**B**), and caudal (C) levels demonstrating the dense DßH-immunoreactive input into the nucleus relative to the surrounding AHA. The third ventricle is to the right. Abbreviations: AHA = anterior hypothalamic area; PVH = paraventricular nucleus of the hypothalamus; f = fornix. Scale bar in C = 100 μm and applies to A and B as well.

Fig. 3. Darkfield photomicrographs demonstrating the distribution of DßH-immunoreactive processes in discrete hypothalamic regions. **A:** Medial preoptic area. The fiber density is greatest in periventricular regions. The third ventricle is to the right. **B:** Suprachiasmatic area. Both the SCN and subventricular nucleus are heavily innervated by DßH-immunoreactive fibers. **C:** Supraoptic nucleus. The nucleus is outlined by the DßH-immunoreactive input. Note the fibers exiting the nucleus into the anterior hypothalamic area. The optic chiasm is to the right. **D:** Perifornical area. The density of DßH-immunoreactive processes is greater medial to the fornix.

Abbreviations: AHA = anterior hypothalamic area; MPA = medial preoptic area; PFAl = perifornical area, lateral region; PFAm = perifornical area, medial region; SCN = suprachiasmatic nucleus; SON = supraoptic nucleus; SVN = subventricular nucleus; III = third ventricle; f = fornix; och = optic chiasm. Scale bar in D = 100 μm and applies to A - C as well.

Fig. 4. Darkfield photomontage illustrating the DβH-immunoreactive innervation of the ARC, DMH, and VMH. Note that the DβH innervation density in the ARC and DMH is continuous in the periventricular zone. The VMH is demarcated from the rest of the mediobasal hypothalamus by its relative lack of DβH immunoreactivity. Abbreviations: ARC = arcuate nucleus; DMH = dorsomedial nucleus; LHA = lateral hypothalamic area; PVZ = periventricular zone; SONr = supraoptic nucleus, retrochiasmatic region; VMH = ventromedial nucleus; III = third ventricle; f = fornix; ot = optic tract. Scale bar = 100 μm.

Fig. 5. Darkfield photomicrographs demonstrating the DβH-immunoreactive innervation pattern in the midline thalamic region. **A:** Paraventricular nucleus of the thalamus. The innervation density is greatest at the midline. **B:** Magnocellular subfascicular nucleus. This nucleus is demarcated from the surrounding nucleus reuniens by a dense plexus of DβH-immunoreactive fibers. Abbreviations: PVT = paraventricular nucleus of the thalamus; RE = nucleus reuniens; SFN = magnocellular subfascicular nucleus; III = third ventricle. Scale bar in B = 100 μm and applies to A as well.

Fig. 6. Total DßH-immunoreactive varicosity counts in the collapsed sampling area in MC and PC regions of 5 rhesus monkeys. Varicosities were counted through successive z-axis optical sections on the LSM for each of the nine PVH samples per animal for a final volume of 9.27×10^{-3} mm^3. Quantitative analysis yielded values of 7865.0 ± 1188.5 (SEM) DßH-immunoreactive varicosities in the MC regions and 10291.4 ± 1461.1 DßH-immunoreactive varicosities in the PC regions. This difference was significant * = ($p < 0.003$), indicating that PC regions have a greater DßH-immunoreactive innervation density.

Fig. 7. Digitized LSM microscope image with overlaid computer graphics of one MC field illustrating the technique for quantifying varicosities through multiple z-axis optical sections. Scale = 50 µm. **A:** Two-dimensional map depicting the computer generated maps of eight collapsed z-axis optical sections quantified for DßH-immunoreactive varicosities. Each colored symbol represented a single profile counted in one of eight successive optical sections, as the immunoreactive structure came clearly into focus. The symbol demarcating previously counted profiles was overlaid on top of each successive optical section image, in order to avoid double counting of immunoreactive structures which appeared in focus on one or more z-axis planes. **B:** Digitized LSM microscope image with overlaid computer graphics of three successive z-axis optical sections (levels 4, 5, and 6) illustrating the DßH-immunoreactive varicosities that were quantified in the three successive planes. Note that varicosities are counted in the first plane in which they come into clear focus. Some varicosities (arrow) were not marked with a

symbol in any of these three z-axis optical sections because they were designated in a previous z-axis optical section.

Fig. 8. Histogram illustrating the DßH-immunoreactive varicosities quantified for each of the 8 optical sections seen graphically in Figure 7. A total of 744 varicosities was tabulated for this MC field (see details in text).

Fig. 9. A representative computer generated map of the anterior hypothalamus designating the MC (**a**) and PC (**b**) regions quantified for DßH-immunoreactive varicosity density. Note that the MC region is dorsal and lateral to the PC region. Abbreviations: PVH = paraventricular nucleus of the hypothalamus; SON = supraoptic nucleus; III = third ventricle; f = fornix; och = optic chiasm. Scale = 1 mm.

Figure 1

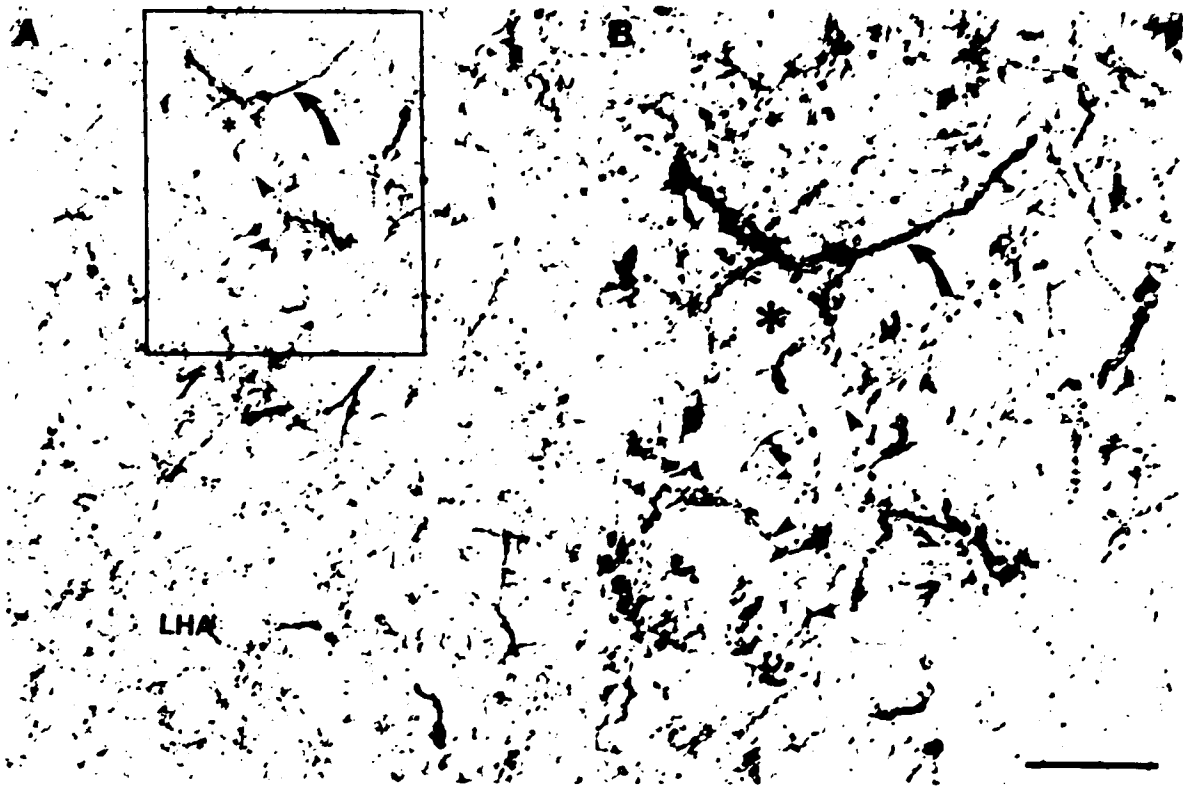

Figure 2

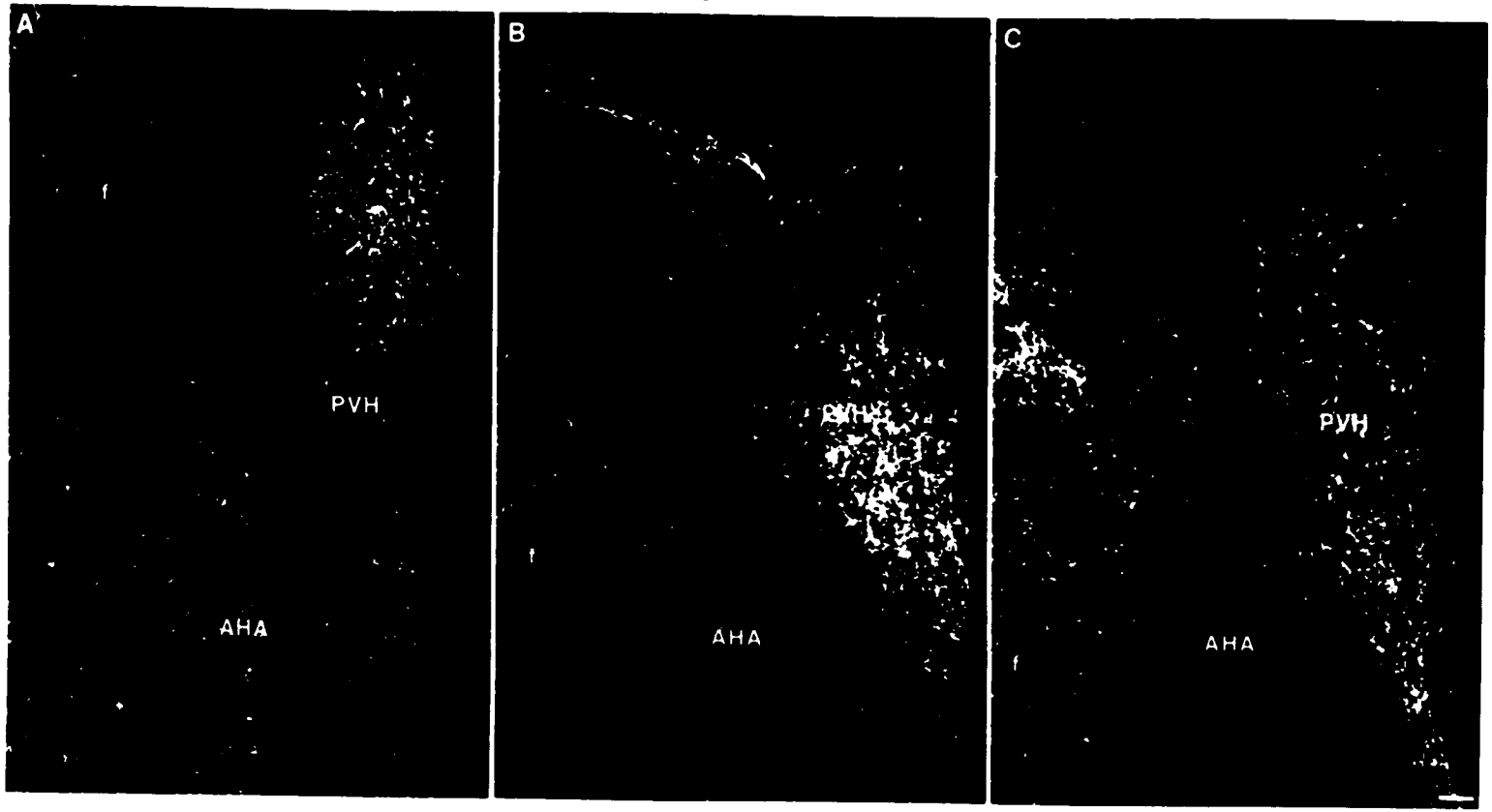

Figure 3

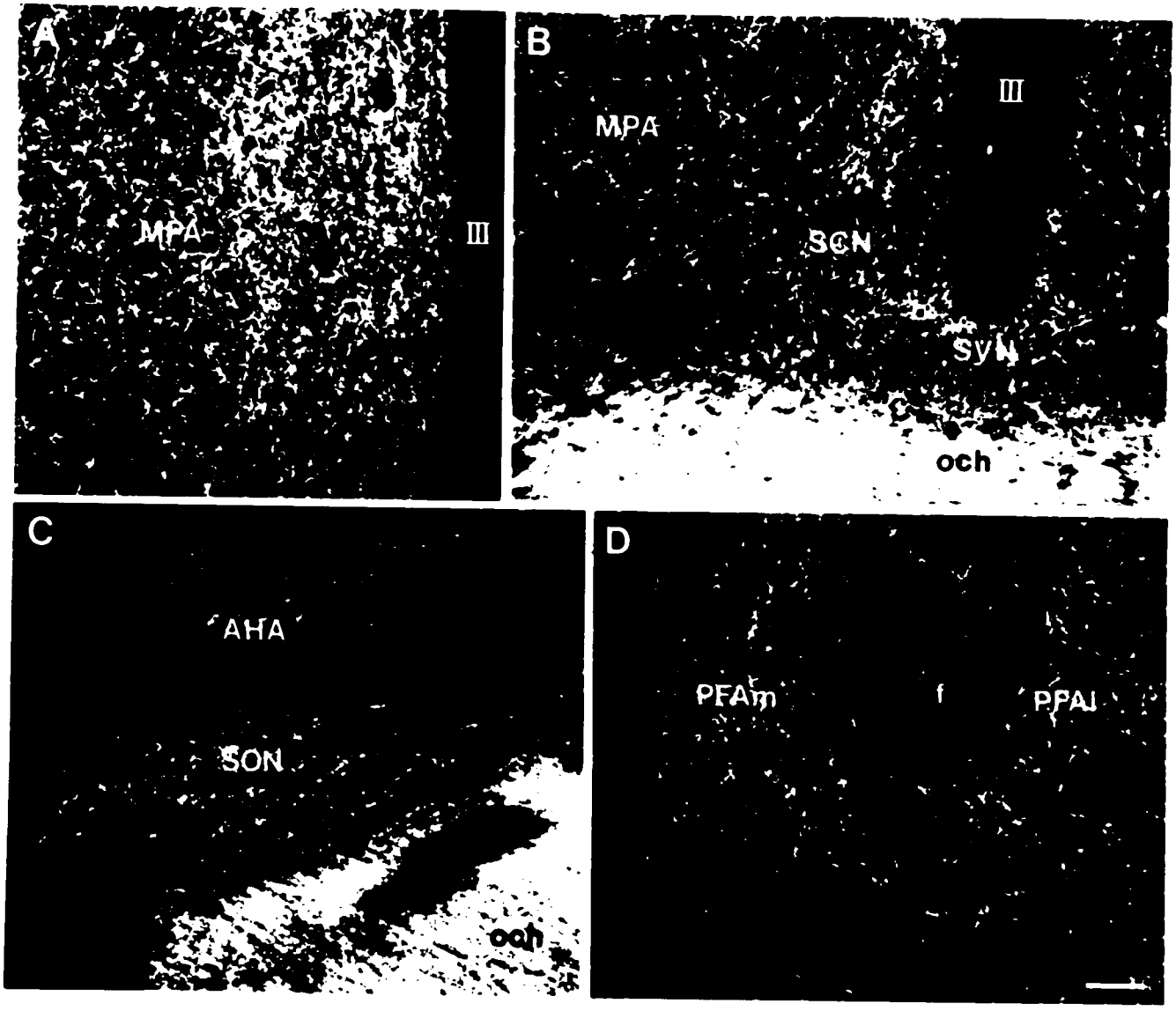

Figure 4

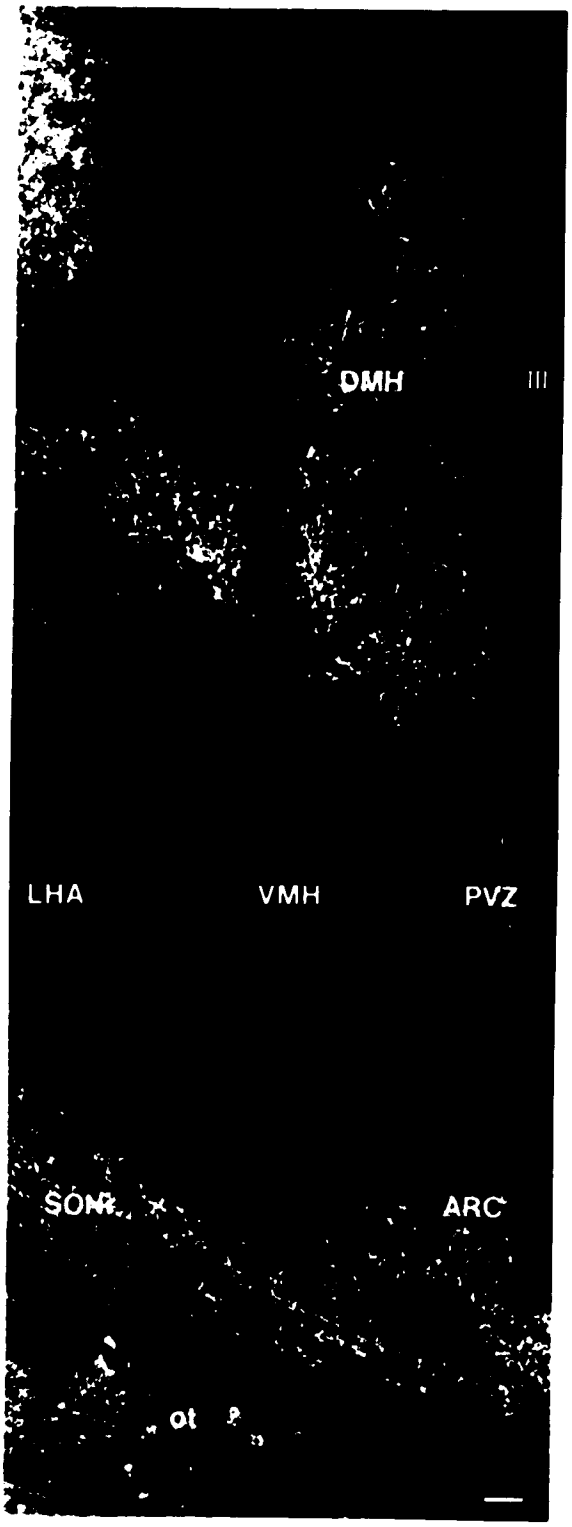

Figure 5

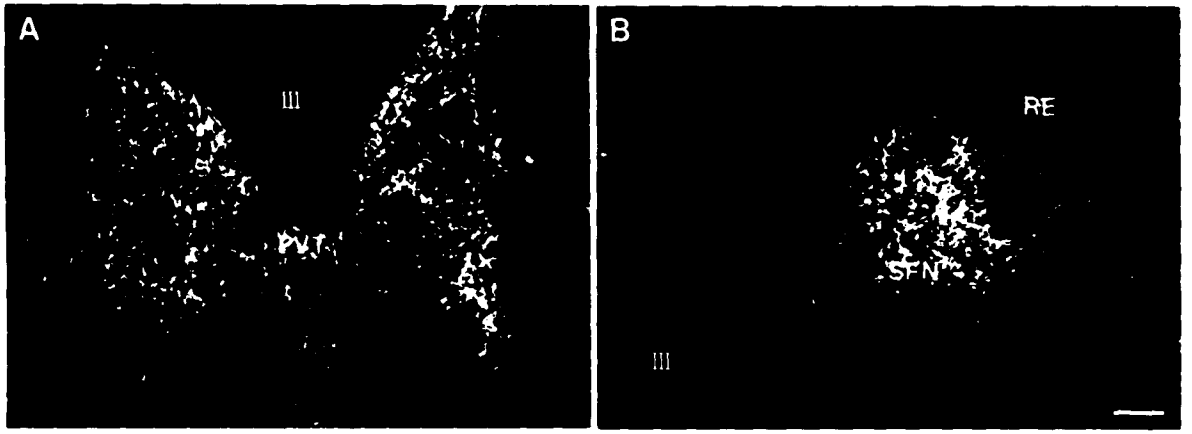

Figure 6

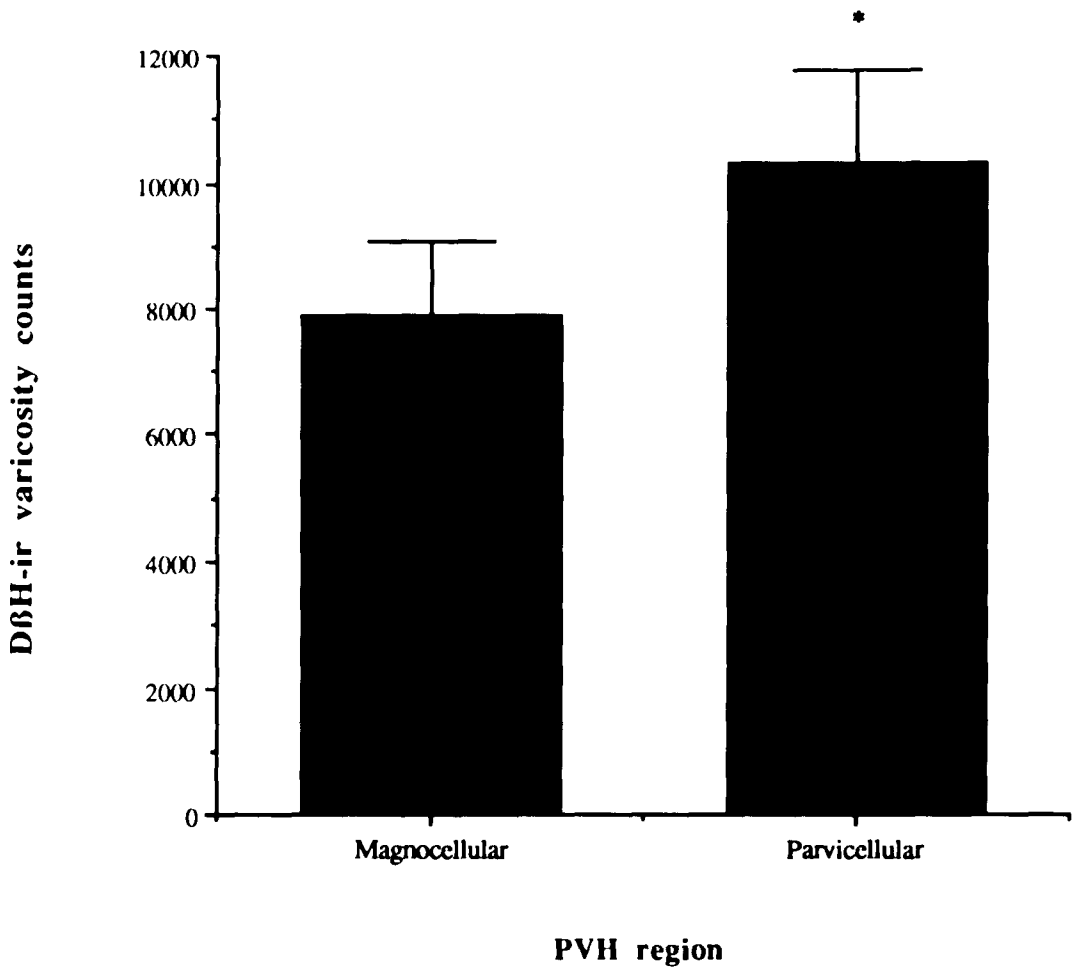
*
12000
10000
8000
6000
4000
2000
0
DßH-ir varicosity counts
Magnocellular
Parvicellular
PVH region

Figure 7

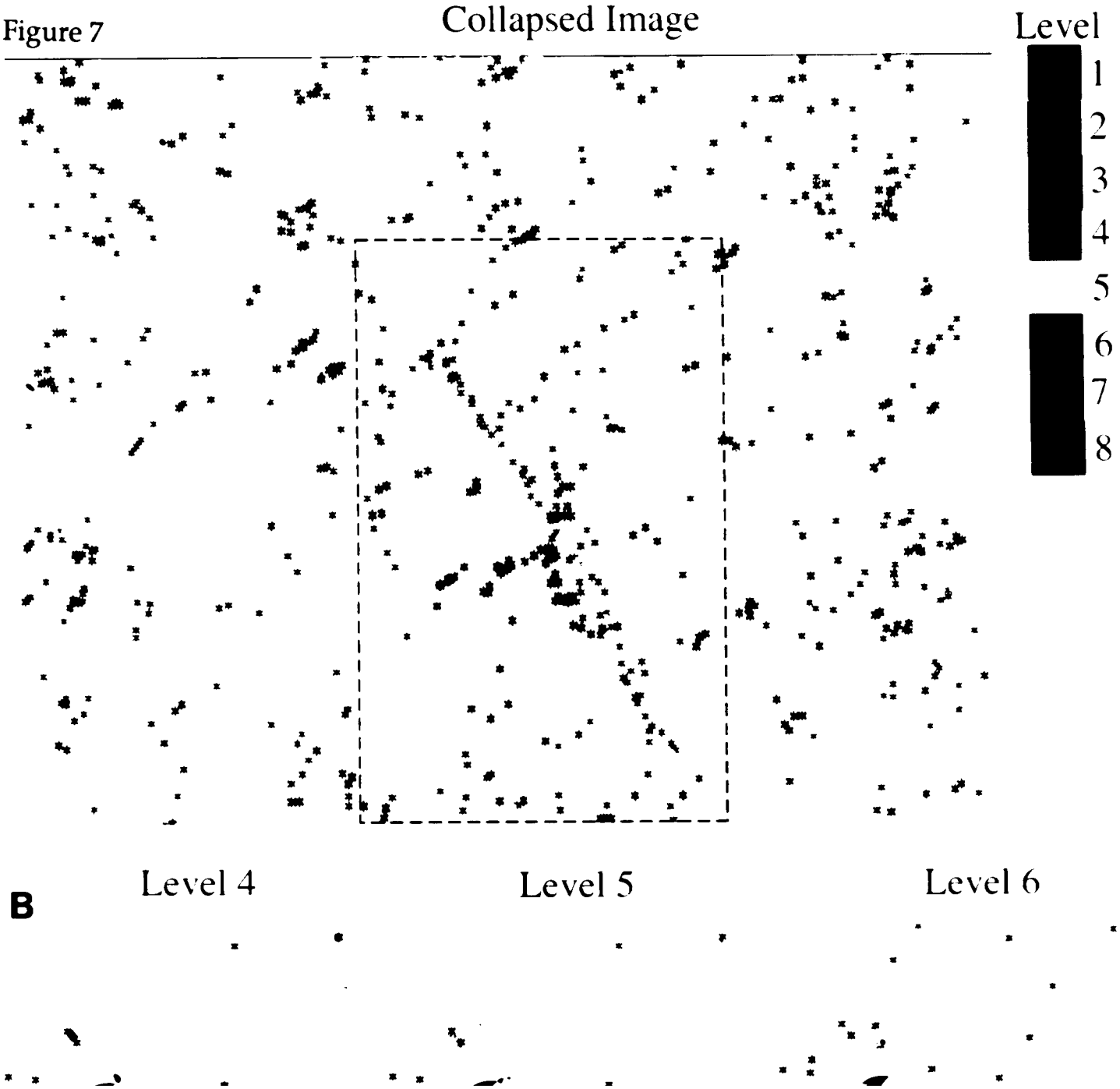

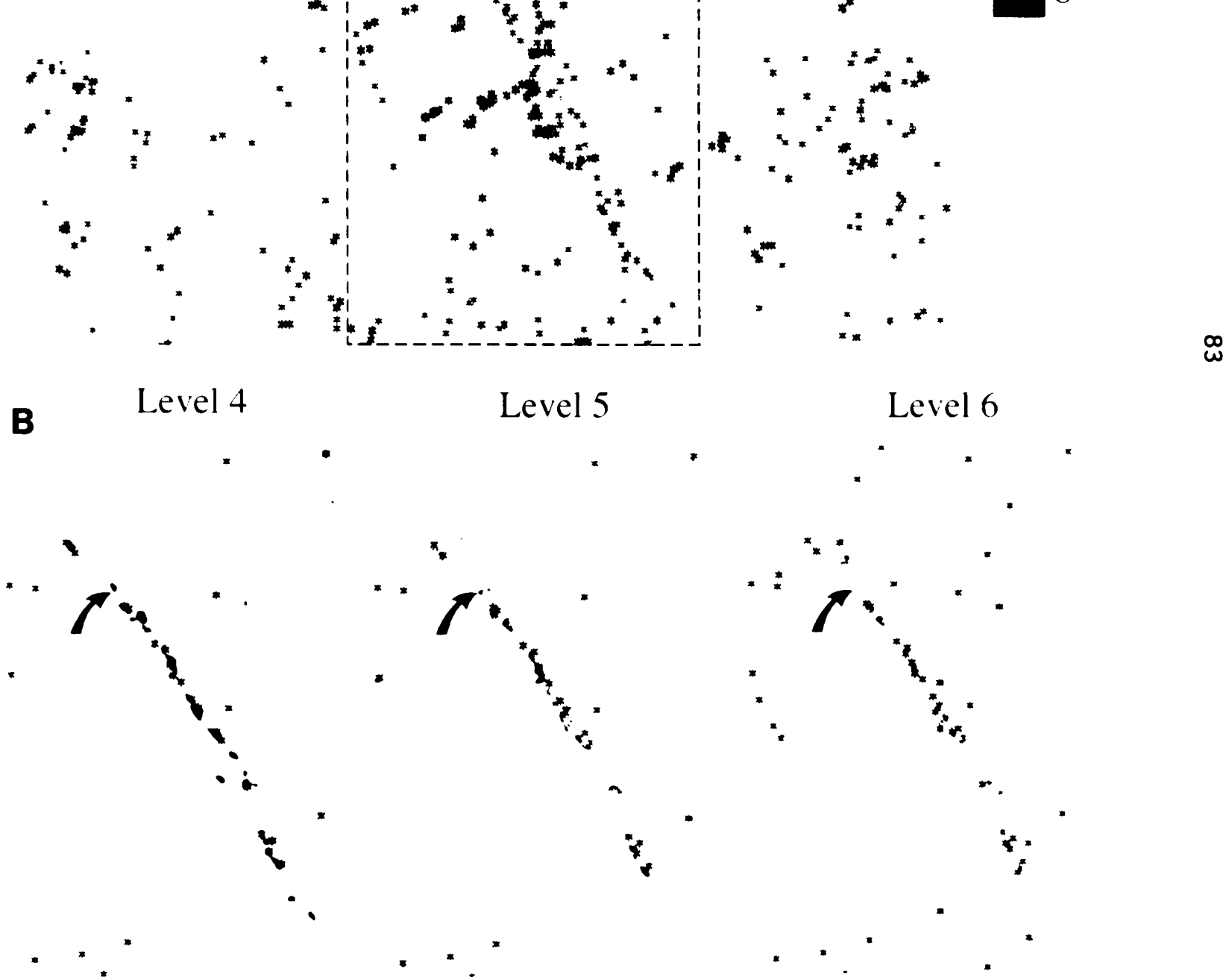
B
Level 4
Level 5
Level 6

Figure 8

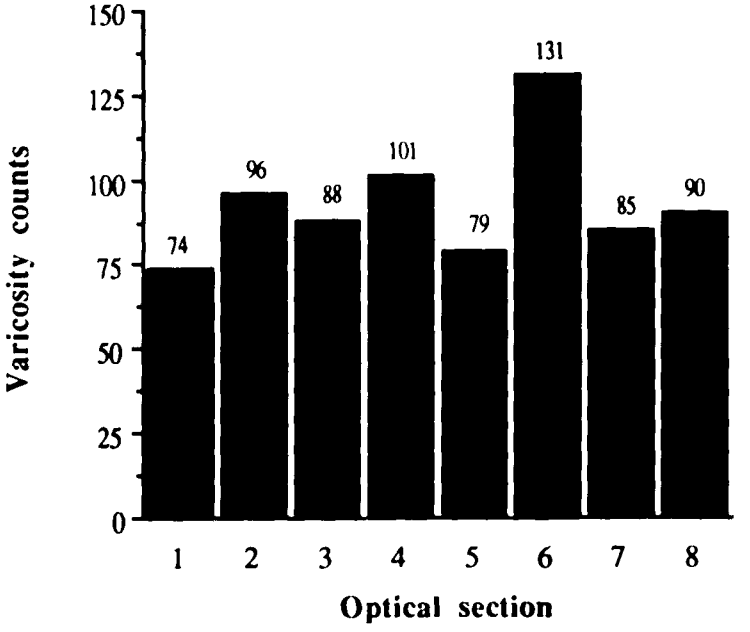
Varicosity counts
150
125
100
75
50
25
0
74
96
88
101
79
131
85
90
1
2
3
4
5
6
7
8
Optical section

Figure 9

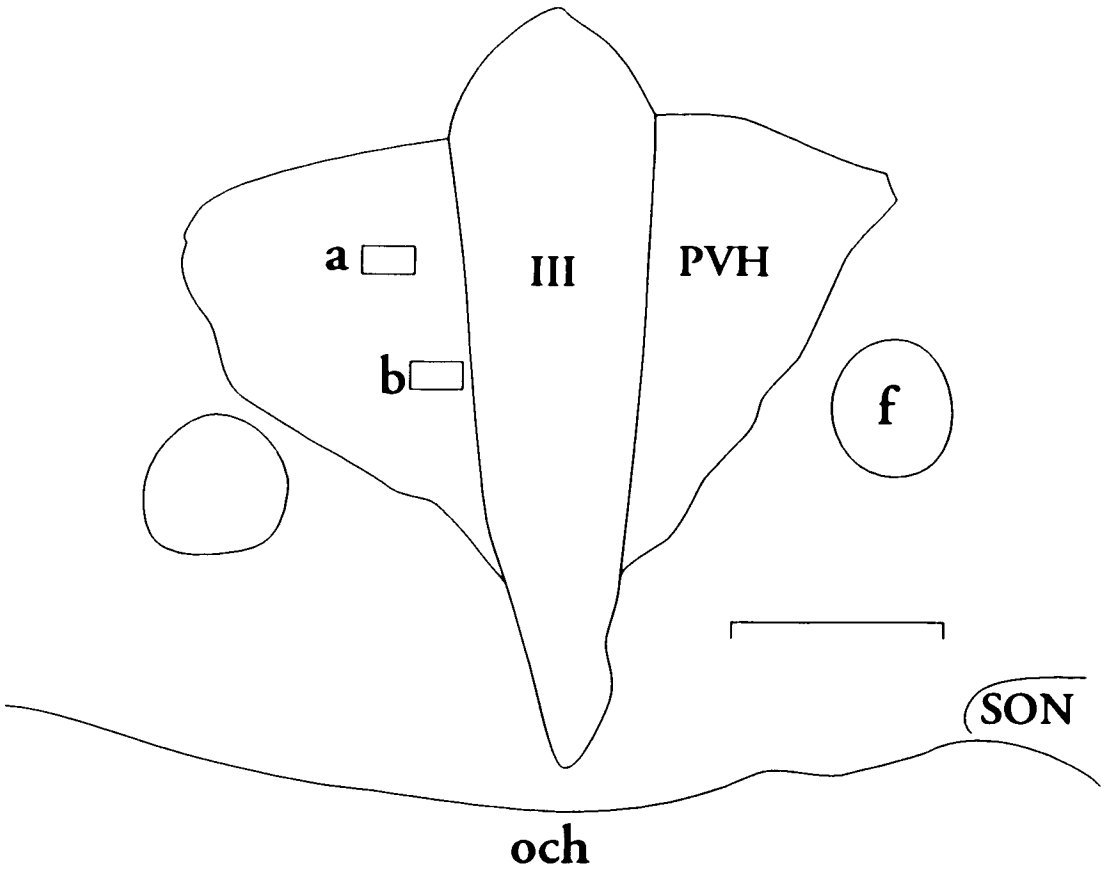

Chapter Four

SUMMARY

Previous reports in rat and monkey hypothalamus have revealed a dense noradrenergic innervation within the PVH as assessed by DßH immunohistochemistry. These single label analyses were unable to delineate the cellular structures which receive this noradrenergic innervation. Double label preparations in rat and monkey have demonstrated that a population of noradrenergic varicosities contact MC neurons within the PVH. However, the density and distribution of noradrenergic varicosities contacting chemically-identified MC neurons has not been assessed. In this report, double label immunohistochemistry was combined with confocal laser scanning microscopy to quantify the number of DßH-immunoreactive varicosities in apposition to MC vasopressin- and oxytocin-immunoreactive neurons in the macaque PVH. In addition, the morphology of chemically-identified neurons was compared to MC neurons in the monkey PVH that were filled with LY in order to assess the somatodendritic labeling of the immunofluorescent preparations. A series of confocal optical sections were assessed through the total somal volume of vasopressin- and oxytocin-immunoreactive neurons along with the corresponding DßH-immunoreactive varicosities in the same volume of tissue, generating a varicosity-to-neuron ratio which was further characterized morphologically to assess noradrenergic input to the soma and proximal dendrites. Quantitative analysis revealed that vasopressin-immunoreactive neurons received approximately two-thirds of their DßH-immunoreactive varicosities in apposition to the proximal dendrites and one-

third in apposition to the somata. Furthermore, vasopressin-immunoreactive neurons received a greater innervation density than oxytocin-immunoreactive neurons, which did not have a differential distribution of varicosities on the proximal dendrites versus the somata. This differential distribution of noradrenergic afferents on MC neurons in the PVH may reflect a physiologic role of this circuit in terms of preferential release of vasopressin from MC neurons upon noradrenergic stimulation.

INTRODUCTION

Early studies of the rat central nervous system using monoamine fluorescence histochemistry revealed a dense catecholaminergic input to the hypothalamus, notably within the PVH and SON (Carlsson et al., '62; Fuxe, '65; Björklund et al., '73). A similar density of catecholaminergic innervation was observed in the monkey hypothalamus (Hoffman et al., '76; Ishikawa and Tanaka, '77; Felten and Sladek, '83). The development of antibodies directed against DßH, the enzyme which converts dopamine into norepinephrine, allowed for the neurochemical and morphologic characterization of the noradrenergic (and adrenergic- see Discussion) innervation within the rat hypothalamus (Palkovits et al., '74; Swanson and Hartman, '75). Previous investigation of the DßH-immunoreactive input to the monkey hypothalamus has revealed a differential distribution of noradrenergic processes, with the PVH receiving a particularly dense innervation. Additionally, quantitative analysis of the monkey PVH revealed an extremely high density of noradrenergic varicosities distributed throughout the rostrocaudal extent of the PVH in both MC and PC divisions (Ginsberg et al., '93c). This single label

immunohistochemical method allowed for the quantification of DßH-immunoreactive varicosities within circumscribed regions of the PVH, but did not delineate the cellular structures receiving this noradrenergic innervation. Potential targets include the MC neurons of the PVH which synthesize the nonapeptides vasopressin and oxytocin. Furthermore, it has been reported in the rat PVH that regions containing vasopressin-immunoreactive neurons receive a denser noradrenergic innervation than regions containing oxytocin-immunoreactive neurons (Sawchenko and Swanson, '81a; Swanson et al., '81). Double label experiments at the light microscopic level in rat and monkey PVH have demonstrated monoamine histofluorescent varicosities in apposition to neurophysin-immunoreactive perikarya (McNeill and Sladek, '80; Sladek and Zimmerman, '82). Dopamine-ß-hydroxylase-immunoreactive varicosities have also been demonstrated to contact vasopressin-immunoreactive neurons in the rat PVH (Hornby and Piekut, '87). Ultrastructural studies in rat PVH and SON using autoradiography after topical application of tritiated norepinephrine combined with immunoelectron microscopy have demonstrated synaptic contacts between noradrenergic varicosities and vasopressinergic perikarya (Silverman et al., '83, '85; Nakada and Nakai, '85; Nakai et al., '86). Double label immunoelectron microscopy experiments in rat have also demonstrated noradrenergic synapses on neurophysin- and vasopressin-immunoreactive neurons (Ochiai et al., '88; Ochiai and Nakai, '90; Shioda and Nakai, '92). In addition in the rat PVH, Cummings and Seybold ('88) have localized alpha-1 and alpha-2 adrenergic receptors to regions containing neurophysin-immunoreactive perikarya using a combined receptor autoradiography and immunohistochemical technique. Preliminary data in rat and monkey have

also detected the presence of subtype-specific adrenergic receptor immunoreactivity in several hypothalamic nuclei, including the PVH (Go et al., '92). Functionally, *in vivo* and *in vitro* electrophysiologic and neuropharmacologic experiments have demonstrated that norepinephrine facilitates the release of several neuropeptides, including vasopressin, and to a lesser extent oxytocin, from MC neurons, and CRF from PC neurons (Day et al., '84; Day and Renaud, '84; Randle et al., '86b; Plotsky, '87; Saphier, '89).

To date, catecholamine-neuropeptide interactions have been described qualitatively in light microscopic examinations and synapses have been verified at the ultrastructural level, however, no quantitative assessment of the number of varicosities per chemically-identified cell or their precise somatodendritic distribution has been undertaken. Such quantitative data are particularly crucial in regard to the evaluation of the overall cytoarchitecture and function of the PVH, notably the relation of potential postsynaptic structures such as neurons, glia, and blood vessels to a neurochemically- and physiologically-defined afferent input.

In this report, a technique using double label immunofluorescence combined with confocal laser scanning microscopy was employed to assess the noradrenergic input to MC vasopressin- and oxytocin-immunoreactive neurons within the macaque hypothalamus. This experimental paradigm allowed for the quantification of DßH-immunoreactive varicosities per vasopressin- or oxytocin-immunoreactive neuron, as well as revealing the noradrenergic input to this subpopulation of neurons relative to the non-identified components of the PVH. The combination of double label immunohistochemistry with confocal microscopy is a method that several investigators have employed to localize immunohistochemically-identified

structures in relation to each other per unit volume of tissue, including varicosities in apposition to perikarya (Mossberg et al., '90; Mossberg and Ericsson, '90; Mason et al., '92). The morphology of the vasopressin- and oxytocin-immunoreactive neurons was also compared to MC neurons in the monkey PVH filled with the intracellular dye LY, to determine whether the immunofluorescent preparation sufficiently labeled dendritic processes within the confines of a tissue section. Some of these data have been reported in abstract form (Ginsberg et al., '92a).

MATERIALS AND METHODS

Immunohistochemical Procedure

These experiments were conducted within NIH guidelines for animal research and were approved by the IACUC board of the Mount Sinai Medical Center. Five cynomolgus monkeys (*Macaca fascicularis*) and two rhesus monkeys (*Macaca mulatta*) were used in this study. All monkeys were sacrificed by transcardiac perfusion. They were sedated with ketamine hydrochloride (25 mg/kg i.m.) and anesthetized with sodium pentobarbital (30 mg/kg i.p.), intubated with an endotracheal tube and ventilated. The chest cavity was exposed and the descending aorta was clamped. To increase vasodilation, 1.5 ml of 1% aqueous sodium nitrite was injected into the left ventricle prior to transcardial perfusion. Ice-cold 1% paraformaldehyde in PBS (0.12 M, pH 7.4) was delivered via a perfusion pump (275 - 325 ml/min) to flush the vascular system for 45 - 60 seconds followed by ice-cold 4% paraformaldehyde in PBS delivered at the same flow rate for an additional 8 - 9 minutes. Brains were removed and blocks containing the entire rostrocaudal

extent of the hypothalamus were prepared in the coronal plane, postfixed in 4% paraformaldehyde for 6 hours, and cryoprotected in a series of 12%, 16%, and 18% sucrose solutions in PBS.

Hypothalamic blocks were removed from 18% sucrose and frozen in dry ice prior to cryostat sectioning. A 1 in 13 series of 30 μm thick sections through the extent of the hypothalamus were used for the immunohistochemical analyses. One series was processed for double label immunohistochemistry using a polyclonal rabbit antiserum directed against human DβH at a working dilution of 1:2,000 and a mouse monoclonal antibody directed against synthetic vasopressin at a working dilution of 1:100. An adjacent series was also prepared for double label immunohistochemistry using the polyclonal anti-DβH and a monoclonal mouse antibody directed against synthetic oxytocin at a working dilution of 1:100. The DβH antibody has been fully characterized and shown to crossreact with monkey DβH (O'Connor et al., '79; Frigon et al., '81; Morrison et al., '82; Ginsberg et al., '93c). Both the vasopressin and oxytocin antibodies have been fully characterized using radioimmunoassay, immunoabsorption, and immunohistochemical techniques (Hou-Yu et al., '82, '86). The vasopressin antibody does not crossreact with oxytocin or vasotocin, and vice versa. No cross reactivity was observed between the DβH/vasopressin or DβH/oxytocin antibodies. Another series was stained with thionin to assign cytoarchitectonic criteria for the delineation of nuclear boundaries in conjunction with Bleier's ('84) atlas of the rhesus monkey hypothalamus.

Tissue sections were incubated overnight in a PBS solution containing both primary antisera (anti-DβH/anti-vasopressin or anti-DβH/anti-oxytocin), 0.3% Triton X-100, and 0.5 mg/ml bovine serum albumin at 4°C.

Since the primary antibodies were raised in different species, the secondary antibody preparations were processed simultaneously (all at a working dilution of 1:200), followed by a tertiary step (also at a 1:200 dilution) for the anti-DßH label. The vasopressin and oxytocin antibodies were visualized with horse anti-mouse IgG conjugated to fluorescein isothiocyanate (Vector Laboratories, Burlingame, CA) and the DßH antibody was visualized with a biotinylated goat anti-rabbit IgG (Vector Laboratories) reagent in the same PBS solution for 2 hours, followed by avidin conjugated to Texas Red (Vector Laboratories) in PBS for two hours. Tissue sections were mounted onto chrome-alum coated slides and coverslipped using PermaFluor (Lipshaw, Pittsburgh, PA) mounting media. The control experiments for the double label immunohistochemistry procedure are similar to those described by Joseph and Piekut ('86). Controls included the omission of the anti-DßH antibody, the omission of the anti- vasopressin or oxytocin antibody; using the same antibody (e.g anti-DßH) twice in the double label procedure; switching the staining sequence (e.g. a secondary and tertiary conjugate for anti-vasopressin); or reversing fluorophores. If the primary, secondary, or tertiary reagents from the protocol were removed, there was no immunohistochemical labeling of the tissue.

Intracellular filling procedure

Two hypothalamic blocks postfixed for 2 hours in 4% paraformaldehyde were cut on a vibratome in ice-cold PBS at a section thickness of 200 µm. Tissue sections were mounted onto nitrocellulose filter paper (Whatman, 0.45 µm pore size, Maidstone, England), connected to the anode of a current microiontophoresis programmer (World Precision Instruments, New Haven, CT). The cathode was attached to a glass

micropipette (outer diameter 0.86 mm, A-M Systems Inc., Everett, WA) pulled to a tip diameter of 0.25 μm with a vertical pipette puller (David Kopf Instruments, Tujunga, CA) and filled with a 5% aqueous solution of the fluorescent dye LY (Sigma, St. Louis, MO). A constant current of 100 nA was applied to iontophorese the LY. The micropipette was lowered into the tissue section by a micromanipulator (Goodfellow, Cambridge, England) and a fluorescence microscope (Labophot, Nikon, Japan) equipped with a 10x objective and a B2A filter allowed for the visualization of the LY and autofluorescent tissue landmarks. Each cell was filled for approximately 10 - 15 minutes, at which time all of the processes within the confines of the tissue section appeared to be labeled. As previously described by de Lima et al. ('90), cells were considered to be completely filled when no cut off processes were visible and fine axonal and dendritic processes were observed to follow their appropriate trajectories.

Double Labeling Data Analysis

Qualitative analysis of DβH-immunoreactive varicosities in relation to vasopressin- and oxytocin-immunoreactive perikarya throughout the PVH was performed using standard epifluorescence optics attached to a LSM (Zeiss, Germany), switching between the appropriate fluorescein and rhodamine/Texas Red barrier filters at 100x and 250x. Immunoreactive neurons were selected for quantification by the following criteria: a) neurons were located within the cytoarchitectonic boundaries of the PVH as assessed by adjacent thionin-stained sections; b) the full somal volume of the neuron was contained within the tissue section; c) the neuron had at least two clearly defined dendritic processes within the tissue section that were not obscured by dendritic processes of an adjacent neuron; d) the neuron displayed the

morphology of a presumed MC neuron as confirmed by intracellular filling with LY in rat and similar to previous descriptions of Golgi-stained MC neurons in rhesus monkey PVH (Randle et al., '86a; Rafols et al., '87; Hoffman et al., '91). According to these criteria, a total of 16 vasopressin-immunoreactive neurons and 11 oxytocin-immunoreactive neurons were subjected to quantitative analysis.

Quantification of DßH-immunoreactive varicosities in apposition to vasopressin- and oxytocin-immunoreactive perikarya was done using the LSM coupled to a computer driven stage (MSP65, Zeiss) and a computer workstation (DEC 3100, Digital Equipment Corp., Maynard, MA). A confocal mode of scanning was selected which allowed for the discrimination and localization of the fluorophore-conjugated structures throughout the entire thickness of a tissue section because images which were only in focus in the specific optical section, (< 0.5 µm in all three planes, Inoué '90) were digitized and transmitted to the computer monitor where the optical sections were overlaid.

A 25x oil objective was selected for the LSM analysis. At this magnification, the resolution on the computer monitor was 2.4 pixels per µm, and allowed for scanning of a relatively large field of view. The precise focus of optical sections in all three planes resulted in a high resolution of DßH-immunoreactive varicosities and vasopressin- and oxytocin-immunoreactive perikarya. The area sampled for each field was 260 µm in the *x* plane, 165 µm in the *y* plane, and the confocal section thickness was < 0.5 µm, creating a volume of 2.15×10^{-5} mm^3 per optical section.

For each *z*-axis interval, tissue sections were scanned twice using argon lasers with specific excitation wavelengths, capturing sequential images for

subsequent computer-generated overlay and analysis. Specifically, a 488 nm and a 514 nm laser were employed to detect the fluorescein-conjugated (i.e., vasopressin or oxytocin) signal and the Texas Red-conjugated (i.e., DßH) signal, respectively. In this manner, vasopressin- and oxytocin-immunoreactive neurons were assessed through their total somal volume, along with the corresponding DßH-immunoreactive varicosities in the same volume of tissue, in a series of optical sections 1 µm apart (neurons ranged approximately from 10 - 14 µm thick in the z-axis plane) while the *x* and *y* coordinates remained fixed for each field. To maintain experimental consistency, the fluorescein image was scanned first, and the analysis always began at the top of a tissue section and the z-axis plane was stepped down. All of the data acquisition procedures were computer automated to insure tightly controlled and accurate scanning parameters for the detection of each signal.

Pairs of confocal optical sections (one fluorescein image and one Texas Red image for each z-axis plane) were scanned on the LSM and digitized to the computer monitor where the images were aligned with respect to the *x*, *y*, and z coordinates, and overlaid to yield a resultant composite image. The scoring of DßH/vasopressin and DßH/oxytocin contacts was characterized morphologically by toggling between the two optical sections (Texas Red/DßH and fluorescein/vasopressin- or oxytocin) and the resultant overlay image for each z-axis plane using custom designed morphometry software. For the vasopressin- or oxytocin-immunoreactive image, pixels which contained a fluorescein signal were coded in yellow and in the DßH image, pixels which contained a Texas Red signal were coded in red. Additionally, pixels in the overlay image which contained both a fluorescein

and a Texas Red signal were coded in blue, signifying that a DßH-immunoreactive varicosity was in apposition (< 0.5 μm apart, with 2.4 pixels per μm) to a vasopressin- or oxytocin-immunoreactive neuron. An apposition was registered only if both signals were present in the same pixels, thus, even excluding profiles where the two independent signals were in adjacent pixels. Every varicosity had a fixed *x*, *y*, and *z* coordinate attributed to it relative to a 0, 0, 0 (home) point stored in a datafile for each section. Once the quantification of varicosities in apposition to a perikaryon through the series of optical section pairs was complete, an outline of the neuron was plotted to illustrate the shape of the cell being counted relative to the apposition contacts. A varicosity-to-neuron ratio was based upon data collected for each immunohistochemically-identified cell which was further characterized morphologically to assess noradrenergic innervation density directly on the soma versus the proximal dendrites. Statistical analyses were performed by a two-tailed Student's *t*-test.

RESULTS

Vasopressin-immunoreactive neurons in the macaque hypothalamus

Magnocellular vasopressin-immunoreactive neurons were present in discrete nuclei within the monkey hypothalamus, notably in the PVH, SON, and accessory magnocellular nuclei. Labeled neurons were intensely immunofluorescent with eccentric nuclei observed to be immuno-negative relative to the rest of the somata. A population of small (10 - 15 μm in diameter), bipolar PC vasopressin-immunoreactive neurons were also located in the SCN. Faint vasopressin-immunoreactive PVH neurons exhibiting PC

morphology were also rarely observed in a few monkeys, but no consistent pattern for the smaller subpopulation was detectable. Within the PVH, MC vasopressin-immunoreactive neurons typically exhibited 2 - 3 aspiny primary dendrites (4 - 6 μm thick in the z-axis plane), exiting from the somata. These dendrites were extremely thick at the somal junction, and tended to taper off distally. Dendritic processes were oriented in the dorsoventral plane, with arborization both medially towards the third ventricle and laterally towards the fornix. Axonal processes were not consistently observed in the immunofluorescent preparations. Vasopressin-immunoreactive neurons appeared throughout the rostrocaudal extent of the PVH, mainly localized to medial MC regions of the nucleus (Fig. 10A). In addition, a smaller population was observed in the periventricular zone ventral to the region known to contain CRF-immunoreactive neurons (Ginsberg et al., '93a). In rostral aspects of the nucleus, vasopressin-immunoreactive neurons were found in a more ventral region, closer to the subependymal layer of the third ventricle than to the fornix. In more caudal regions, however, the vasopressin-immunoreactive neurons were localized closer to the fornix, as the nuclear boundaries of the PVH shifted to a more dorsolateral position within the hypothalamus.

Oxytocin-immunoreactive neurons in the macaque hypothalamus

Magnocellular neurons containing oxytocin immunoreactivity were found in the PVH, SON, and accessory magnocellular nuclei. No oxytocin-immunoreactive neurons displayed PC morphology, nor were there any oxytocin-immunoreactive neurons found in the SCN. The morphology of the oxytocin-immunoreactive PVH neurons was similar to the vasopressin-immunoreactive neurons, except that they appeared smaller and the proximal

dendrites were not as thick, especially at the dendritic-somal junction. Additionally, oxytocin-immunoreactive neurons were consistently observed in a more lateral position than the vasopressin-immunoreactive neurons throughout the rostrocaudal extent of the PVH (Fig. 11A). The only exception, however, was in the periventricular zone, where oxytocin- and vasopressin-immunoreactive perikarya were intermixed. Oxytocin and vasopressin immunoreactivity did not colocalize through adjacent section analysis. Rather, the two neuropeptides appeared to exist in discrete subpopulations of MC neurons. There was no apparent difference in oxytocin- and vasopressin-immunoreactive neuron density.

Morphology of MC neurons as assessed by intracellular filling

Intracellular filling with LY in 200 μm thick sections revealed MC neurons which were strikingly similar in morphology to the vasopressin- and oxytocin-immunoreactive neurons in 30 μm thick sections. Specifically, large multipolar cells oriented in the dorsoventral plane were observed, with dendrites exiting both medially towards the third ventricle and laterally towards the fornix (Fig. 12). The full complement of the distal dendritic field was observed for several millimeters in the LY preparation, whereas the distal dendrites could only be followed 500 - 750 μm in the immunohistochemical preparation on 30 μm thick sections. Very thin axonal processes could also be observed exiting the somata, or occasionally, the shaft of proximal dendrites in the LY preparations. The axonal processes of these MC neurons could be visualized as they arched laterally around the fornix, presumably en route to the posterior pituitary via the hypothalamo-neurohypophysial tract. Intracellularly filled neurons which displayed a PC morphology were also observed in medial and periventricular PVH regions. These neurons were

smaller, bipolar, with long, thin dendrites that could be followed beyond the roof of the third ventricle to the level of the zona incerta. The morphology and location of such PC neurons were similar to those described for monkey CRF-immunoreactive neurons (Ginsberg et al., '93a), except that the proximal dendrites observed in the immunohistochemical preparations did not sufficiently label the dendritic field in the 30 μm thick section.

Noradrenergic innervation of the macaque PVH

Dopamine-ß-hydroxylase-immunoreactive fibers with punctate varicosities were densely distributed throughout the rostrocaudal extent of the PVH, as characterized previously by nonconfocal LSM analysis in the monkey hypothalamus and by electron microscopy in rat PVH and basal forebrain (Olschowka et al., '81; Liposits et al., '86b; Chang, '89; Ginsberg et al., '93c). Briefly, DßH-immunoreactive varicosities clearly demarcated the PVH from the surrounding AHA, with areas containing both vasopressin- and oxytocin-immunoreactive neurons receiving a dense DßH-immunoreactive input (Figs. 10B, 11B). The greatest noradrenergic innervation density, however, appeared in more medial, PC PVH regions known to contain CRF-immunoreactive neurons (Ginsberg et al., '93a).

Noradrenergic innervation of vasopressin-immunoreactive neurons in the macaque PVH

Qualitative observations of the double label immunohistochemical preparations revealed clear appositions of DßH-immunoreactive varicosities to vasopressin-immunoreactive neurons, notably on the proximal portions of aspiny, primary dendrites (Fig. 10C). More distal aspects of vasopressin-immunoreactive dendrites did not appear to receive substantial noradrenergic input. Dopamine-ß-hydroxylase-immunoreactive varicosities

in apposition to vasopressin-immunoreactive somata were also observed, although less frequently than on the proximal dendrites. Typically, a DßH-immunoreactive varicosity was observed in apposition to an immunohistochemically-identified dendrite or somata through one z-axis optical section. Occasionally, a large varicosity (approximately 1.5 - 2.5 μm in diameter) would be observed in contact with a perikaryon across several z-axis optical sections. Another large subset of DßH-immunoreactive varicosities were located near (< 5 μm away), but not directly in apposition to, vasopressin- or oxytocin-immunoreactive perikarya, suggesting that there are other postsynaptic targets that receive noradrenergic innervation. A computer generated map of DßH-immunoreactive varicosities in apposition to a representative vasopressin-immunoreactive neurons is shown in Figure 13. Quantitative confocal LSM analysis through the total somal volume of 16 vasopressin-immunoreactive neurons in the PVH of 6 monkeys demonstrated a mean of 8.8 ± 1.8 (SEM) DßH-immunoreactive varicosities in apposition to vasopressin-immunoreactive somata and 24.3 ± 3.8 DßH-immunoreactive varicosities in apposition to vasopressin-immunoreactive dendrites. The number of DßH-immunoreactive varicosities quantified in apposition to vasopressin-immunoreactive dendrites was significantly greater ($P < 0.005$) than the number counted in apposition to vasopressin-immunoreactive somata (Fig. 14). A two-dimensional representation of DßH-immunoreactive varicosities in apposition to a vasopressin-immunoreactive neuron through successive optical sections is shown in Figure 15.

Noradrenergic innervation of oxytocin-immunoreactive neurons in the macaque PVH

Appositions between DßH-immunoreactive varicosities and oxytocin-immunoreactive somata and dendrites were observed, similar to the description of vasopressin-immunoreactive neurons. However, fewer appositions were tallied as quantitative analysis of 11 oxytocin-immunoreactive neurons in the PVH of 4 monkeys revealed 2.6 ± 0.6 (SEM) DßH-immunoreactive varicosities in apposition to oxytocin-immunoreactive somata and 4.8 ± 2.2 DßH-immunoreactive varicosities in apposition to oxytocin-immunoreactive dendrites. In contrast to the population of vasopressin-immunoreactive neurons, the number of DßH-immunoreactive varicosity appositions was not significantly different between the somata and dendrites of oxytocin-immunoreactive neurons (Fig. 14). Accordingly, vasopressin-immunoreactive neurons received a significantly greater noradrenergic innervation density than oxytocin-immunoreactive neurons ($P < 0.005$). In addition, confocal LSM assessment of somal volume of the immunohistochemically-identified neurons indicated that vasopressin-immunoreactive neurons had a greater somal volume than oxytocin-immunoreactive neurons, with a mean of 7686.4 ± 2020.6 μm^3 versus 3321.8 ± 993.5 μm^3 ($P < 0.005$). Therefore, double label immunohistochemistry combined with confocal LSM methodology revealed that macaque PVH vasopressin-immunoreactive neurons have a larger somal volume and receive a greater noradrenergic innervation density than oxytocin-immunoreactive neurons, especially on the proximal dendrites.

DISCUSSION

Antibody specificity

Previous descriptions of the catecholaminergic innervation of neuropeptide-containing neurons within the primate PVH have been performed using monoamine fluorescence histochemistry combined with neurophysin immunohistochemistry, however, these techniques do not discriminate between the specific catecholamine neurotransmitters nor the neurohypophysial hormones (Hoffman et al., '76; Ishikawa and Tanaka, '77; Antunes and Zimmerman, '78; Sladek and Zimmerman, '82). A double label immunofluorescence preparation was used in this study to delineate noradrenergic varicosities in apposition to vasopressin- and oxytocin-immunoreactive perikarya. The antibodies directed against synthetic vasopressin and oxytocin were more specific than previous immunohistochemical analyses using antibodies directed against the neurophysin carrier proteins. Similarly, the antibody directed against DßH allowed for the discrimination of noradrenergic varicosities from dopaminergic varicosities. However, adrenergic varicosities could not be distinguished from noradrenergic varicosities, since DßH is also located in adrenergic-containing structures. Neurochemical and morphologic studies in rat using an antibody directed against PNMT, the enzyme which converts norepinephrine into epinephrine, have shown that an adrenergic terminal field exists within the medial PC PVH, with MC regions receiving little adrenergic input (van der Gugten et al., '76; Swanson et al., '81; Liposits et al., '86a). Therefore, our assumption is that the vast majority of DßH-immunoreactive varicosities in apposition to MC vasopressin- and oxytocin-immunoreactive neurons in the monkey PVH are noradrenergic.

Qualitative observations on the vasopressin, oxytocin, and DβH immunoreactivity within the PVH

The immunohistochemical localization of vasopressin- and oxytocin-containing neurons in this report using mouse monoclonal antibodies is consistent with earlier descriptions in rat (Swaab et al., '75a, 75b) and human (Dierickx and Vandesande, '77, '79) using various polyclonal antisera. Magnocellular neurons within the PVH and SON are believed to synthesize either vasopressin or oxytocin, but not both hormones (Dierickx and Vandesande, '79). In addition, several neuropeptides have been colocalized within MC neurons in rat including dynorphin, galanin, and TH in vasopressin-containing neurons, and CRF and CCK in oxytocin-containing neurons (Swanson and Sawchenko, '83; Meister et al., '90). The morphology and distribution of immunohistochemically-identified neurons within the PVH in this report is consistent with the existing literature in monkeys that subpopulations of both MC and PC neurons express vasopressin, but only a subpopulation of MC neurons expresses oxytocin, with the oxytocin-containing neurons tending to be located more laterally than the vasopressin-containing neurons (Sofroniew et al., '81; Kawata and Sano, '82; Caffé et al., '89). In addition, Kawata and Sano ('82) have demonstrated in monkey that vasopressin-immunoreactive neurons are larger than oxytocin-immunoreactive neurons, although their analysis was performed two-dimensionally rather than the three-dimensional analysis of somal volume used in this study. Taken together, these data indicate that macaque PVH MC neurons are parcellated by the nonapeptide they express, their somal size, and the number of noradrenergic appositions that they receive.

The noradrenergic innervation of the primate hypothalamus as assessed immunohistochemically with an antibody directed against DßH has been previously reported (Ginsberg et al., '93c). Briefly, the present immunofluorescent preparation demonstrated extremely dense DßH-immunoreactive terminal fields with punctate varicosities throughout the rostrocaudal extent of the PVH, including both MC and PC regions. No qualitative differences were observed in the staining intensity, density, and distribution of immunoreactive profiles between the immunofluorescent preparation and the previous immunoperoxidase-DAB method.

Noradrenergic innervation of vasopressin- and oxytocin-immunoreactive perikarya

The quantification of DßH-immunoreactive varicosities in optical sections throughout the somal volume of immunohistochemically-identified PVH neurons yielded a varicosity-to-neuron ratio and provides an indication of the distribution of synapses, that in turn, will allow for a precise anatomic characterization of this neurotransmitter-identified circuit. These quantitative data revealed a dense noradrenergic input to MC vasopressin-immunoreactive PVH neurons as compared to MC oxytocin-immunoreactive neurons. Since there was no apparent bias in the choice of vasopressin- or oxytocin-immunoreactive neurons analyzed, the data suggests that each MC vasopressin-immunoreactive neuron in the monkey PVH receives an average of 33 noradrenergic varicosity contacts, with approximately two-thirds of these appositions on the proximal dendrites and one-third on the soma, whereas MC oxytocin-immunoreactive neurons receive an average of 8 noradrenergic varicosity contacts evenly distributed on the proximal dendrites and soma. This quantitative assessment is in agreement with

previous qualitative observations in rat and monkey PVH that regions containing vasopressin-immunoreactive neurons are more heavily innervated by noradrenergic fibers (McNeill and Sladek, '80; Sawchenko and Swanson, '81a; Sladek and Zimmerman, '82).

The intracellular injections of LY in 200 μm thick sections demonstrated that the quantitative and morphologic analyses of immunohistochemically-identified neurons in 30 μm thick sections likely omitted the distal portion of the dendritic tree. Even though the majority of appositions were observed on the proximal portions of MC dendrites, it is possible the present quantitative analysis slightly underestimates the number of appositions because the distal dendritic regions were not fully analyzed. The high density of noradrenergic afferent input to the proximal dendrites and somata of vasopressin-immunoreactive neurons is in a position to have profound effects on the activity of these cells, and may be functionally a more dominant input to this group of neurons than the noradrenergic input that has been described in several telencephalic areas (Morrison et al., '81, '82). For instance, the distribution of noradrenergic synapses in neocortex tends to be localized to spines and shafts on distal dendritic branches of pyramidal neurons (Papadopoulos et al., '87, '89) as opposed to the noradrenergic appositions on the proximal dendrites and soma of MC vasopressin-immunoreactive neurons in the PVH.

The substantial noradrenergic input to vasopressin-immunoreactive neurons represents an anatomic substrate of a defined physiologic response in the hypothalamus, as pharmacologic applications of norepinephrine or electrophysiologic stimulation of brainstem noradrenergic cell groups elevates plasma levels of vasopressin, and to a lesser degree, oxytocin (Day et

al., '84; Blessing and Willoughby, '85; Brooks et al., '86; Randle et al., '86b). This well characterized circuit is believed to be involved in the regulation of several homeostatic functions, including appetitive behaviors and cardiovascular responses (Swanson, '87; Leibowitz, '88; Li et al., '92). Retrograde tract tracing methods combined with immunohistochemistry have localized projections from noradrenergic-containing cell groups in the caudal medulla (A1 and A2) and pons (locus coeruleus) terminating in the PVH and SON of rats (Cunningham and Sawchenko, '88). Additionally, the rat A1 cell group preferentially innervates MC vasopressin neurons (Cunningham and Sawchenko, '88), which may explain the greater DßH-immunoreactive varicosity input to this subpopulation found in the present report. It is interesting to note that a non-catecholaminergic subset of neurons adjacent to the A2 cell group (within the nucleus of the solitary tract) preferentially innervates oxytocinergic neurons in the rat PVH and expresses a combination of inhibin ß, somatostatin, and enkephalin immunoreactivities (Sawchenko et al., '90). These discrete, chemically-specified brainstem projections may carry functional significance relating to the separate effects of the two hormones. Several catecholamine-containing cell groups projecting to the PVH of rhesus monkeys have been described using monoamine histofluorescence (Schofield and Everitt, '81; Tanaka et al., '82; Felten and Sladek, '83). However, further retrograde tracing/immunohistochemistry experiments are necessary to test whether specific cell groups preferentially innervate regions of the primate PVH or SON. Moreover, norepinephrine modulates the HPA axis through the activation of CRF-containing neurons, possibly via alpha-1 adrenergic receptors (Szafarczyk et al., '87; Plotsky et al., '89; Saphier and Feldman, '91). Noradrenergic activation of vasopressinergic and oxytocinergic neurons in

the PVH may also affect the HPA axis as both hormones stimulate the release of ACTH by themselves (vasopressin being a more potent secretagogue than oxytocin) as well as potentiating CRF secretion (Gillies et al., '82; Antoni et al., '83; Negro-Vilar et al., '87).

In addition to the DßH-immunoreactive varicosities which are in apposition to vasopressin- and oxytocin-immunoreactive perikarya, there are several other potential targets for this noradrenergic innervation within the macaque PVH. Since numerous DßH-immunoreactive varicosities were observed to terminate near (< 5 μm), but not in apposition to immunohistochemically-identified neurons, one possibility is that these noradrenergic afferents are contacting the processes of interneurons, which have been observed to form synapses with rat MC neurons and demonstrated to express the fast inhibitory neurotransmitter GABA (van den Pol, '85; Buijs et al., '87; Decavel et al., '89). The present technique of confocal microscopy/double label immunohistochemistry would be extremely useful to determine if noradrenergic inputs contact processes of GABAergic interneurons within the PVH. If appositions were localized, then a triple label preparation to identify potential glomeruli where noradrenergic afferents target chemically-specified interneuronal processes and/or MC PVH neurons would ultimately lead to a greater understanding of the anatomic relationships between extrinsic and intrinsic PVH signaling, as well as give better insight into overall neuroendocrine function.

Another population of monkey PVH neurons likely to receive a substantial DßH-immunoreactive input is the PC neurons, which are localized to more medial and periventricular aspects of the PVH that from a quantitative standpoint in monkey, receive the greatest DßH-immunoreactive

input (Ginsberg et al., '93a, '93c). Several investigators have demonstrated that CRF-, somatostatin-, and thyrotropin-releasing factor-containing neurons in rat all are contacted by catecholaminergic afferents (Nakada and Nakai, '85; Nakai et al., '86; Shioda et al., '86).

In lieu of morphologic and physiologic data suggesting that norepinephrine plays a role in the regulation of CRF-containing neurons, the confocal microscopy/double label immunofluorescence technique using antibodies directed against DßH and CRF was to be undertaken. However, comparisons between CRF-immunoreactive neurons and intracellularly filled PC PVH neurons suggested that the immunohistochemical procedure did not sufficiently label proximal dendritic processes, and colchicine administration was not a viable option. Since the assessment of vasopressin- and oxytocin-immunoreactive neurons depended on complete immunohistochemical labeling of the dendritic field within the confines of the tissue section, double immunohistochemistry for DßH and CRF was not performed.

Glial cells may also be targets for noradrenergic innervation within the PVH as both alpha- and beta-adrenergic receptors have been localized *in vitro* to astrocytes in cultures derived from rat cortical and pituitary tissue (Bicknell et al., '89; Lerea and McCarthy, '89; Salm and McCarthy, '89; Hatton et al., '91). Another possible target for noradrenergic innervation are blood vessels within the PVH, which have been shown to receive monoaminergic innervation (Swanson et al., '77). Thus, the noradrenergic input to the PVH appears to have multiple termination sites, both neuronal and non-neuronal.

Norepinephrine-containing varicosities have been demonstrated to form primarily asymmetric, axodendritic and axosomatic synaptic contacts in the rat PVH, basal forebrain, and neocortex (Olschowka et al., '81; Liposits et

al., '86b; Chang, '89; Papadopoulos et al., '89). Moreover, each DßH-immunoreactive varicosity in apposition to an identified soma or dendrite in monkey PVH is likely to contain at least one release site in the form of a functional synapse, as observed in rat double label electron microscopy preparations (Silverman et al., '83, '85; Nakada and Nakai, '85; Ochiai et al., '88; Ochiai and Nakai, '90). Quantitative confocal analysis expands on previous qualitative descriptions in monkey and rat where catecholamine-neuropeptide interactions have been described at the light microscopic level by providing greater two point resolution and the ability to overlay optical sections in the same z-axis plane. Although electron microscopy is necessary to verify synaptic relationships, confocal microscopy allows for the characterization of appositions in a larger volume of tissue to include the total somal volume of an identified neuron, effectively becoming a practical interface between conventional light microscopy and electron microscopy. Future morphologic characterization of other neurotransmitters such as glutamate and GABA in apposition to PVH neurons in the primate will help clarify the anatomic organization of this complex neurosecretory circuit. In addition, with the development of antibodies against subtype-specific receptors (e.g. alpha adrenergic and glutamate receptors) the use of confocal microscopy combined with double label immunohistochemistry may help elucidate the relationship(s) between terminal varicosities and the localization of receptor complexes on neurons with well characterized, physiologically defined neurosecretory functions. In addition, such precise quantitative analysis of neurotransmitter-identified circuits will be useful in assessing potential developmental and/or neuropathological changes in the density and distribution of synaptic interactions.

ACKNOWLEDGMENTS

The authors thank Dr. A.-J. Silverman and Dr. D.T. O'Connor for donating the antisera, Dr. P.C. Goldsmith for helpful discussions, P. Good for assistance with the intracellular filling, and R. Woolley for photographic assistance. This research was supported in part by a pilot research grant from the John D. and Catherine T. MacArthur Foundation Mental Health Research Network I, the Brookdale Foundation, and NIH grant MH45212.

FIGURE LEGEND

Figure 10. Fluorescence photomicrographs demonstrating the DβH-immunoreactive innervation of vasopressin-immunoreactive neurons within the macaque PVH. **A)** Fluorescein-conjugated vasopressin-immunoreactive neurons located within a medial MC region at the mid-rostral level the PVH. **B)** Texas Red-conjugated DβH-immunoreactive varicosities in the same field as (**A**), demonstrating the concomitant noradrenergic innervation of the region. **C)** Double exposure of the two fluorophores demonstrating the association between DβH-immunoreactive varicosities and vasopressin-immunoreactive perikarya. Several contacts are observed, including DβH-immunoreactive varicosities in apposition to vasopressin-immunoreactive somata (white arrowheads) and dendrites (white arrows). Additionally, a substantial population of DβH-immunoreactive varicosities are near, but not in apposition to vasopressin-immunoreactive perikarya, suggesting that there are also other targets for this noradrenergic innervation within the monkey PVH. The third ventricle is to the right. Scale = 25 μm.

Figure 11. Fluorescence photomicrographs demonstrating the DβH-immunoreactive innervation of oxytocin-immunoreactive neurons within the macaque PVH. **A)** Fluorescein-conjugated oxytocin-immunoreactive neurons located laterally to the vasopressin-immunoreactive neurons observed in Fig. 1A. **B)** Texas Red-conjugated DβH-immunoreactive varicosities in the same field as (**A**), demonstrating the noradrenergic innervation of the region. Curved arrows point to contacts between DβH-immunoreactive varicosities and oxytocin-immunoreactive perikarya. There appear to be fewer DβH-

immunoreactive varicosities in apposition to oxytocin-immunoreactive neurons as compared to vasopressin-immunoreactive neurons. The third ventricle is to the right. Scale = 50 μm.

Figure 12. Fluorescence photomicrograph of a monkey PVH neuron intracellularly filled with LY displaying MC morphology in a 200 μm thick tissue section. Note that several dendrites and a fine caliber axonal process (arrowhead) exit the somata. The morphology of this neuron filled with LY is similar to the vasopressin-immunoreactive neurons quantitatively assessed in 30 μm thick tissue sections, indicating that the immunofluorescent preparation is sufficiently labeling the proximal dendrites of these MC neurons. The third ventricle is to the right. Scale = 25 μm.

Figure 13. Computer-generated two-dimensional map depicting DβH-immunoreactive varicosities in apposition to a vasopressin-immunoreactive neuron in the macaque PVH. A total of 8 DβH-immunoreactive varicosities were counted on the soma, and 29 on the proximal dendrites through the total volume of the neuron. Note that the two dendrites that appear to cross (asterisk) are in fact separated in space through the z-axis plane. The third ventricle is to the right. Scale = 20 μm.

Figure 14. Histogram illustrating the number of DβH-immunoreactive varicosities quantified in apposition to vasopressin- and oxytocin-immunoreactive somata and proximal dendrites. The proximal dendrites of vasopressin-immunoreactive neurons received a significantly greater density of noradrenergic innervation as compared to the somata (* = $P < 0.005$). In

contrast to the vasopressin-immunoreactive neurons, no significant difference in the distribution of appositions was observed between the proximal dendrites and the somata of oxytocin-immunoreactive neurons.

Figure 15. A sequential series of optical sections with overlaid computer graphics demonstrating the relationship between DβH-immunoreactive varicosities and a vasopressin-immunoreactive neuron through 7 μm in the *z*-axis plane. Pairs of confocal optical sections (one fluorescein/vasopressin image and one Texas Red/DβH image for each *z*-axis plane) were scanned on a laser scanning microscope (LSM) and digitized to the computer monitor where the images were aligned with respect to the *x*, *y*, and *z* coordinates, and overlaid to yield a resultant image. The scoring of DβH/vasopressin contacts was characterized morphologically by toggling between the two optical sections (Texas Red/DβH and fluorescein/vasopressin) and the resultant overlay image for each *z*-axis plane using custom designed morphometry software. For the vasopressin-immunoreactive image, pixels which contained a fluorescein signal were coded in yellow and in the DβH image, pixels which contained a Texas Red signal were coded in red. Additionally, pixels in the overlay image which contained both a fluorescein and a Texas Red signal were coded in blue, signifying that a DβH-immunoreactive varicosity was in apposition (< 0.5 μm apart, with 2.4 pixels per μm) to a vasopressin-immunoreactive neuron. An apposition was registered only if both signals were present in the same pixels, excluding profiles where two signals were in adjacent pixels. Once the quantification of varicosities in apposition to a perikaryon through the series of optical section pairs was complete, an outline of the neuron was plotted (in red) to illustrate the shape of the cell

being counted relative to the apposition contacts. Note that the outline and appositions are present in each optical overlay and the data is specific to the z-axis plane. A total of 10 DßH-immunoreactive varicosities were counted in apposition to the vasopressin-immunoreactive somata and 27 on the dendrites. One dendrite (asterisk) did not receive any direct noradrenergic innervation. The blue coded regions outside the boundaries of the vasopressin-immunoreactive neuron are due to autofluorescence of lipofuscin granules in the neuropil. Bar = 25 μm.

Figure 10

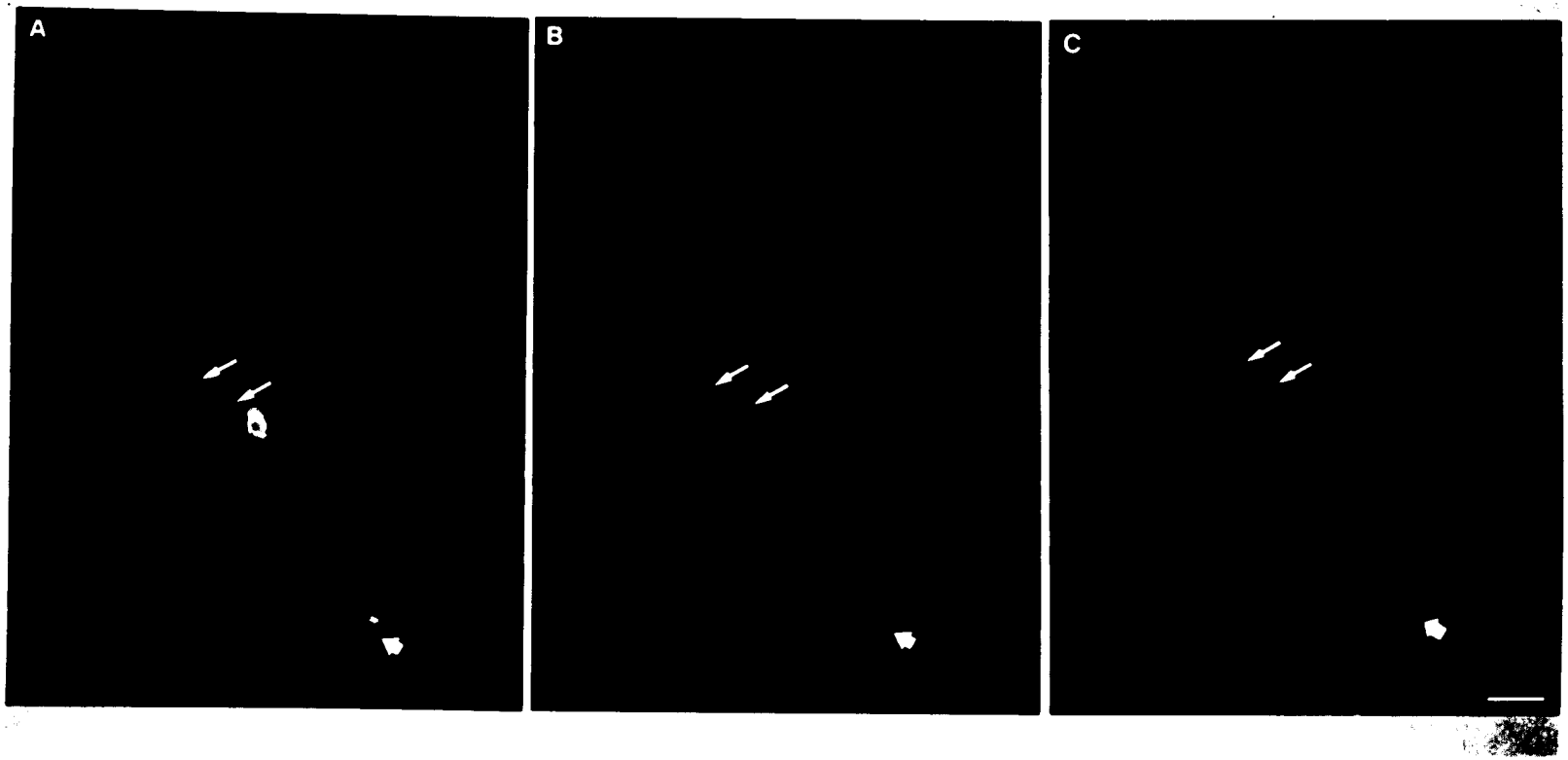

Figure 11

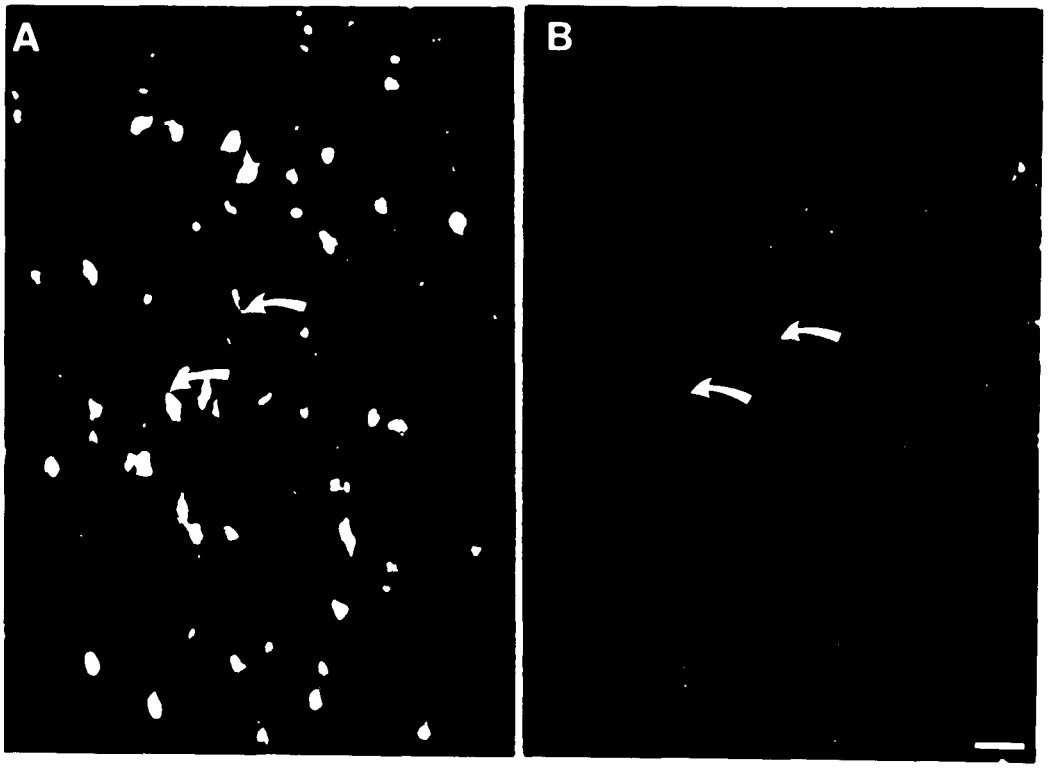

Figure 12

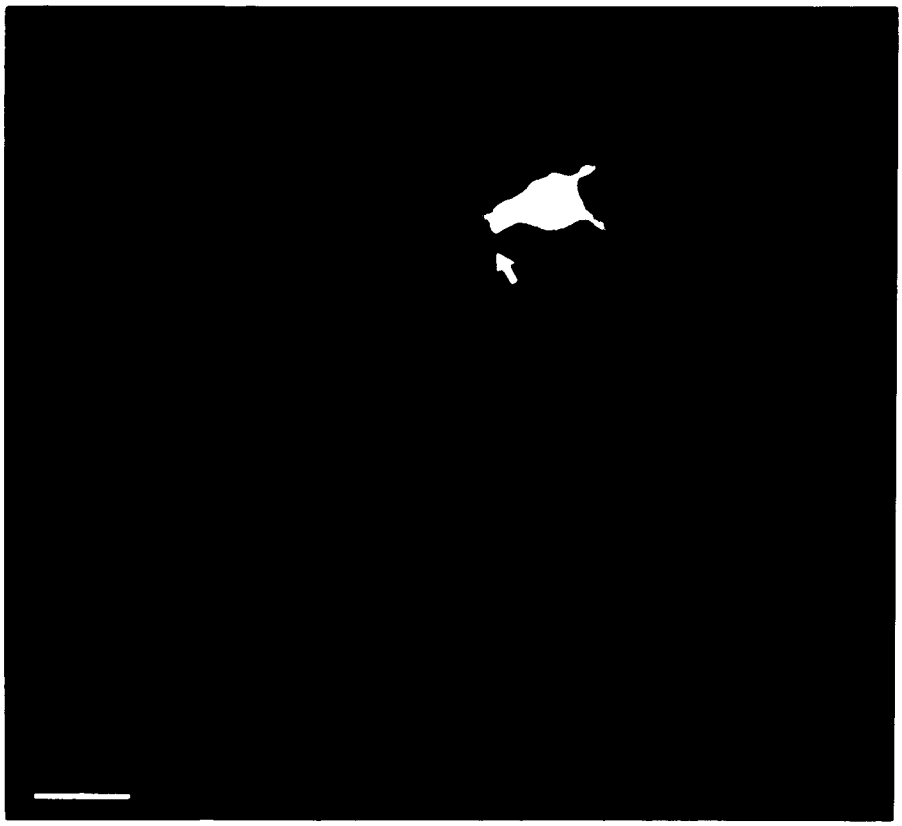

Figure 13

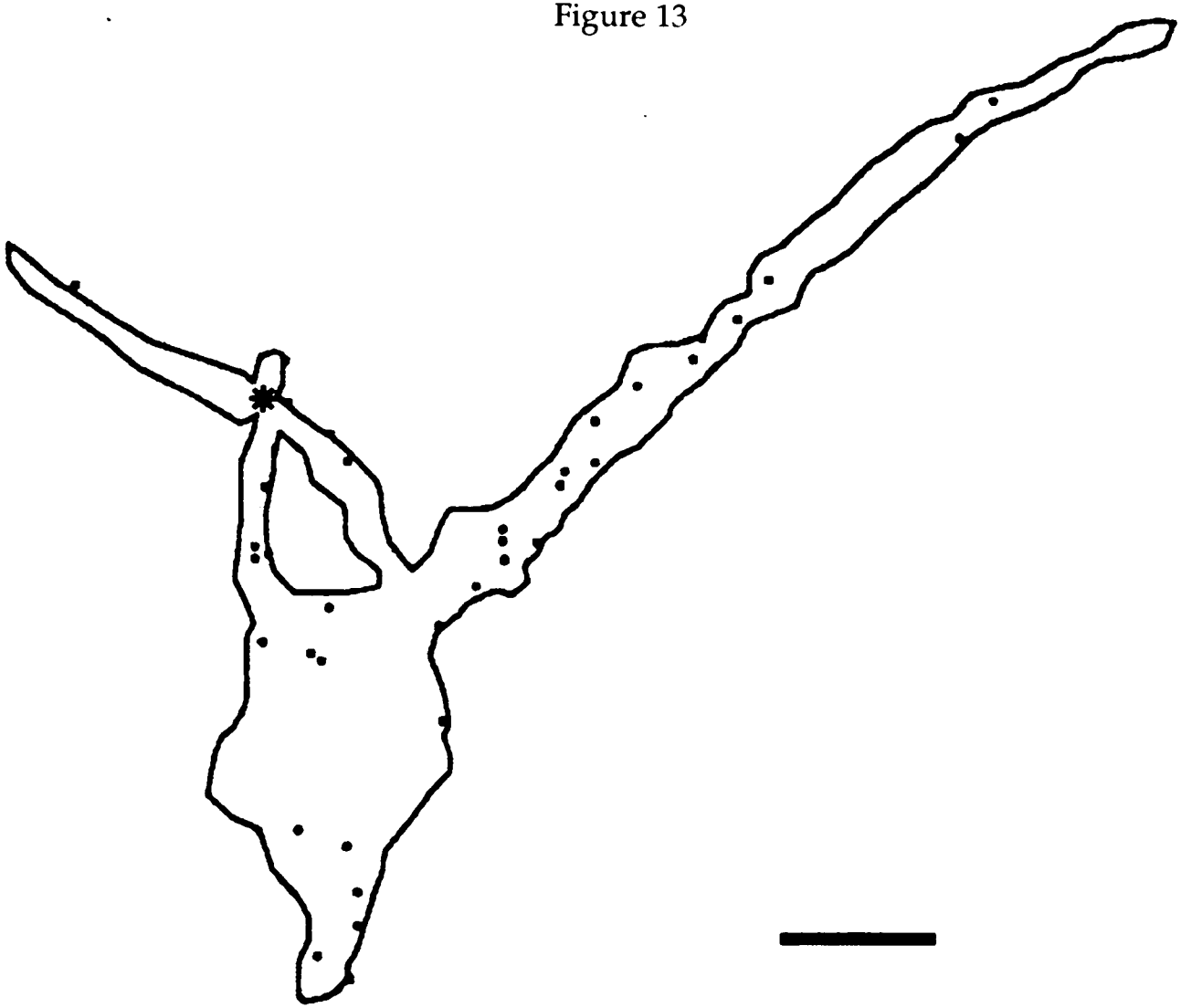

Figure 14

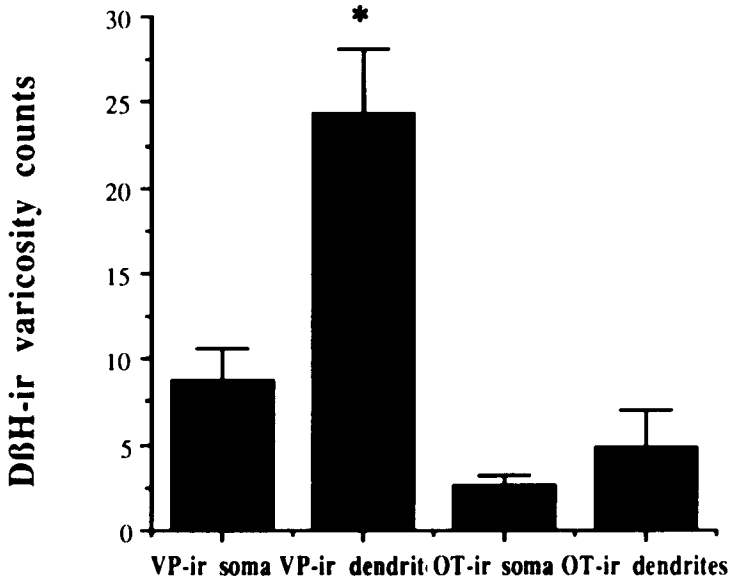
DßH-ir varicosity counts
30
25
20
15
10
5
0
*
VP-ir soma
VP-ir dendrit
OT-ir soma
OT-ir dendrites

Figure 15

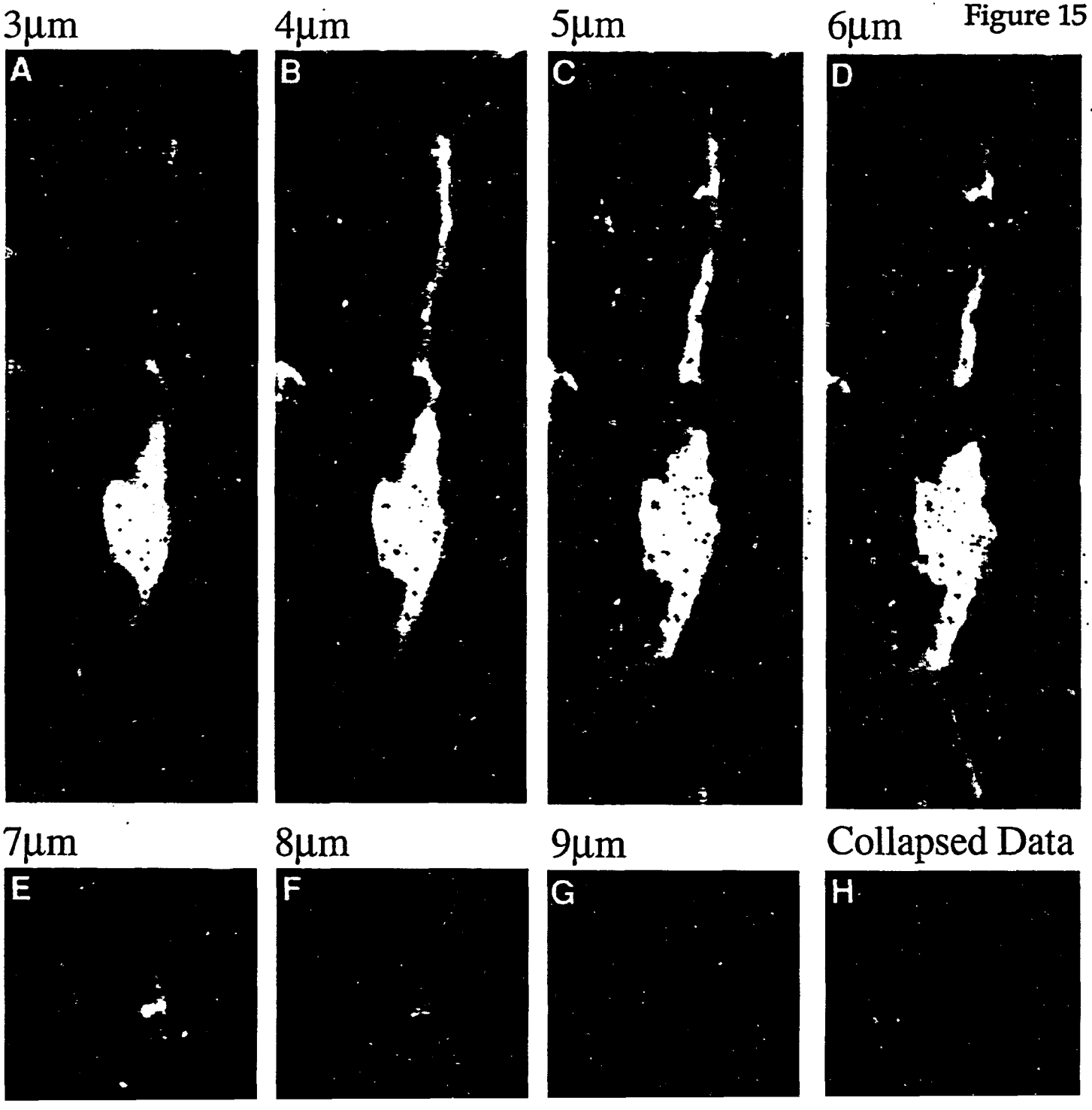

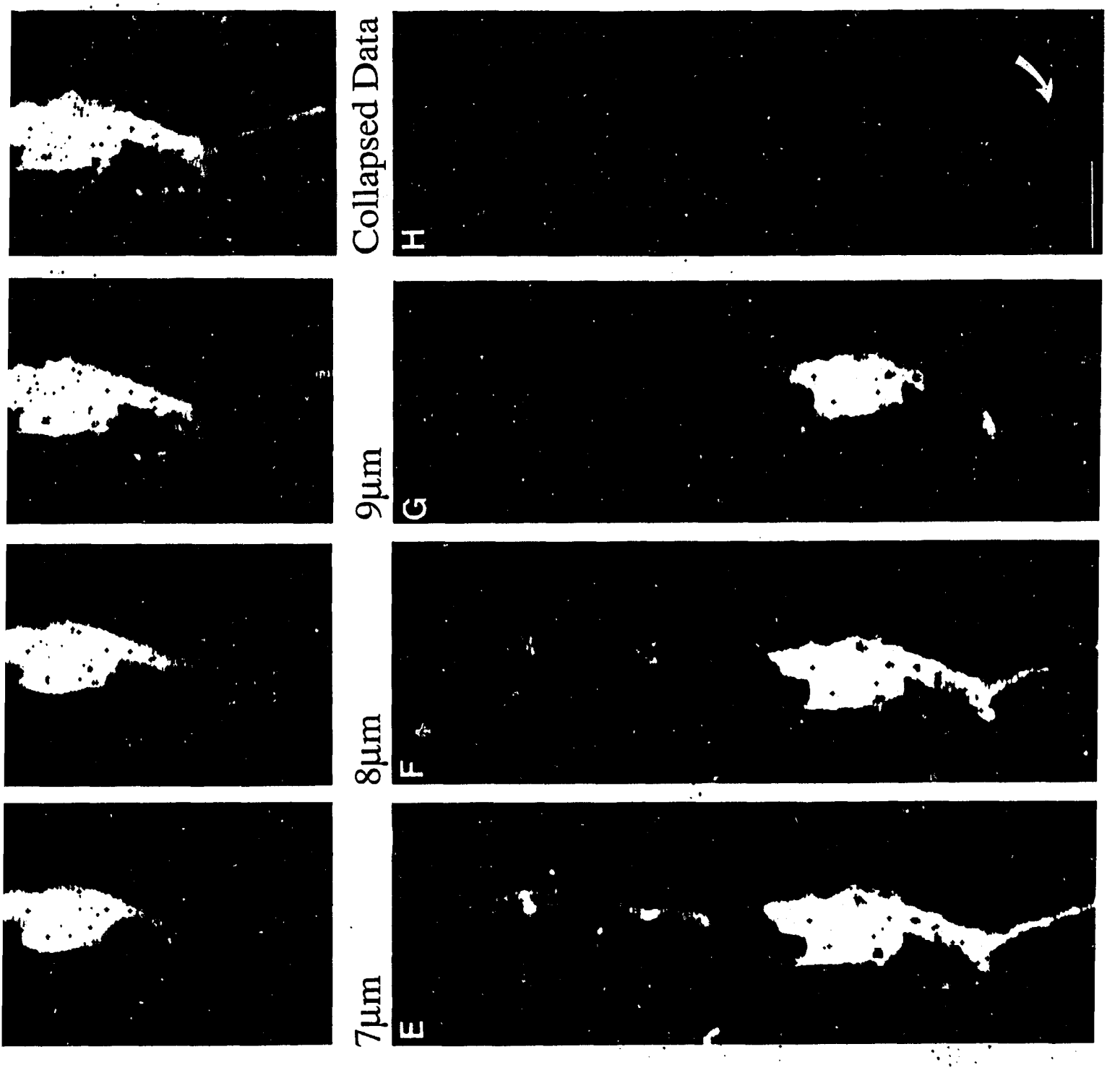
Collapsed Data
H
9µm
G
8µm
F
7µm
E

Chapter Five

SUMMARY

A series of neuroanatomic analyses have been undertaken to identify potential neuropathological changes seen in monkeys exposed to early social deprivation, which leads to psychopathology, inappropriate responses to stress, and appetitive disorders. The animals used in this study were either socially reared or maternal and peer deprived. Within this framework, the distribution and density of noradrenergic varicosities was assessed in the PVH of rhesus monkeys using DßH immunohistochemistry combined with laser scanning microscopy. Quantitative analysis of DßH-immunoreactive varicosity density within MC and PC regions revealed no significant differences between rearing conditions, suggesting that the noradrenergic innervation of the PVH was not affected by the early environmental insult of social deprivation.

INTRODUCTION

Social deprivation in non-human primates has been demonstrated to produce a variety of psychosocial abnormalities including appetitive disorders (hyperphagia and polydipsia), increased fear and aggressive behaviors, sexual dysfunction, and prolonged and inappropriate responses to stress that are suggestive of severe neuroendocrine deficits (Mitchell et al., '66; Miller et al., '69; Kraemer, '92). In an attempt to correlate potential neurochemical and morphologic changes to behaviors which are disrupted by

social deprivation, the noradrenergic innervation of the PVH was evaluated in rhesus monkeys (*Macaca mulatta*) raised in differential rearing conditions using an antibody directed against DßH, the enzyme which converts dopamine into norepinephrine. The density and distribution of DßH-immunoreactive varicosities was chosen for analysis because of the potent effects of norepinephrine on physiologic circuits within the PVH, notably the stimulation of feeding behaviors (possibly through post synaptic alpha-2 receptors), the release of vasopressin from MC neurons, and CRF from PC neurons (Leibowitz, '78, '88; Day et al., '84; Plotsky, '87). In addition, previous neurochemical measurements in socially deprived rhesus monkeys have demonstrated a decrease in cerebrospinal fluid norepinephrine concentrations (Kraemer et al., '84, '89). The characterization of chemically-identified systems within the PVH (see Ginsberg et al., '93a) is part of a larger series of analyses within discrete brain structures including amygdala, brainstem, hippocampus, and neocortex that may be involved in some of the aberrant behavioral and cognitive responses displayed by socially deprived monkeys. A previous report included the quantitative analysis of DßH-immunoreactive varicosities in MC and PC PVH regions of socially reared animals (Ginsberg et al., '93c), which in turn, was used in this study as a normative database to probe for potential neuropathological changes in noradrenergic innervation density within the PVH of maternal and peer deprived monkeys.

MATERIALS AND METHODS

Animals

The animals used in this study were born at the Harlow Primate Laboratory, Madison, Wisconsin, and reared either in a socially enriched environment or in a socially deprived environment. Socially reared animals were housed from birth to the age of 6 months with their mother and then housed in peer groups of 4 young monkeys per cage. Socially deprived animals were born and kept with their mother in her home cage for 3 days prior to separation, and then taken to the nursery where they remained for 1 month. After 1 month, socially deprived animals were transferred to single cages, and had auditory, olfactory, and visual, but not tactile, contact with other subjects. Both male and female monkeys were used in this study. These experiments were conducted within NIH guidelines for animal research and were approved by the IACUC board of the University of Wisconsin. The animals were sacrificed in pairs between 19 - 27 months of age. Monkeys were sedated with ketamine hydrochloride (25 mg/kg i.m.) and anesthetized with sodium pentobarbital (30 mg/kg i.p.), then intubated with an endotracheal tube and ventilated. Monkeys were perfused with ice-cold 1% paraformaldehyde in phosphate buffered saline PBS (0.12 M, pH 7.4) delivered via a perfusion pump (275 - 325 ml/min) as an initial rinse of the vascular system for 45 - 60 seconds followed by ice-cold 4% paraformaldehyde in PBS delivered at the same flow rate for an additional 8 - 9 minutes. Brains were removed and hypothalamic blocks were cut in the coronal plane and post fixed in 4% paraformaldehyde for 6 hours then cryoprotected in a series of 12%, 16%, and 18% sucrose solutions in PBS. A 1 in 13 series of 30 μm thick sections were cut throughout the hypothalamus on

a cryostat. One series was stained with thionin and used in conjunction with Bleier's ('84) atlas of the rhesus monkey hypothalamus. An adjacent series was processed for immunohistochemistry using a polyclonal rabbit antiserum directed against human DßH at a working dilution of 1:2,000. The primary antibody has been fully characterized previously and shown to crossreact with monkey DßH (O'Connor et al., '79; Ginsberg et al., '93c). Tissue sections were incubated overnight in a PBS solution containing the primary antiserum, 0.3% Triton X-100, and 0.5 mg/ml bovine serum albumin at 4°C. The secondary and tertiary steps were processed using a Vectastain ABC kit (Vector Laboratories, Burlingame, CA) with DAB as a chromogen. The reaction product was intensified with 0.05% cobalt chloride and 0.05% nickel ammonium sulfate.

Data analysis

Quantitative assessment of DßH-immunoreactive varicosity density within both MC and PC PVH regions was performed in 5 socially deprived rhesus monkeys and compared to the varicosity density in 5 socially reared monkeys (Ginsberg et al., '93c). The quantitative analysis scheme has been described in detail elsewhere (Ginsberg et al., '93c). Briefly, 9 immunostained sections evenly spaced throughout the rostrocaudal extent of the PVH were analyzed per animal (a total of 45 sections each for the socially reared and socially deprived conditions) on a LSM (Zeiss, Germany). Magnocellular and parvicellular regions were identified on thionin-stained sections and the adjacent immunostained section for DßH-immunoreactive varicosity density. The LSM used an argon laser as an illumination source, and was coupled to a computer driven stage (MSP65, Zeiss) and a computer workstation (DEC 3100, Digital Equipment Corp., Maynard, MA). Eight z-axis planes with a

vertical resolution < 3 μm were collected for one MC and one PC region per PVH tissue section. Dopamine-ß-hydroxylase-immunoreactive structures were characterized morphologically as the axon traversed through all three planes of view. Specifically, varicosities were identified within the plane of focus as punctate, spherical processes (approximately 1 μm in diameter), intensely labeled with DAB reaction product, either discontinuous with adjacent labeled profiles or attached to an intervaricose segment. A 25x oil objective was used for the LSM analysis, yielding a pixel-to-micron ratio of 2.4 on the computer monitor where the actual quantification was performed. The area sampled for each field was 260 μm in the *x* plane, 165 μm in the *y* plane, and the section thickness was 24 μm, creating a volume of 1.04×10^{-3} mm^3 per field. The varicosity quantification for each tissue section on the LSM yielded 2 collapsed two-dimensional maps, one for each of MC and PC regions, which provided a quantitative assessment for the density of DßH innervation within a circumscribed region of monkey PVH. The number of varicosities that were quantified for each of the 9 tissue sections per subject was collapsed to yield a final effective volume of 9.27×10^{-3} mm^3 per subject. Statistical analyses were performed using an ANOVA.

RESULTS

No qualitative differences were observed within the PVH of socially deprived monkeys and socially reared monkeys in terms of the size, staining intensity, or distribution of DßH-immunoreactive processes (Fig. 16). In all of the subjects examined, coarse, varicose fibers with dense terminal fields were

found throughout the rostrocaudal extent of the PVH, clearly delineating the nucleus from the surrounding anterior hypothalamic area. Magnocellular and parvicellular regions received a dense DßH-immunoreactive terminal input, making any differences in innervation density difficult to assess through qualitative observation. A total of 90,782 DßH-immunoreactive varicosities were counted in the PVH of 5 socially reared monkeys and 80,600 DßH-immunoreactive varicosities were counted in the PVH of 5 socially deprived monkeys. Quantitative analysis within both MC and PC regions revealed no statistical differences between rearing conditions as 7,865.0 ± 1,188.5 (SEM) DßH-immunoreactive varicosities were tabulated in MC regions and 10,291.4 ± 1,461.1 in PC regions of 5 socially reared monkeys compared to 7,173.8 ± 755.8 DßH-immunoreactive varicosities in MC regions and 8,946.2 ± 473.4 in PC regions of 5 socially deprived monkeys (Fig. 17). These data suggest that social deprivation does not alter the density or distribution of the noradrenergic innervation within MC and PC regions of the primate PVH.

DISCUSSION

The noradrenergic innervation of the rat and monkey hypothalamus has been demonstrated to be extremely dense, especially within the PVH, as assessed by DßH immunohistochemistry and monoamine fluorescence histochemistry (Fuxe, '65; Swanson and Hartman, '75; Felten and Sladek, '83; Ginsberg et al., '93c). In addition, double labeling studies in rat have shown that noradrenergic afferents form synapses with vasopressin-immunoreactive neurons (Silverman et al., '85; Ochiai and Nakai, '90). The noradrenergic innervation of the rat PVH is derived from three brainstem nuclei (see Fuxe,

'65 for nomenclature), as assessed by retrograde tract tracing combined with DßH immunohistochemistry. Specifically, the A1 cell group projects preferentially to vasopressinergic MC neurons, and the A2 cell group projects to MC and PC PVH regions, whereas the locus coeruleus projects to a restricted region of the PC PVH, notably within the periventricular region (Cunningham and Sawchenko, '88). The monkey PVH receives catecholaminergic input from several fiber bundles originating in the brainstem (Felten and Sladek, '83), however, tract tracing/DßH immunohistochemistry experiments need to be conducted in the primate in order to identify the specific nuclei supplying this innervation pattern.

Dopamine-ß-hydroxylase immunohistochemistry allowed for the discrimination of noradrenergic varicosities from dopaminergic varicosities, however, adrenergic varicosities could not be distinguished from noradrenergic varicosities. Studies in rat using an antibody directed against PNMT, the enzyme which converts norepinephrine into epinephrine, have demonstrated that the dense noradrenergic innervation of the PVH contains a smaller subset of adrenergic terminals (Swanson et al., '81; Liposits et al., '86a). These PNMT-immunoreactive processes are localized to medial PC regions of the PVH and form synaptic contacts with CRF-immunoreactive neurons, whereas regions containing MC neurons have a sparse adrenergic innervation (Swanson et al., '81; Liposits et al., '86a). Experiments have not been conducted in the monkey hypothalamus to assess potential adrenergic innervation. Our present assumption is that the majority of DßH-immunoreactive varicosities quantified in this study are noradrenergic, however it is possible that some are adrenergic, especially within PC regions

and may have contributed to the significant difference that was observed between MC and PC regions.

Behavioral and cognitive characterization of non-human primates deprived of their mother and/or peers has been performed by several investigators (Mitchell et al., '66; Miller et al., '69; Kraemer, '92), and has led to speculation as to what brain regions may be most affected by this early environmental insult. In lieu of the aberrant stress responses, hyperphagia, and decrease in cerebrospinal fluid concentrations of norepinephrine reported in socially deprived macaques, quantitative analysis of the noradrenergic innervation density within MC and PC regions of the PVH was performed. In a previous report in socially reared monkeys, PC regions received a greater innervation density than MC regions (Ginsberg et al., '93c). These results suggested that a single PC neuron receives more DßH-immunoreactive varicosities than a single MC neuron. However, PC neurons outnumber MC neurons in the rat PVH (Swanson and Sawchenko, '83; Kiss et al., '91), possibly indicating that PC neurons receive a greater DßH-immunoreactive input because there are more per unit volume than MC neurons. Also, by virtue of their smaller size, this increase in density may reflect a tighter cell packing phenomena in PC regions of the PVH. In order to assess the number of appositions per chemically-identified neuron, experiments using a double label immunohistochemical procedure have been performed within monkey PVH quantifying the number of DßH-immunoreactive varicosities in apposition to vasopressin- and oxytocin-immunoreactive neurons (Ginsberg et al., '93d). This study demonstrated that vasopressin-immunoreactive neurons received a greater noradrenergic innervation density, especially on

the proximal dendrites, than oxytocin-immunoreactive neurons (Ginsberg et al., '93d).

In addition to the alteration of cerebrospinal fluid norepinephrine content, structural differences in the brains of socially deprived monkeys have been reported in the basal ganglia, cerebellum, hippocampal formation, and neocortex (Struble and Riesen, '78; Floeter and Greenough, '79; Morrison et al., '90; Martin et al., '91; Siegel et al., '92). To date, no changes in the chemoarchitecture of the PVH have been identified. Specifically, this report in conjunction with an assessment of the TIDA neurons and CRF-immunoreactive neurons have demonstrated no significant differences between rearing conditions (Ginsberg et al., '93a). This raises the possibility that chemically-identified circuits within the PVH are not as vulnerable to the early environmental insult of social deprivation in non-human primates as other brain regions (Morrison et al., '90; Martin et al., '91; Ginsberg et al., '92b; Siegel et al., '92). Further quantitative characterization of chemically-specified circuits within several regions that modulate the affected behaviors may reveal additional circuits that are resistant and/or vulnerable to maternal and peer deprivation.

ACKNOWLEDGMENTS

The authors thank Dr. G.W. Kraemer for providing the animals used in the study and detailed description of the rearing conditions and behavior. We also thank Dr. D.T. O'Connor for donating the antiserum, Dr. S.L. Foote and S.J. Siegel for helpful discussions, and R. Woolley for photographic assistance. This research was supported in part by a pilot research grant from the John D.

and Catherine T. MacArthur Foundation Mental Health Research Network I, the Brookdale Foundation, and NIH grant MH45212.

FIGURE LEGEND

Figure 16. Darkfield photomontages within the PVH of a socially reared (**A**) and socially deprived (**B**) rhesus monkeys demonstrating no gross differences in the density and distribution of DßH-immunoreactive processes. Abbreviations: PVH = paraventricular nucleus; III = third ventricle. Scale = 100 µm.

Figure 17. Histogram illustrating the total DßH-immunoreactive varicosity counts in the collapsed sampling area in MC and PC regions for socially reared and socially deprived monkeys. No significant differences were observed between rearing conditions.

Figure 16

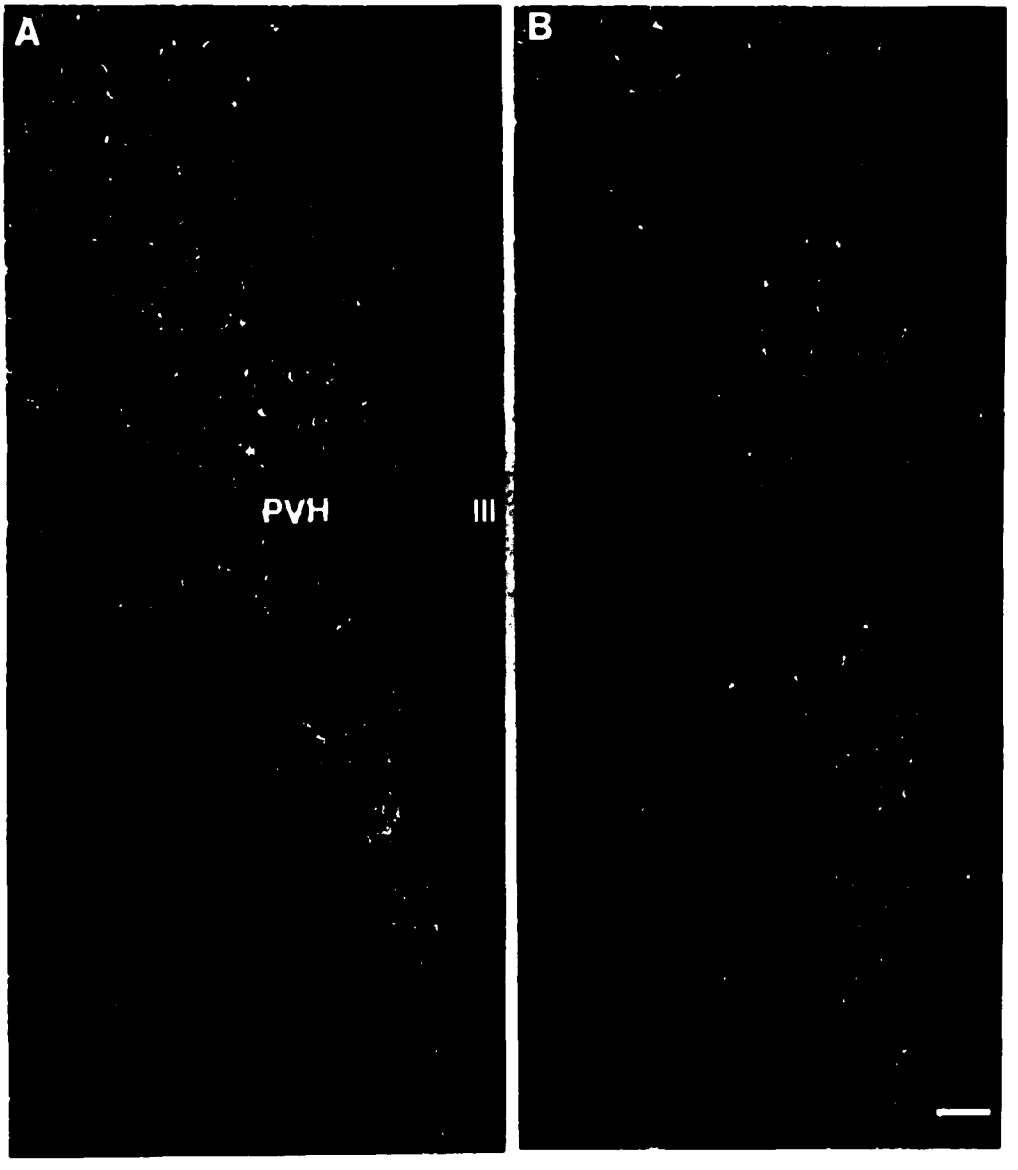

Figure 17

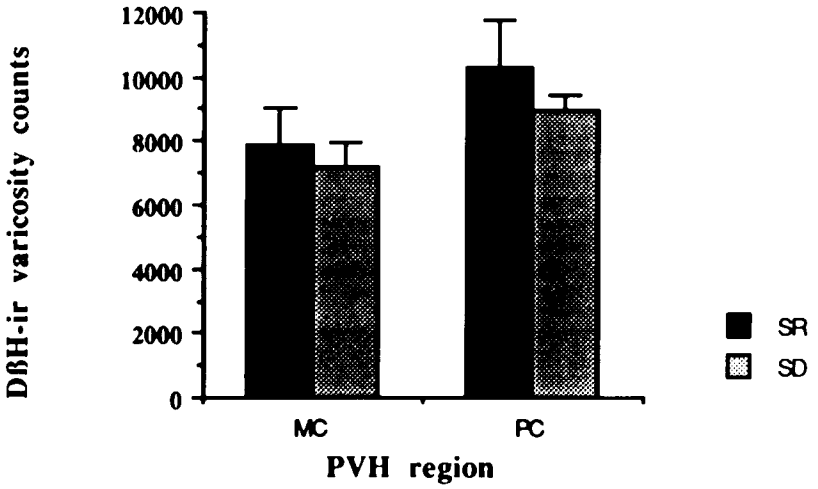
DßH-ir varicosity counts
12000
10000
8000
6000
4000
2000
0
MC
PC
PVH region
SR
SD

Chapter Six

SUMMARY

A major goal in assessing biological determinants of behavior lies in studying the effect(s) of rearing on the development of the central nervous system. Specifically, a series of neuroanatomic analyses have been undertaken to identify potential neuropathological changes seen in monkeys exposed to early social deprivation, which leads to profound psychopathology and inappropriate responses to stress. The animals used in this study were either raised with their mother and peers (socially reared) or raised without maternal/peer contact (socially deprived). Within this context, the distribution of TIDA neurons in the PVH and ARC of rhesus monkeys was determined by immunohistochemistry using an antibody against the enzyme TH, a marker for dopamine-containing systems. Additionally, the distribution of CRF-containing neurons in the PVH was assessed immunohistochemically. The majority (97.5%) of dopaminergic neurons in the PVH displayed PC morphology, with a small (2.5%), but consistently observed population of MC neurons immunoreactive for TH. Within the ARC, TH-immunoreactive neurons were similar in morphology to the PC neurons of the PVH. Qualitative assessment of CRF-immunoreactive neurons in the PVH revealed a PC population of neurons located in medial aspects of the nucleus, similar to what has been observed in the rat. Quantitative analysis revealed no differences in the number of TH- and CRF-immunoreactive neurons between rearing conditions, suggesting that these neurons were not affected, in terms of overall cell counts, by the early environmental insult of social deprivation.

INTRODUCTION

Early social deprivation in primates is known to produce behavioral abnormalities including prolonged and inappropriate responses to stress, alternating hypo- and hyper-aggression, appetitive disorders, and sexual dysfunction that are suggestive of severe neuroendocrine deficits (Kraemer, '91, '92). In this report, the TIDA and CRF systems of rhesus monkeys (*Macaca mulatta*) raised in differential rearing conditions were assessed in regard to their cell density and distribution due to their respective involvement in prolactin secretion and regulation of the HPA axis. Cell counts collected from socially reared animals comprised a normative database that was used as one measure to assess potential neuropathological changes induced by social deprivation. The examination of hypothalamic nuclei involved in the regulation and integration of the reproductive and stress cascades is part of a larger series of experiments within discrete brain regions including amygdala, brainstem, hippocampus, and neocortex designed to assess structures which may be involved in some of the aberrant behavioral and cognitive responses displayed by socially deprived subjects.

The PVH was selected since connectivity studies in rat have demonstrated direct links to multiple structures that include limbic areas (Sawchenko and Swanson, '83b; Oldfield et al., '85; Oldfield and Silverman, '85), circumventricular organs (Sawchenko and Swanson, '83b; McKinley et al., '90), other hypothalamic nuclei (Bai et al., '85; Luiten et al., '87; Ter Horst and Luiten, '87), and brainstem nuclei (Sawchenko et al., '83; Cunningham and Sawchenko, '88; Ter Horst et al., '89; Cunningham et al., '90). Furthermore, the PVH in rat projects to the posterior pituitary, anterior pituitary (via a neurovascular link through the median eminence), brainstem,

and spinal cord (Armstrong et al., '80; Swanson and Kuypers, '80). Thus, the PVH is likely to play a crucial role in the regulation and integration of neuroendocrine and autonomic responses. The ARC was also analyzed because of its dense projection through the external lamina of the median eminence towards the hypophysial portal capillary plexus and resultant modulation of anterior pituitary hormone release, notably prolactin and the gonadotropins (Plant et al., '78; Weigand and Price, '80; Kawano and Daikoku, '87).

Catecholaminergic neurons within the hypothalamus were first described and categorized with monoamine histofluorescence, including a caudal hypothalamic group (A11), an arcuate group (A12), an incertohypothalamic group (A13), and a periventricular group (A14) (Dahlström and Fuxe, '64; Björklund et al., '73; Felten and Sladek, '83). Monoamine histofluorescent neurons intrinsic to the PVH were also described (Felten and Sladek, '83). Immunohistochemical techniques have also been used to analyze the catecholamine-containing systems within the hypothalamus. In particular, antibodies against TH, the rate limiting enzyme in the synthesis of catecholamines, were used to identify putative dopaminergic neurons in the hypothalamus of mouse (Ruggiero et al., '84), rat (Chan-Palay et al., '84; van den Pol et al., '84; Kawano and Daikoku, '87), cat (Kitahama et al., '87), monkey (Goldsmith et al., '90), and human (Li et al., '88).

Corticotropin-releasing factor, a 41 amino acid peptide originally isolated from ovine hypothalamus by Vale et al. ('81), has been demonstrated to be one of the most potent secretagogues for ACTH *in vivo* and *in vitro* (Rivier and Vale, '83; Rivier and Plotsky, '86; Negro-Vilar et al., '87). The human CRF sequence is identical to rat, and differs from the ovine CRF by 7

amino acids (Furutani et al., '83; Shibahara et al., '83). Antibodies directed against human/rat CRF have been used to characterize the distribution of immunoreactive profiles in a variety of species, including rat (Kawano et al., '88; Sawchenko and Swanson, '90), and both New- and Old World monkeys (Paull et al., '84; Foote and Cha, '88). The majority of CRF-immunoreactive neurons are PC cells localized to dorsal medial divisions of the PVH and have been shown in rat to project to the median eminence by retrograde tracing techniques (Weigand and Price, '80; Kawano et al., '88). Since socially deprived monkeys have exaggerated stress responses, the number of CRF-immunoreactive neurons in the PVH were assessed in both rearing conditions to determine whether social deprivation led to changes in the number of this chemically-specified subclass of PC PVH neurons. Some of these data have been reported in abstract form (Ginsberg et al., '91).

MATERIALS AND METHODS

Animals

The animals used in this study were born at the Harlow Primate Laboratory, Madison, Wisconsin, and reared either in a socially enriched environment or in a socially deprived environment. Briefly, socially reared animals were housed from birth to the age of 6 months with their mother and then housed in peer groups of 4 young monkeys per cage. Socially deprived animals were born and kept with their mother in her home cage for 3 days prior to separation, and then taken to the nursery where they remained for 1 month. After 1 month, socially deprived animals were transferred to single cages, and had auditory, olfactory, and visual, but not tactile, contact with

other subjects. Monkeys had free access to water and were fed a fixed amount of monkey chow based upon age and weight. Both male and female monkeys were used in this study. These experiments were conducted within NIH guidelines for animal research and were approved by the IACUC board of the University of Wisconsin.

Immunohistochemical Procedure

The animals were sacrificed in pairs at 1.5 to 2.5 years of age. Monkeys were sedated with ketamine hydrochloride (25 mg/kg i.m.) and anesthetized with sodium pentobarbital (30 mg/kg i.p.), then intubated with an endotracheal tube and ventilated. Prior to transcardial perfusion, 1.5 ml of 1% aqueous sodium nitrite was injected into the left ventricle to induce vasodilation. Ice-cold 1% paraformaldehyde in PBS (0.12 M, pH 7.4) was delivered via a perfusion pump (275 - 325 ml/min) as an initial rinse of the vascular system for 45 - 60 seconds followed by ice-cold 4% paraformaldehyde in PBS delivered at the same flow rate for an additional 8 - 9 minutes. Brains were removed and hypothalamic blocks were cut in the coronal plane and post fixed in 4% paraformaldehyde for six hours then cryoprotected in a series of 12%, 16%, and 18% sucrose solutions in PBS.

Hypothalamic blocks were removed from 18% sucrose and frozen in dry ice prior to being cut on a cryostat. A 1 in 13 series of 30 μm thick sections through the extent of the hypothalamus was taken, effectively sampling every 390 μm. One series was stained with thionin and used in conjunction with Bleier's ('84) atlas of the rhesus monkey hypothalamus. An adjacent series was processed for immunohistochemistry using a polyclonal rabbit antiserum directed against TH that was purified from a rat pheochromocytoma clonal cell line and used at a working dilution of 1:2,000. Another adjacent series

was processed for immunohistochemistry using a polyclonal rabbit antiserum directed against human/rat CRF. Both primary antisera have been fully characterized previously and shown to crossreact with monkey TH and CRF, respectively (Markey et al., '80; Vale et al., '83; Lewis et al., '87; Foote and Cha, '88).

Tissue sections were incubated overnight in a PBS solution containing the primary antisera, 0.3% Triton X-100, and 0.5 mg/ml bovine serum albumin at 4°C. The secondary and tertiary steps were done using the Vectastain method (Vector Laboratories, Burlingame, CA) with DAB (Sigma, St. Louis, MO) as a chromogen. The reaction product was intensified with 0.05% cobalt chloride and 0.05% nickel ammonium sulfate added to the DAB solution. The tissue sections were then mounted on chrome-alum coated slides, cleared through an ascending ethanol series and coverslipped with DPX (Fluka, Germany) mounting media. Failure to add the primary, secondary, or tertiary reagents resulted in no immunohistochemical labeling of the tissue.

Data Analysis

All investigators were blind to the rearing conditions of the monkeys. Qualitative inspection of TH- and CRF-immunoreactive profiles was done using a Zeiss Axiophot photomicroscope at a magnification of 100x and 200x. Quantitative assessment of TH- and CRF-immunoreactive neurons was performed on 9 immunostained sections evenly spaced throughout the rostrocaudal extent on the left PVH (and ARC for TH) of each animal for a total of 90 tissue sections analyzed per antibody series. The analysis was done at a magnification of 200x on a computer-assisted microscopy system consisting of a Zeiss Axiophot photomicroscope equipped with a Zeiss

MSP65 computer-controlled stage, a DEC 3100 workstation, a Macintosh IIci server, and custom designed morphometry software. In this analysis scheme, each selected immunoreactive cell had a fixed *x*, *y*, and z coordinate attributed to it relative to a 0, 0, 0 (home) point recorded in a datafile for each section. Immunoreactive neurons were counted if one or more processes were immunolabeled and/or the nucleus was visible by being immuno-negative relative to the stained perikarya. The TH-immunoreactive incertohypothalamic (A13) and periventricular (A14) cell groups were not included in the quantitative study. The number of TH- and CRF-immunoreactive neurons for 9 sections per animal was collapsed to yield a total value for comparison across conditions. Statistical analysis was performed using a Student's *t*-test.

RESULTS

TH-immunoreactive neurons in the PVH

Tyrosine hydroxylase-immunoreactive dendritic processes, fibers, and cell bodies were observed throughout the rostrocaudal extent of the PVH. One to two unbranched, primary dendrites were typically identified exiting TH-immunoreactive cell bodies at the apical and basal poles. Tyrosine hydroxylase-immunoreactive fibers contained both intervaricose segments and small (approximately 1 μm in diameter), punctate varicosities. Within the PVH, the majority (97.5%) of TH-immunoreactive cells displayed PC morphology, as determined by their size and fusiform shape, and dispersed throughout medial regions of the PVH, approximately 225 - 275 μm lateral to the third ventricle. A few (2.5%) large, multipolar MC neurons were observed

to contain TH immunoreactivity and were scattered in lateral aspects of the PVH, bordering the surrounding AHA (Fig. 18). Tyrosine hydroxylase-immunoreactive MC neurons were significantly larger in long axis cross section than PC neurons (n = 30 neurons in 4 monkeys for both MC and PC neurons, mean 31.9 ± 0.9 (SEM) μm versus 17.4 ± 0.6 μm, $p < 0.001$). Quantitative analysis of both PC and MC TH-immunoreactive neurons on 9 tissue section levels within the PVH demonstrated a clear rostrocaudal distribution of cells. The mid portion of the nucleus, corresponding to levels 3 - 6 in this study and plates 8 - 10 in Bleier's ('84) atlas, contained approximately 80% of all the neurons counted in the PVH (Table 4). Both the rostral and caudal regions of the nucleus contained approximately 10% of the TH-immunoreactive neurons. A representative distribution of TH-immunoreactive neurons through the rostrocaudal extent of the PVH in one monkey is shown in Figure 19.

TH-immunoreactive neurons in the ARC

Both TH-immunoreactive perikarya and fibers were observed in the ARC. Fibers which contained TH immunoreactivity tended to be located in the periventricular zone lateral to the subependymal layer of the third ventricle. Tyrosine hydroxylase-immunoreactive neurons were similar in size and morphology to the PC neurons in the PVH. Within the ARC, TH-immunoreactive neurons tended to cluster in ventrolateral portions of the nucleus and in the periventricular zone ventral and lateral to the subependymal layer of the third ventricle (Fig. 20).

CRF-immunoreactive neurons in the PVH

Corticotropin-releasing factor-immunoreactive neurons were primarily localized in vertical arrays approximately 140 - 210 μm lateral to the third

ventricle in rostral and middle regions of the PC portion of the PVH (Fig. 21). Few, if any, CRF-immunoreactive profiles were observed in caudal regions of the PVH. The CRF-immunoreactive neurons were small, fusiform, with darkly stained perikarya and faintly labeled dendrites. Two primary dendrites typically exited from both the apical and basal aspects of the somata. Lightly stained neurons exhibiting MC morphology were very rarely observed in a few monkeys, and no consistent pattern was detectable. Compared with the TH-immunoreactive neurons of the PVH, the CRF-immunoreactive neurons were smaller, tightly packed, and found in a more medial location. These two PC populations did not appear to colocalize through adjacent section analysis.

Social Deprivation

Qualitative observations revealed no significant differences in the size, shape, or distribution of TH-immunoreactive neurons in the PVH or ARC between rearing conditions. Similarly, no appreciable differences were seen in the intensity of immunostaining or distribution of dendritic processes, fibers, or terminals. Quantitative analysis of total TH-immunoreactive neurons counted in this analysis scheme revealed no significant differences between the two rearing conditions, as 880.0 ± 66.0 (SEM) immunoreactive PC neurons were tabulated in the PVH of 5 socially reared monkeys, and 879.4 ± 39.1 were counted in 5 socially deprived monkeys (Fig. 22). Similarly, no significant differences were observed for MC TH-immunoreactive neurons, as 21.4 ± 2.3 cells were tabulated in the PVH of socially reared monkeys, and 23.6 ± 1.4 were counted in the socially deprived monkeys. No significant differences were observed between rearing conditions for TH-immunoreactive neurons in the ARC, as 310.6 ± 17.4 cells were counted in the

socially reared monkeys and 281.0 ± 21.7 were counted in the socially deprived monkeys. Additionally, no significant differences were observed in the number of CRF-immunoreactive neurons in the PVH as 671.0 ± 83.1 cells were counted in 5 socially reared monkeys and 867.0 ± 89.2 were tabulated in 5 socially deprived monkeys (Fig. 21). These data indicated a low degree of variability in TH- and CRF-immunoreactive neuron counts within and across the rearing conditions, suggesting that the TH and CRF immunoreactivity of these neurons within the PVH was consistent across animals with identical rearing history and was not affected by the early environmental insult of social deprivation.

DISCUSSION

TH immunoreactivity in the PVH and ARC

In this report TIDA neurons in the PVH and ARC of rhesus monkeys were visualized and quantified by using an antibody against TH. Tyrosine hydroxylase-immunoreactive neurons in the hypothalamus are presumed to be dopaminergic as these cells in rat and monkey are not labeled by antibodies directed against DßH and PNMT, the enzymes involved in the conversion of dopamine to norepinephrine, and norepinephrine to epinephrine, respectively (Swanson et al., '81; Liposits et al., '86b; Ginsberg et al., '93c). Similarly, an equivalent distribution of cell bodies and fibers has been described in the rat PVH using an antibody directly against glutaraldehyde-conjugated dopamine (Buijs et al., '84). Pharmacological and surgical lesioning studies which destroyed ascending catecholaminergic fibers to the diencephalon did not affect TH-immunoreactive fibers in the

PVH of rats, also suggesting that an intrinsic dopamine-containing system exists in the PVH along with the well characterized noradrenergic and adrenergic inputs (Lindvall et al., '84; Liposits and Paull, '89). Furthermore, the presence of TH-immunoreactive fibers and terminals is in agreement with previous reports in rat using monoamine histofluorescence and TH immunohistochemistry (Swanson et al., '81; Lindvall et al., '84; Decavel et al., '87). The total number of TH-immunoreactive neurons counted in this report is in agreement with a quantitative analysis of TH-immunoreactive neurons in the hypothalamus of juvenile cynomolgus monkeys (Goldsmith et al., '90).

Dopamine has been proposed to subserve many functions within the neuroendocrine axis, notably in the stress and maternal/reproductive responses (Moore et al., '87). In MC neurons, which project through the internal lamina of the median eminence to the posterior pituitary, dopamine has been reported electrophysiologically and pharmacologically *in vivo* and *in vitro* to modulate vasopressin- and oxytocin-containing cells, as well as having a direct effect on the neurohypophysis, indicating an effect at the cell body and at the terminals (Bridges et al., '76; Moos and Richard, '82; Mason, '83; Buijs et al., '84). Hyperosmotic stress, such as salt loading, has been demonstrated in rat to increase TH immunohistochemical staining and TH mRNA levels in MC neurons of the PVH (Kiss and Mezey, '86; Young et al., '87). Dopamine has also been reported to facilitate the milk ejection reflex in lactating rats (Moos and Richard, '82). Additionally, reports in rabbit and human indicate that TH immunoreactivity is colocalized with oxytocin immunoreactivity in a subset of MC neurons (Schimchowitsch et al., '83; Li et al., '88). Alternatively, dopamine has been proposed to affect anterior pituitary function via the projection of PC neurons to the portal capillary

plexus through the external lamina of the median eminence, notably to inhibit prolactin release from lactotrophs (Neill et al., '81; Moore et al., '87). Approximately 66% of TH-immunoreactive neurons in the monkey PVH, ARC, and adjacent periventricular zone have been demonstrated by retrograde labeling to project to the median eminence, suggesting that these neurons belong to the TIDA system (Goldsmith et al., '90). Within the rat ARC, TIDA neurons have been demonstrated immunohistochemically to colocalize a variety of neuropeptides, including GABA and GAD (Everitt et al., '84b; Schimchowitsch et al., '91), growth hormone-releasing factor (Okamura et al., '85), and neurotensin (Ibata et al., '83). Another small population of PC dopaminergic neurons has been reported in rat to project to the brainstem and thoracic spinal cord, as determined by retrograde labeling combined with immunohistochemistry and/or monoamine histofluorescence, suggesting a role for dopamine in the modulation of autonomic responses, such as the regulation of sympathetic outflow (Swanson et al., '81; Skagerberg and Lindvall, '85).

In addition to extrahypothalamic projections, the TH-immunoreactive neurons of the PVH have dendritic arborizations within the nuclear borders, suggesting that this chemically-defined subclass of neurons plays a role in the local circuitry of the PVH, notably influencing neurons which synthesize and secrete CRF. An immunoelectron microscopy study of rat PVH revealed that asymmetric synapses exist between TH-immunoreactive processes and CRF-immunoreactive perikarya (Liposits et al., '86c). A similar study performed in monkey PVH indicated that CRF-immunoreactive terminals synapse on TH-immunoreactive perikarya (Thind and Goldsmith, '89). These two reports implicate a local short loop feedback circuit within the PVH that may

modulate the stress response prior to the resultant stress cascade. Therefore, these data suggest that dopamine in the PVH subserves both extra- and intra-hypothalamic functions, potentially modulating endocrine and autonomic responses at multiple levels.

CRF immunoreactivity in the PVH

In addition to the analysis of TIDA neurons, the distribution of CRF-immunoreactive perikarya in the PVH of rhesus monkeys was assessed quantitatively. Previous observations in the PVH of both New- and Old World monkeys are in agreement with the distribution of CRF-immunoreactive neurons in this report (Paull et al., '84; Foote and Cha, '88). The majority of CRF-immunoreactive neurons were localized to a medial PC portion of the PVH, which is also consistent with observations in the rat (Kawano et al., '88; Sawchenko and Swanson, '90). In terms of overall PVH organization in the primate, the CRF-immunoreactive neurons appear as a distinct cluster of PC neurons, smaller, more densely packed, and medial to the PC population of TH-immunoreactive neurons. Magnocellular neurons which express either vasopressin or oxytocin have been identified laterally to both populations of TH- and CRF-immunoreactive neurons, and are currently being assessed in regard to their location and relationship to noradrenergic afferents (Ginsberg et al., '93d). To date, a comprehensive parcellation of PVH subnuclei, as described in rat (Armstrong et al., '80; Swanson and Kuypers, '80), cannot be properly ascribed in monkey due to the lack of retrograde and/or anterograde tracing studies.

Corticotropin-releasing factor has been demonstrated to be a powerful central regulator of the HPA axis, specifically stimulating the release of ACTH from anterior pituitary corticotrophs. Corticosteroid manipulation has

direct effects on CRF mRNA and peptide levels in rat PVH, as assessed by *in situ* hybridization and immunohistochemistry, respectively (Kovacs and Mezey, '87; Swanson and Simmons, '89). Glucocorticoid receptors have been immunohistochemically localized to CRF-immunoreactive neurons in the rat PVH, and are also responsive to corticosteroid administration (Liposits et al., '87). Norepinephrine has also been reported to facilitate the release of CRF into the portal vasculature (Plotsky, '87). Similarly, in rhesus monkey PVH, DßH-immunoreactive varicosities are extremely dense in the PC region that contains the CRF neurons (Ginsberg et al., '93c). In addition to the effects on the HPA axis, CRF administration has been reported in a dose- and environment-dependent fashion, to increase arousal, specifically eliciting anorexigenic, anxiety-like, and self-directed responses in rhesus monkeys (Kalin, '85; Glowa and Gold, '91). In light of these stress and pronounced behavioral responses to CRF, the location and distribution of CRF-immunoreactive neurons was examined in both socially reared and socially deprived monkeys to see if rearing environment affected the overall number of cells expressing the peptide.

Social Deprivation

Social deprivation, including maternal/peer deprivation, has been investigated in several monkey species for almost four decades (Harlow et al., '71; Kraemer, '91, '92). Behavioral and cognitive testing has allowed for some speculation as to what brain regions may be most affected. In this report, hypothalamic nuclei were investigated in order to relate the observed neuroendocrine deficits with structural alterations as part of a larger series of experiments designed to identify potential neuropathological changes in the brains of socially deprived rhesus monkeys. Specifically, cell counts were

performed on TIDA and CRF PVH neurons as one measure to assess the effect of rearing on hypothalamic structure. Ideally, cell counts would be augmented with receptor density, neurotransmitter turnover, and ultrastructural analyses. However, the tissue in this series of experiments was dedicated to systematic light microscopic examination and quantification in several discrete brain regions, excluding the possibility for neurochemical and/or ultrastructural assessment.

To date, relatively few, precise neuropathological changes in the brains of socially deprived animals have been identified. Structural differences have been reported in the basal ganglia, dentate gyrus of the hippocampus, vestibular cerebellum, and neocortex of socially deprived monkeys (Struble and Riesen, '78; Floeter and Greenough, '79; Morrison et al., '90; Martin et al., '91; Siegel et al., '92). Within dopaminergic systems, Morrison et al. ('90) reported fewer TH-immunoreactive fibers in neocortex of socially deprived rhesus monkeys. Martin et al. ('91) reported alterations in the chemoarchitecture of the basal ganglia in rhesus monkeys, notably a loss of TH immunoreactivity in the striatal matrix, but not in the amygdala and other basal forebrain regions. In addition, Martin et al. ('91) reported that 40% of the neurons synthesizing TH in the substantia nigra/ventral tegmental area, the major source of striatal and cortical dopamine, lose the ability to express this enzyme, although these cell bodies appear normal in Nissl preparations. A potential confound is that this study was conducted in aged socially deprived animals, and that the substantia nigra has been demonstrated to be susceptible to neuronal cell loss in normal human aging (Fearnley and Lees, '91). The study by Martin et al. ('91) was performed using rhesus monkeys exposed to total social isolation as opposed to the partial social isolation

paradigm used in the present experiments. The severity of the deprivation paradigm may also be an important factor in the lack of affect of rearing condition on the PVH. Nonetheless, a picture of differential involvement of dopaminergic systems emerges when comparing the results of this report with the former findings. The apparent sparing of the TH-immunoreactive neurons in the PVH and ARC relative to those in the substantia nigra/ventral tegmental area may underscore distinct morphological and connectivity patterns of these chemically-defined neurons which have differential vulnerability to an early environmental insult. Further investigation of the substantia nigra/ventral tegmental area should be examined in young socially deprived animals to minimize the potential confounding effect of age-related neuronal loss. A similar resistance to morphologic changes in response to aberrant rearing conditions is reported for CRF-containing neurons in the PVH of this same group of subjects, indicating that the chemoarchitecture of the PVH may not be as vulnerable to the early environmental insult as other brain regions (Morrison et al., '90; Martin et al., '91; Ginsberg et al., '92b; Siegel et al., '92). Additional anatomic and biochemical evaluation of central and peripheral sites within the HPA axis is necessary to clarify the degree to which other components of this system are susceptible to the effects of social deprivation.

ACKNOWLEDGMENTS

The authors thank Dr. G.W. Kraemer for providing a detailed description of the rearing conditions and behavior of the animals used in this study. We thank Dr. M. Goldstein (anti-TH) and Dr. W.W. Vale (anti-CRF) for donating the antisera, Dr. W.G. Young for software development, Dr. S.L.

Foote for helpful discussions, and R. Woolley for photographic assistance. This research was supported in part by a pilot research grant from the John D. and Catherine T. MacArthur Foundation Mental Health Research Network I, the Brookdale Foundation, and NIH grant MH45212.

Table 4. Rostrocaudal distribution of TH-immunoreactive neurons in the PVH of 10 monkeys

PVH region	TH-ir cells % ± SEM
rostral (levels 1-2)	10.3 ± 1.5
mid (levels 3-6)	79.1 ± 1.8
caudal (levels 7-9)	10.6 ± 1.2

Note Percentage of TH-immunoreactive neurons in rostral, mid, and caudal regions in the PVH of ten rhesus monkeys. Approximately 80% of all TH-immunoreactive neurons lie within the mid portion of the nucleus.

FIGURE LEGEND

Figure 18. Brightfield photomicrographs of TH-immunoreactive neurons in the PVH of a rhesus monkey demonstrating the cell morphology of immunoreactive profiles **A**: A representative field of PC TH-immunoreactive neurons lateral to the third ventricle. **B**: A TH-immunoreactive MC neuron. The third ventricle is to the right. Abbreviations: PVH = paraventricular nucleus of the hypothalamus; III = third ventricle. Scale = 100 μm.

Figure 19. Histogram demonstrating the distribution of TH-immunoreactive neurons counted in the PVH of one rhesus monkey in each of the nine levels used in the analysis. A total of 924 TH-immunoreactive neurons were tabulated for this animal. Note that levels 3 - 6, which correspond to the mid portion of the nucleus, contain the majority of immunoreactive neurons.

Figure 20. Brightfield photomontage of TH-immunoreactive neurons and fibers the ARC in a rhesus monkey demonstrating the distribution of immunoreactive profiles. Abbreviations: ARC = arcuate nucleus; PVZ = periventricular zone; III = third ventricle. Scale = 100 μm.

Figure 21. Brightfield photomicrographs in the medial PC region of the PVH demonstrating the distribution of CRF-immunoreactive neurons in a socially reared (**A**) and a socially deprived (**B**) rhesus monkey. No alterations in the size, shape, or number of CRF-immunoreactive perikarya was observed. Abbreviations: PVH = paraventricular nucleus; III = third ventricle. Scale = 100 μm.

Figure 22. Brightfield photomicrographs of the PVH in a socially reared (**A, C, E**) and a socially deprived (**B, D, F**) rhesus monkey through rostral, mid, and caudal levels demonstrating no gross differences in TH-immunoreactive neuron distribution or relative density. Abbreviations: PVH = paraventricular nucleus; III = third ventricle. Scale = 100 μm.

Figure 18

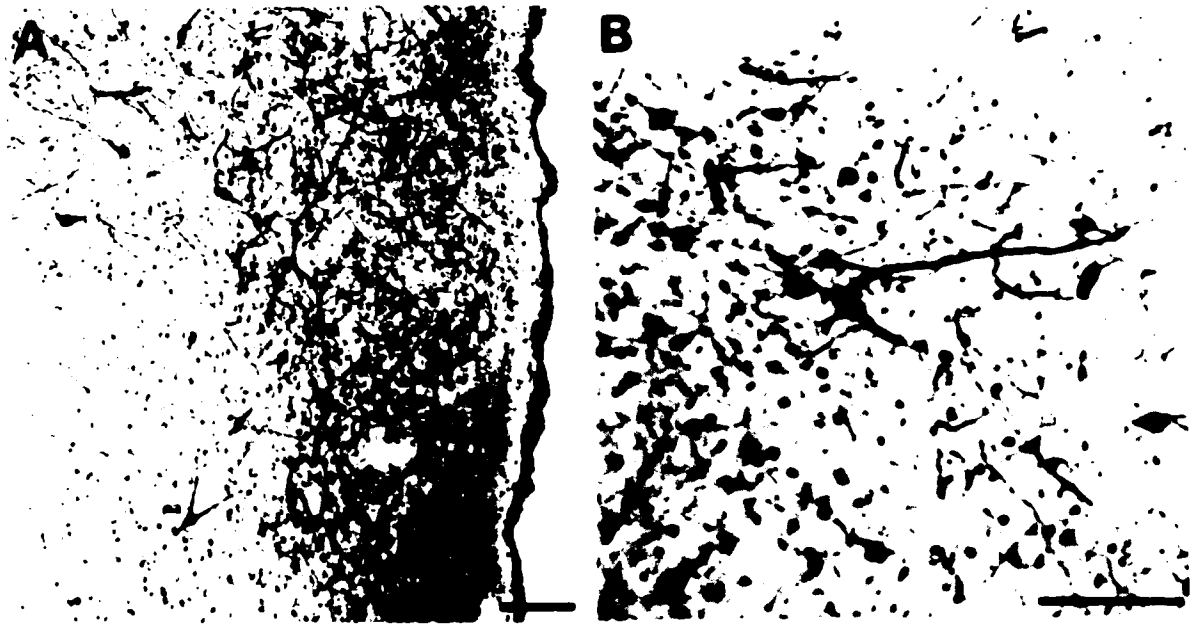

Figure 19

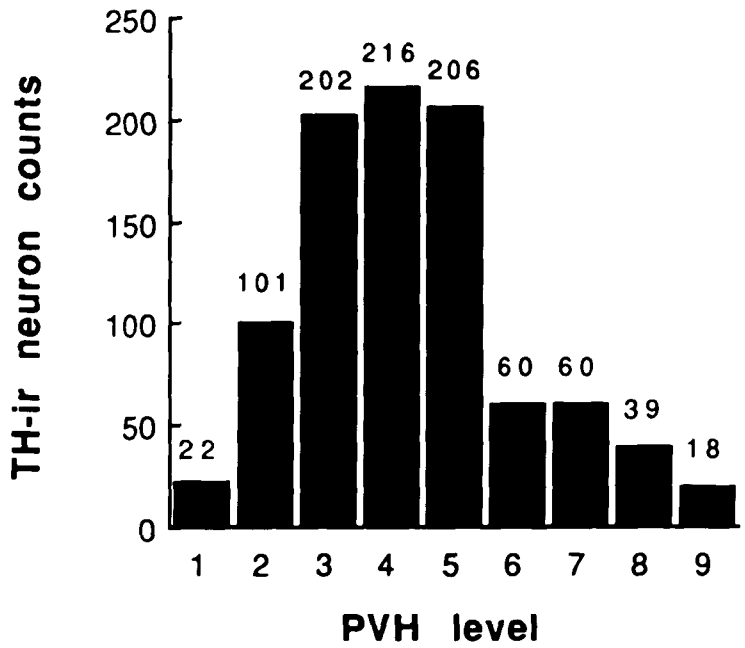
250
200
150
100
50
0
TH-ir neuron counts
22
101
202
216
206
60
60
39
18
1
2
3
4
5
6
7
8
9
PVH level

Figure 20

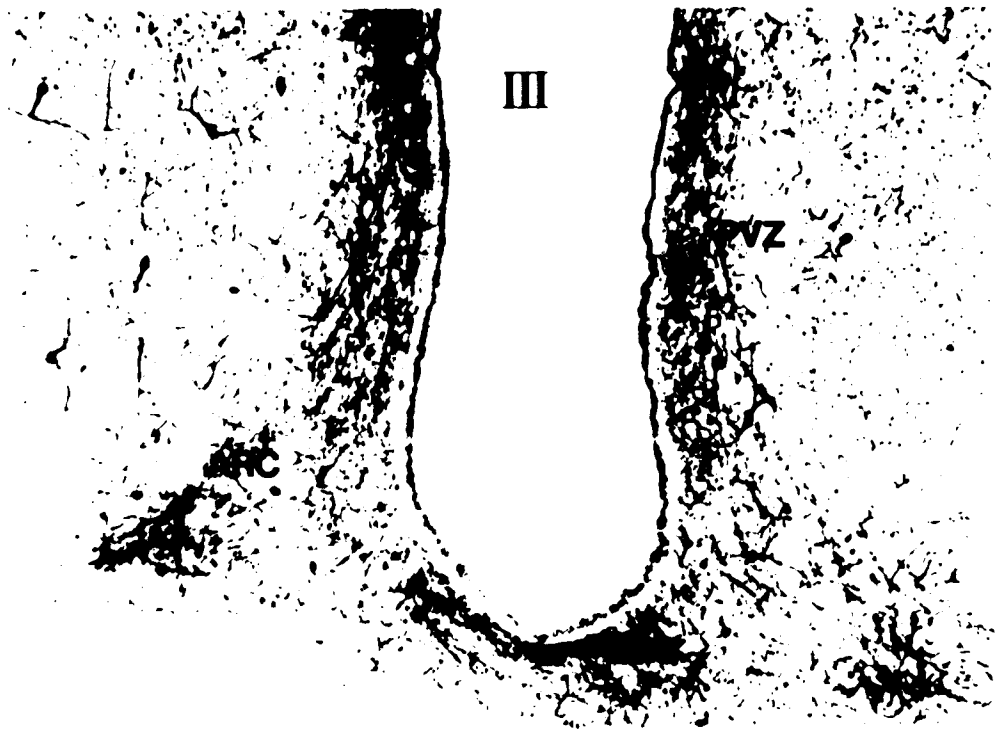

Figure 21

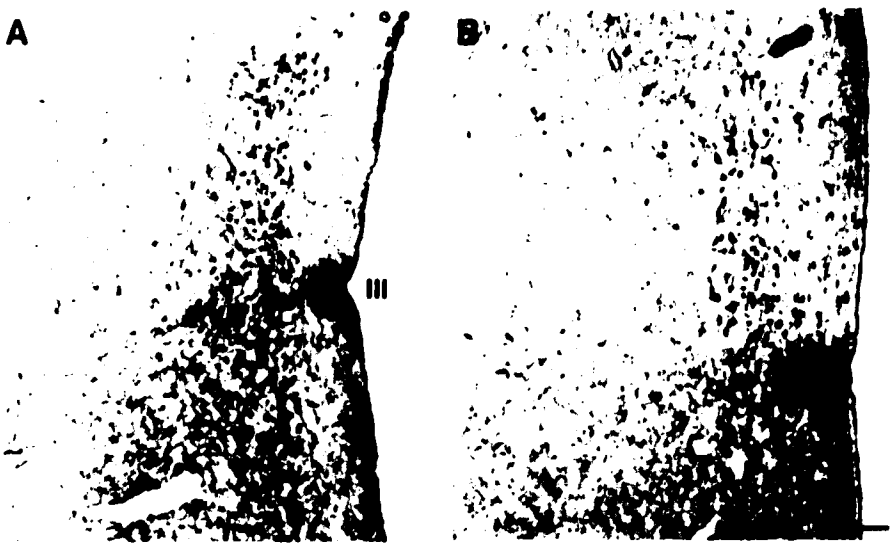

Figure 22

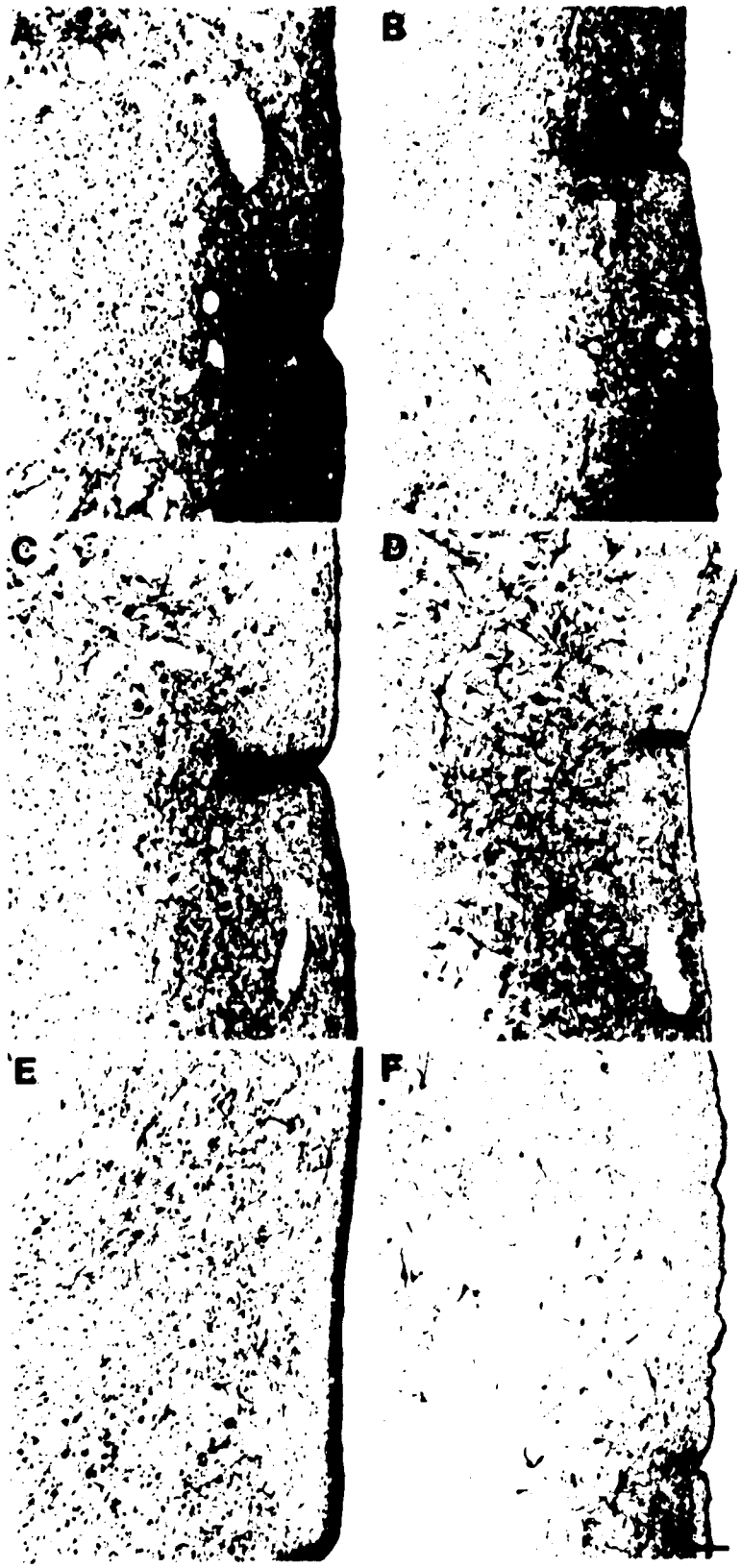

Chapter Seven

Noradrenergic innervation of the monkey hypothalamus

In specific aim 1, the distribution of noradrenergic-containing structures was assessed in the rhesus monkey hypothalamus, midline thalamus, and subthalamic areas using an antibody directed against DßH. Qualitative observations within these diencephalic areas revealed striking interregional differences in DßH immunoreactivity which are summarized in Chapter Three. Within the hypothalamus, a rostrocaudal distribution of DßH-immunoreactive fibers was observed, where the rostral two-thirds contained a greater noradrenergic innervation density than the caudal one-third. Additionally, a mediolateral gradient in the distribution of hypothalamic DßH immunoreactivity was observed, with medial regions tending to be more densely innervated than lateral regions. This pattern of DßH immunoreactivity may reflect the multiple noradrenergic fiber tracts innervating the monkey hypothalamus, with anteromedial regions receiving inputs from at least three different fiber tracts, including the dorsal, ventral, and periventricular noradrenergic bundles, which have been characterized in rhesus monkey by monoamine histofluorescence (Schofield and Everitt, '81; Tanaka et al., '82; Felten and Sladek, '83). One exception to the mediolateral gradient, however, was the dense DßH-immunoreactive innervation of the laterally-located SON, which clearly demarcated this nucleus from the surrounding AHA and LHA. This preferential innervation of the SON may reflect a neurotrophic effect of vasopressin, and to a lesser degree, oxytocin on noradrenergic afferents as an ontogenetic study in rat SON and PVH

demonstrated that neurophysin immunoreactivity within MC neurons precedes the visualization of monoamine histofluorescent varicosities (Khachaturian and Sladek, '80). Similarly, in the Brattleboro rat, which has a vasopressin deficiency due to a single base deletion in the second exon encoding part of the neurophysin carrier protein (Schmale and Richter, '84), there appears to be an alteration in noradrenergic input (Versteeg et al., '78; Schöler and Sladek, '81, '82). The neurotrophic effect of vasopressin and oxytocin on noradrenergic afferents may be specific to the hypothalamo-neurohypophysial system, since ontogenetic studies in rat have suggested that the development of the locus coeruleus noradrenergic system precedes the differentiation of cerebellar and hippocampal target neurons (Lauder and Bloom, '74, '75). Detailed ontogenetic studies characterizing the development of intrinsic and afferent inputs within the monkey hypothalamo-neurohypophysial system are presently lacking. These experiments would be of comparative value in relation to the development of normal and Brattleboro rats as well as humans suffering from diabetes insipidus.

In terms of a marker for norepinephrine in the primate hypothalamus, DßH immunohistochemistry reported in Chapter Three is in agreement with previous investigations within the monkey hypothalamus using monoamine fluorescence histochemistry where the catecholaminergic innervation was attributed to norepinephrine-containing structures as opposed to dopamine-containing structures. For example, Hoffman et al. ('76) and Ishikawa and Tanaka ('77) have suggested that the dense plexus of histofluorescent fibers in the internal lamina, rather than the external lamina, of the median eminence were noradrenergic. Similarly, the histofluorescent neurons within the monkey hypothalamus have been demonstrated to be dopaminergic since

TH, but not DßH, immunoreactivity has been localized within hypothalamic perikarya (Felten and Sladek, '83; Goldsmith et al., '90). In addition, DßH immunohistochemistry in monkey hypothalamus has revealed a continuity of the DMH and ARC that has received little attention using cytoarchitectonic methods. Broadwell and Bleier ('76) and Bleier ('84) have reported in mouse and rhesus monkey, respectively, the similarity of cell types within the PNZ which connects the ARC and DMH. The DßH innervation pattern may therefore indicate some shared function of these two nuclei, possibly modulating a NPY-immunoreactive input into the PVH (Bai et al., '85; Ter Horst and Luiten, '87). Furthermore, early lesion and neuropharmacologic studies attributed noradrenergic induced feeding behaviors to the VMH (Booth, '68; Albert et al., '71; Martin and Myers, '75). In lieu of the dense DßH-immunoreactive innervation of the ARC and DMH relative to the paucity of DßH-immunoreactive input to the VMH, the possibility exists that the ARC and DMH may also be in involved in feeding behavior. Discrete assessment of the ARC, DMH, and VMH in relation to noradrenergic varicosity input, adrenergic receptor localization, and feeding behavior is necessary to clarify these relationships.

Noradrenergic innervation of the PVH

In specific aim 2, quantification of DßH-immunoreactive varicosities within MC and PC regions of the PVH was performed using the LSM. The PVH was chosen as a circumscribed nucleus within the monkey hypothalamus for regional DßH innervation density assessment due to the potent effects of norepinephrine on the release of vasopressin and oxytocin from MC neurons and CRF from PC neurons. Both MC and PC divisions of the PVH contained extremely dense terminal field input, making any

differences in innervation density within the PVH difficult to assess through qualitative observations. Therefore, a hypothesis was tested to see if any quantitative differences in noradrenergic innervation density between MC and PC regions existed. The results in Chapter Three suggested that PC neurons received a greater noradrenergic innervation density than MC regions, a result that was replicated in a group of socially deprived monkeys in Chapter Five. These data indicated that PC neurons receive more DßH-immunoreactive varicosities per unit volume than MC neurons, even though there appear to be size, packing density, and numeric differences between PC and MC neurons (see Chapters Three and Five). The specific brainstem noradrenergic cell groups which supply these projections to the monkey PVH need to be elucidated. However, studies in rat suggest that PC regions are innervated by the A2 and locus coeruleus, whereas MC regions are preferentially innervated by A1 afferents (Cunningham and Sawchenko, '88; Day, '89). The convergence of noradrenergic inputs to PC neurons may be a determining factor in terms of the total number of varicosities present relative to MC neurons.

The DßH immunohistochemical method used in specific aim 2 allowed for the quantification of DßH-immunoreactive varicosities within circumscribed regions of the PVH, but did not delineate the cellular structures receiving this noradrenergic innervation. Potential targets included MC neurons, PC neurons, glia, and blood vessels (Ginsberg et al., '93c, '93d). Since several qualitative double labeling studies in rat and monkey PVH have suggested that MC vasopressin-immunoreactive neurons receive a denser noradrenergic innervation than oxytocin-immunoreactive neurons (McNeill and Sladek, '80; Sladek and Zimmerman, '82), specific aim 3 was designed to

quantitatively assess the density and distribution of DßH-immunoreactive varicosities in apposition to vasopressin- and oxytocin-immunoreactive perikarya using double label immunohistochemistry combined with laser scanning microscopy. The hypothesis being tested was that quantitative analysis would reveal differential input to vasopressin- or oxytocin-immunoreactive neurons which could not be precisely assessed qualitatively. The results reported in Chapter Four demonstrated that vasopressin-immunoreactive neurons received a greater noradrenergic innervation density than oxytocin-immunoreactive neurons, with approximately two-thirds of the DßH-immunoreactive varicosities in apposition to proximal dendrites, and the other one-third in apposition to the somata. In contrast, oxytocin-immunoreactive neurons did not receive a differential input of DßH-immunoreactive varicosities on the proximal dendrites relative to the somata. The confocal analysis is in agreement with a previous double labeling electron microscopic study in the rat PVH where approximately two-thirds of the asymmetric, noradrenergic synapses on vasopressin-immunoreactive neurons were axodendritic and approximately one-third were axosomatic (Silverman et al., '85). The high density of noradrenergic afferent input to the proximal dendrites and somata of vasopressin-immunoreactive neurons is in a position to have profound effects on the activity of these cells. Clearly, noradrenergic afferent input has robust physiological effects on vasopressinergic neurons (Day et al., '84; Blessing and Willoughby, '85; Day, '89).

Thus, a goal of this project was achieved through qualitative and quantitative assessment of the noradrenergic innervation of the PVH as outlined by specific aims 1 - 3. Specifically, a regional, qualitative study of the

DßH-immunoreactive input within the macaque hypothalamus revealed a dense noradrenergic input to the PVH. Quantitative analysis of this restricted region indicated a dense DßH-immunoreactive input to both MC and PC regions, with the latter receiving a greater noradrenergic input per unit volume. Further quantitative assessment of DßH-immunoreactive varicosities in apposition to postsynaptic targets yielded distribution and density differences between the two subpopulations of MC neurons, with vasopressin-immunoreactive perikarya receiving more noradrenergic contacts, coinciding with a potent physiologic response. In summary, this cohesive series of specific aims and hypotheses addresses an important structure-function correlation within a non-human primate brain structure that is critical for homeostatic functioning, notably the integration and modulation of nutrient intake, stress, and autonomic outflow (Luiten et al., '87; Swanson '87). This approach is by no means restricted to the rhesus monkey hypothalamus. However, the PVH was an ideal region to commence these types of analyses on anatomic circuits with defined physiologic functions because the output of the target neurons (e.g. MC vasopressin and oxytocin and PC CRF neurons) have been well characterized morphologically, pharmacologically, and physiologically (Harris, '48; Bargmann and Scharrer, '51; Antunes and Zimmerman, '78; Swanson and Kuypers, '80; Sawchenko and Swanson, '90; Renaud and Bourque, '91). In addition, another goal of this project was to develop a normative, quantitative database for chemically-specified hypothalamic circuits that will allow for the assessment of a wide variety of experimental manipulations, including those that are environmentally induced, such as social deprivation (see specific

aims 4 - 6) as well as perturbations that are developmental or neurodegenerative in nature.

Social Deprivation

Maternal and peer deprivation has been demonstrated to cause severe behavioral abnormalities in rhesus monkeys (Harlow et al., '71; Kraemer, '92; see Appendix). In an attempt to correlate structural alterations associated with the observed behavioral dysfunction, a series of neuropathological examinations was conducted within discrete brain regions of socially deprived monkeys. In specific aims 4 - 6, DßH-, CRF-, and TH-immunoreactive processes were investigated within the PVH (and ARC for TH) in order to relate the observed neuroendocrine deficits with structural changes (see Table 5).

The hypothesis tested in specific aim 4 was to see if the noradrenergic innervation within the PVH that was characterized in specific aims 1 - 3 varied as a function of rearing history. The results reported in Chapter Five suggested that DßH varicosity density within both MC and PC regions of the PVH was not affected by the early environmental insult of social deprivation since no significant differences were tabulated between rearing conditions. This investigation did not assess adrenergic receptor density or noradrenergic turnover, however, the afferent input into the PVH appeared to be preserved. A possible explanation for this sparing of noradrenergic input is that synaptic formation on target neurons within the PVH has occurred prior to the onset of social deprivation. For example, an ontogenetic report in rat PVH demonstrated that catecholaminergic varicosities appeared in apposition to neurophysin-immunoreactive perikarya by E 21 (Khachaturian and Sladek, '80). In contrast, the granule cells of the dentate gyrus in rhesus monkey

continue to develop throughout the first 6 months of life, and have been demonstrated to have an altered expression of the neurofilament triplet protein in the same group of socially deprived monkeys used in specific aims 4 - 6 (Eckenhoff and Rakic, '88; Siegel et al., '92). Developmental characterization of the noradrenergic innervation of the PVH in rhesus monkeys of known and controlled rearing conditions is necessary to fully assess the existence of a sensitive period for synaptic formation on PVH neurons.

The hypothesis being tested in specific aim 5 was to see if the distribution of TIDA neurons within the PVH and ARC was altered by social deprivation. These regional quantitative experiments reported in Chapter Six suggested that the total number of TH-immunoreactive neurons were not significantly different between rearing conditions. This result contrasted examinations of the TH-immunoreactive varicosity density in neocortex (Morrison et al., '90), and chemoarchitecture of the basal ganglia in aged socially deprived monkeys where approximately 40% of the dopaminergic neurons within the substantia nigra/ventral tegmental area lost the ability to express TH (Martin et al., '91). Notwithstanding the potential confounds of aging and post-deprivation rearing conditions (Fearnley and Lees, '91; Ginsberg et al., '92b; Siegel et al., '92), a differential involvement of dopaminergic systems may occur in maternal and peer deprivation. Specifically, the apparent sparing of the TIDA neurons relative to the mesocortical and mesostriatal neurons suggests that these neuronal subpopulations have a differential vulnerability to social deprivation. Since socially deprived monkeys display a variety of motor disturbances, including stereotypic rocking and huddling behaviors (Mitchell et al., '66; Kraemer, '92),

the loss of dopaminergic input to the neostriatum and neocortex is significant in correlating underlying neuropathologic changes to observed behavioral abnormalities. Further morphologic characterization of the cellular constituents of the TH-immunoreactive neurons within the TIDA and mesostriatal/cortical systems of age- and rearing-matched monkeys may help identify potential differences between the two subpopulations. For example, the examination of subtype-specific receptor distribution (e.g. glutamate and/or dopaminergic receptors- see Moore et al., '87; Huntley et al., '93; Vickers et al., '93) and cytoskeletal characterization (e.g. neurofilaments and/or microtubule associated proteins- see Siegel et al., '92) may reveal constitutive patterns intrinsic to each dopaminergic subpopulation and may provide a neuroanatomic basis for differential vulnerability.

The hypothesis being tested in specific aim 6 was to see if an alteration in the number of CRF-immunoreactive neurons occurs as a function of rearing history. Similar to the TIDA neurons, CRF-immunoreactive neuron distribution reported in Chapter Six did not vary as a result of maternal and peer deprivation. Since socially deprived monkeys have an inability to regulate their stress responses, other factors within the HPA axis may be underlying these behavioral deficits. The hippocampal formation, which has been demonstrated in rat and monkey to be a central site for glucocorticoid receptor-mediated negative feedback on ACTH release, may be another structure within the HPA axis to investigate (Sapolsky et al., '84, '91; Herman et al., '89). The hippocampal formation is believed to be the cortical mediator of HPA inhibition due to the high density of Type I and Type II glucocorticoid receptors localized to hippocampal subfields and the molecular layer of the dentate gyrus (McEwen et al., '86; Ahima et al., '91;

Ahima and Harlan, '91). In addition, studies in monkey have demonstrated that deafferentation of the hippocampus (ablation of the perirhinal and parahippocampal cortices) has no effect on the tonic inhibition of ACTH release (Insausti et al., '87; Sapolsky et al., '91). Another site within the HPA axis to assess is the median eminence. For example, in the external lamina of the rat median eminence, vasopressin-immunoreactive terminal density, but not CRF-immunoreactive terminal density, has been demonstrated to vary as a result of chronic psychosocial stressors (de Goeij et al., '92). In addition, analysis of the peripheral limb of the HPA axis may provide further insight into the potential affects of social deprivation on stress systems. Of particular interest would be to sample hypophysial portal concentrations of ACTH, CRF, norepinephrine, and vasopressin in conscious, behaving socially reared and socially deprived monkeys, possibly via a push-pull perfusion method (see Terasawa et al., '88) as well as plasma levels of bound (corticosteroid binding globulins) and free glucocorticoids.

In summary, maternal and peer deprivation in a group of rhesus monkeys caused severe behavioral abnormalities that were assessed using neuropathological examinations in an attempt to correlate brain structure with altered behavioral function. Structural differences have been reported in the basal ganglia, dentate gyrus of the hippocampus, vestibular cerebellum, and neocortex of socially deprived monkeys (Struble and Riesen, '78; Floeter and Greenough, '79; Morrison et al., '90; Martin et al., '91; Siegel et al., '92). In contrast, the results of the hypothalamic examinations outlined in specific aims 4 - 6 suggested that several chemically-identified systems within the PVH are not affected, in terms of overall number of varicosity and cell counts, by the early environmental insult of social deprivation. Further quantitative,

morphologic characterization of the normative developmental pattern of these neurotransmitter-identified systems within the PVH may help to elucidate neurochemical substrates for this apparent lack of affect of social deprivation. Other neurotransmitter-identified systems within the monkey hypothalamus, including enkephalin and GnRH, may also warrant quantitative assessment. However, within the confines of this project, the selected neurotransmitter systems were also used as neurochemical markers to evaluate the neurochemical organization of the monkey PVH.

Chemoarchitecture of the macaque PVH

In addition to the quantitative analyses of noradrenergic innervation of the PVH and an assessment of the potential affects of social deprivation within the PVH, the normative data generated in this project also provided insight into the chemoarchitecture of the non-human primate PVH. Unlike the tract tracing / immunohistochemical studies which have been performed within the rat PVH (Armstrong et al., '80; Swanson and Kuypers, '80; Sawchenko and Swanson, '82, '83b), the specific origin of afferents and targets of efferent within the monkey PVH have not been properly assessed. However, precise qualitative and quantitative assessments of multiple neurotransmitter-identified systems throughout the rostrocaudal extent of the PVH yielded insight into the neurochemical organization of the macaque PVH. Specifically, a mediolateral gradient of chemically-specified PC and MC neurons has been observed in addition to the density gradient of noradrenergic innervation within the PVH.

As depicted in Figure 23, DßH-immunoreactive varicosities were found throughout the PVH, with PC regions receiving a denser noradrenergic innervation than MC regions. In terms of PC cytoarchitecture, small, bipolar

CRF-immunoreactive neurons were found approximately 140 - 210 μm lateral to the subependymal layer of the third ventricle, localized to a vertical array throughout the medial PC region. These CRF-containing neurons project through the external lamina of the median eminence to the portal capillary plexus and stimulate the release of ACTH from anterior pituitary corticotroph cells (Vale et al., '81; Kawano et al., '88; Sawchenko and Swanson, '90). In addition, approximately 225 - 275 μm lateral to the third ventricle were a subpopulation of TH-immunoreactive neurons. The majority (97.5%) of these TH-immunoreactive neurons display PC morphology and are part of the TIDA system which inhibits prolactin release from anterior pituitary lactotroph cells (Neill et al., '81; Kawano and Daikoku, '87; Goldsmith et al., '90). Another small population of PC dopaminergic neurons have been reported in rat to project to the brainstem and thoracic spinal cord, suggesting a role for dopamine in the modulation of autonomic responses, such as the regulation of sympathetic outflow (Swanson et al., '81; Skagerberg and Lindvall, '85). Approximately 2.5% of TH-immunoreactive neurons within the PVH display MC morphology, and were located slightly lateral to the PC TH-immunoreactive neurons. These dopamine-containing neurons may be involved in osmoregulation and potentially colocalize oxytocin (Schimchowitsch et al., '83; Young et al., '87; Li et al., '88). Moreover, electron microscopic studies in rat and monkey have demonstrated synaptic contacts between CRF- and TH-immunoreactive processes, suggesting that these two chemically-specified subpopulations of neurons are interconnected, potentially modulating both endocrine and autonomic responses (Liposits et al., '86c; Thind and Goldsmith, '89).

In medial MC regions of the PVH, large (approximate somal volume of 7700 μm^3), multipolar vasopressin-immunoreactive neurons were found, which are known to project via the hypothalamo-neurohypophysial tract through the internal lamina of the median eminence and terminate in the perivascular spaces of the posterior pituitary to maintain water balance. These MC vasopressin-immunoreactive neurons received a dense noradrenergic input, with approximately two-thirds of the innervation in apposition to the proximal dendrites and one-third contacting the somata. In colchicine treated and adrenalectomized rats, vasopressin-immunoreactive neurons displaying PC morphology have been observed in the periventricular PVH, and are likely to affect anterior pituitary secretion as well as autonomic outflow (Swanson and McKellar, '79; Whitnall et al., '85b; Sawchenko, '87; Cechetto and Saper, '88; Whitnall, '88). In more lateral aspects of the MC PVH, oxytocin-immunoreactive neurons were found, which were smaller than MC vasopressin-immunoreactive neurons (approximate somal volume of 3300 μm^3) which most likely terminate in the perivascular spaces of the posterior pituitary, releasing oxytocin into the systemic circulation for the stimulation of the milk ejection reflex and uterine contractility in the female. In addition, an intermixed population of MC vasopressin- and oxytocin-immunoreactive neurons were found within the periventricular PVH.

In conclusion, through specific aims 1 - 6 the chemoarchitecture of the macaque PVH has been assessed using immunohistochemical techniques to localize several neurotransmitter-identified substances within PC, MC, medial, and lateral regions. Further analysis using tract tracing methods in combination with immunohistochemistry are necessary to develop an organizational scheme of the monkey PVH similar to what has been

performed in rat PVH. In addition, triple label immunohistochemistry combined with confocal laser scanning microscopy for the assessment of subtype-specific adrenergic receptors and DßH-immunoreactive varicosities on vasopressin- and oxytocin-immunoreactive neurons would clarify the relationship between afferent input and receptor complexes on immunohistochemically-identified neurons.

FIGURE LEGEND

Figure 23. A schematic map representing the chemoarchitecture of the macaque PVH. The darkly shaded region indicates the PC PVH region and the lightly shaded region indicates the MC region. The small black triangles represent CRF-immunoreactive neurons within the PC PVH. The large black triangles represent MC vasopressin-immunoreactive neurons. The small white triangles represent PC TH-immunoreactive neurons. The large white triangles represent MC oxytocin-immunoreactive neurons. The small gray triangles represent PC vasopressin-immunoreactive neurons. The large gray triangles represent MC TH-immunoreactive neurons.

Figure 23

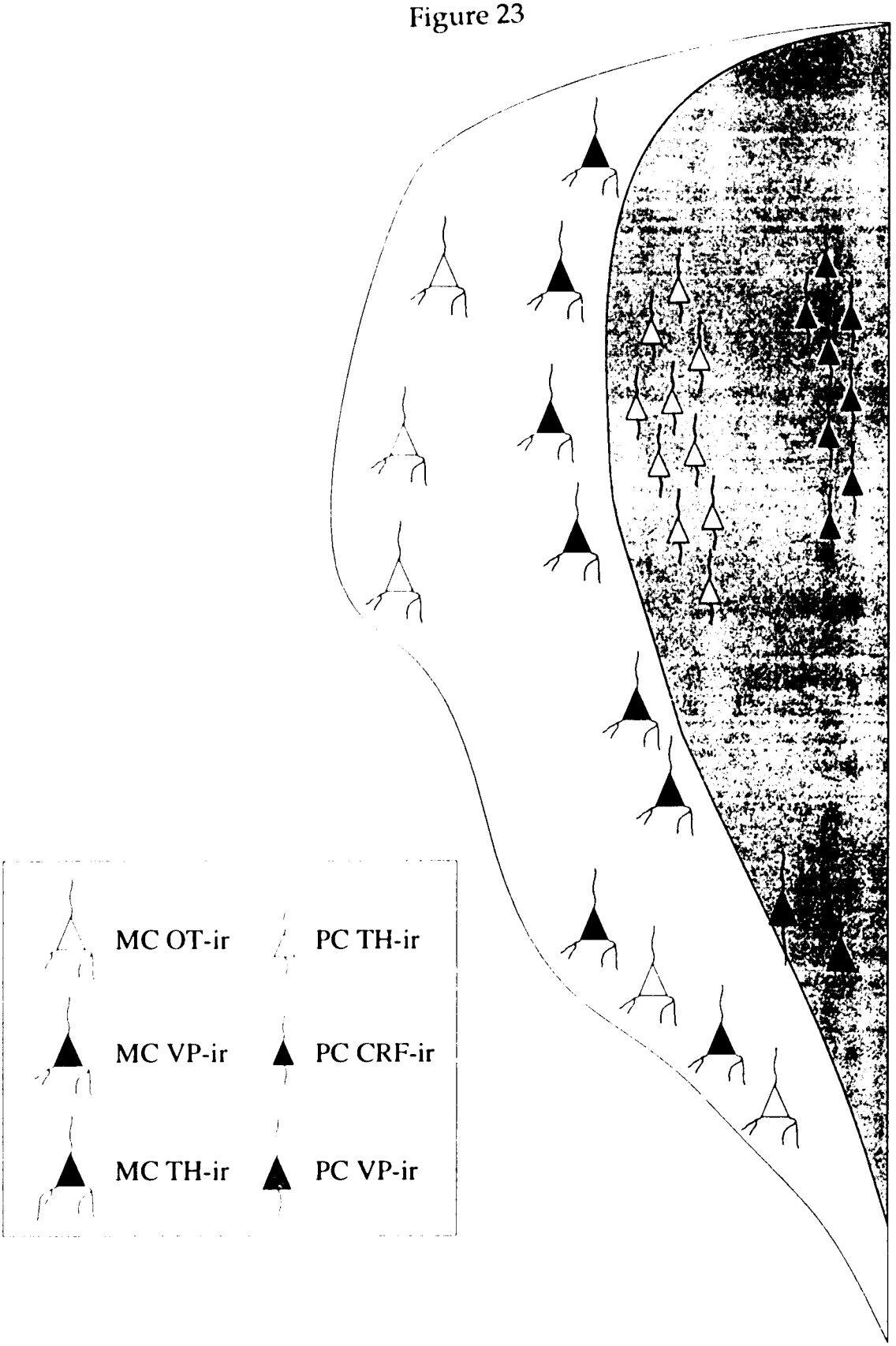

APPENDIX

History and present status of social deprivation

The initial research on social deprivation in rhesus monkeys came from the laboratory of H.F. Harlow, who was studying the effects of cortical lesions on learning (see Harlow, '58 for a review). A standard rearing protocol was implemented to minimize developmental variability across subjects. This was done by separating the mother and infant at birth, and raising the newborn monkey in a single cage with the assistance of a human caretaker. Harlow ('58) observed that these subjects became emotionally attached to their cloth diapers, and were extremely distressed when the diapers were removed for sanitary reasons. Further investigation of this phenomena revealed that attachment was a necessary event for the development of a normal rhesus monkey. This attachment has been demonstrated to be independent of the need for sustenance, since infants will readily cling to a non-nutritive soft cloth surrogate rather than a milk secreting hard wire surrogate (Harlow, '58; Kraemer, '91). Moreover, when the surrogate is removed, these infants become upset and display aberrant behaviors (Harlow et al, '71; Kraemer, '91). Some subjects actually died, apparently from starvation, even though they had ample access to food and water. This observation clearly demonstrated that monkey infants need more than food and shelter to survive. In addition, this behavior in monkeys resembles anaclitic depression and subsequent failure to thrive in human infants separated from their mother (Bowlby, '69; Harlow et al, '71; Kraemer, '91, '92).

The critical parameters for the expression of the isolation syndrome are: how long the subject is separated from the mother or peers; at what age the subject experiences the separation; the physical environment which creates the separation (Harlow, '58; Cross and Harlow, '65). All three of these factors have been examined experimentally to some degree. In terms of age of separation, subjects who are raised for the first 3 months of life in isolation can be placed in a social environment and partially adapt (Harlow et al., '71). However, subjects reared in isolation for 6, 12, and 16 months have permanent behavioral disturbances, especially in social situations, where they are incompetent and unable to comprehend external social cues from other monkeys within the colony (Griffin and Harlow, '66; Harlow, et al., '71). For instance, socially deprived monkeys will exhibit inappropriate behavioral cues, such as a fear grimace (an expression of fear) coupled with the flattening of the ears (an aggressive behavior) which indicate emotional disconnection (Kraemer, '92). These behavioral abnormalities increase in severity as the time in isolation is prolonged. Maternal and peer deprived macaques also have severe sexual dysfunction, as the males cannot successfully copulate, and the deprived females kill their offspring when mated (Harlow et al., '71; Kraemer, '91).

Social "rehabilitation" of 6 month old maternally deprived subjects has been described (Harlow et al., '71). Essentially, 6 month old isolates are paired with 3 month old socially reared "therapists", who are just beginning to develop complex social patterns. The initial cling response of the therapist elicits complete withdrawal by the isolate, but eventually mutual contact cling behavior (a hugging type response which is expressed in many primate species) develops, and subsequent play ensues (Harlow et al., '71).

Rehabilitated subjects appear normal behaviorally at 2-3 years of age, yet are hypersensitive to low doses of d-amphetamine (exhibiting aggression and stereotypic motor abnormalities) whereas socially reared controls have no observable behavioral deficits at the same dose (Kraemer et al., '89). Thus, time is a critical factor in the development of the isolation syndrome. A sensitive period appears to exist between 3-6 months of age where psychopathology is permanently manifested (Griffin and Harlow, '66). The possibility exists, however, that early social deprivation has both behavioral and structural sequelae prior to the 3 - 6 month sensitive period that has not been adequately tested.

The age at which separation occurs is also an important variable in the development of the isolation syndrome. Separation at birth clearly produces subsequent psychopathology (Harlow, '58; Griffin and Harlow, '66; Harlow et al., '71; Kraemer, '91, '92; Martin et al., '91). Separation at 3 months of age has been shown to cause protest and despair responses as well as long lasting behavioral deficits (Griffin and Harlow, '66). Interestingly, repeated separation of 3 month old rhesus monkeys reared in peer groups caused protest and despair responses as well as maturational arrest. At 9 months of age, monkeys who were subjected to 6 months of repeated peer separation displayed the skills of 3 month old monkeys as opposed to their actual age (Harlow et al., '71).

At approximately 1 year of age, rhesus monkeys are considered to be young juveniles and are capable of living by themselves. For a variety of reasons, including financial constraints, space limitations, and lack of detailed developmental data on monkeys, most macaques are separated from their mother and peers at 6 - 12 months of age and housed in single cages for the

remainder of their lives. This institutional procedure may very well constitute social deprivation for a species such as the rhesus monkey, which is dependent on social attachments for normal development.

A third factor in producing the isolation syndrome is the environment in which the subject is housed. Harlow ('58) originally described an infamous "pit" where subjects were reared. Later, stainless steel cages were implemented whereby subjects had no visual, tactile, and little auditory and olfactory interaction with other monkeys. This paradigm produced severe psychopathology. A "partial" social isolation setup was devised which also creates the full blown isolation syndrome, albeit not as severe as in the stainless steel cage. Subjects were reared from birth in wire cages where visual, auditory, olfactory, but not tactile contact with other subjects is possible. In lieu of the psychological distress that these subjects are forced to endure, partial social isolation, rather than isolation in stainless steel cages, is the paradigm selected for the present experiments. This is in contrast to the more severe social deprivation paradigm used by Martin et al. ('91) in which neuropathological changes were observed in the chemoarchitecture of the basal ganglia.

In addition to studying the behavior of socially deprived monkeys, a substantial body of cognitive research has been conducted on maternal and peer deprived subjects to assess learning ability. Few cognitive deficits have been found using such diverse tests as delayed response, avoidance, Wisconsin General Test Apparatus, two choice discrimination, and complex learning-set (Griffin and Harlow, '66; Beauchamp et al., '91; Kraemer '92). However, deficits have been found when socially deprived subjects have to discriminate relevant from irrelevant cues such as oddity tasks and

redundant cue tests (Beauchamp et al., '91; Kraemer, '91, '92). In these tasks, socially deprived subjects fail apparently presumably due to poor sequencing of information and altered cognitive processing.

The behavioral response to separation in a variety of species including monkeys and humans can be considered to have two phases, protest and despair. The protest response occurs early after mother-infant separation and is typified by increased locomotor activity and vocalization (Kraemer, '91). The immune system is also involved, as lymphocyte proliferation decreases after mother-infant separation in squirrel monkeys (Friedman et al, '91). Interestingly, lymphocyte suppression is greatest after two days of separation, the time at which plasma cortisol levels are highest, suggesting an interaction between immune and stress systems (Friedman et al., '91). In rat pups, Hofer ('87) has observed that the protest response can be reduced by stimuli such as nest odor, litter mates, and fur. Furthermore, the separated rat pup does not discriminate between the mother and the environment of the litter mates (Hofer, '87). Protest is proposed to be an adaptive behavior which increases the probability that the mother will locate her infant. After a prolonged period, protest responses become maladaptive, since there is an increased risk of predation. The despair response is thought to be a more energy efficient state for the isolated infant, once the chance of finding their mother is slim (Kraemer, '91, '92). The despair response in often characterized by withdrawal, anorexia, and self stimulation. Despair in monkeys has been compared anthropomorphically to states of learned helplessness, or depression (Kraemer, '91, '92). These behaviors are not, however, observed in all subjects who are separated from their mother. For example, protest

responses do not always precede despair, nor does despair occur in all infants who are separated from their mother (Hofer, '87; Friedman et al., '91).

Experimental evidence demonstrates that the noradrenergic system plays a significant role in the despair response. Neurochemical measurements have shown that maternally-deprived and surrogate-reared infants have lower levels of norepinephrine and its metabolites in the cerebrospinal fluid as compared to mother reared controls (Kraemer et al., '84, '89). a-methyl-p-tyrosine, a catecholaminergic synthesis inhibitor, has also been demonstrated to intensify the despair response in maternally deprived macaques (Kraemer et al., '84). Within the PVH, norepinephrine has been demonstrated in rats to stimulate feeding behaviors, possibly through a postsynaptic alpha-2 receptor mediated mechanism (Leibowitz, '78, '88). Since socially deprived monkeys are hyperphagic, a specific aim was designed to see if noradrenergic innervation density varied as a function of rearing history. The results of this experiment are reported in Chapter Five.

Additionally, two chemically-identified neuronal subpopulations within the PVH were assessed in an attempt to correlate aberrant behavioral responses to underlying structural neuropathology. In specific aim 5, quantitative analysis of TH-immunoreactive neurons within the PVH and ARC was performed. The TH-immunoreactive neurons (approximately 98% of all TH-immunoreactive neurons within the PVH display PC morphology, see Chapter Six) comprise the majority of TIDA neurons which project through the external lamina of the median eminence and terminate in the portal capillary plexus, notably to inhibit prolactin from anterior pituitary lactotrophs and somatotrophs (Neill et al., '81; Kawano and Daikoku, '87; Goldsmith et al., '90). A small subpopulation of TH-immunoreactive neurons

display MC morphology and have been demonstrated in rat to be osmosensitive (Young et al., '87; Watts, '92). Since socially deprived monkeys have sexual dysfunction and are polydipsic, a hypothesis was tested to see if the total number of TH-immunoreactive neurons varied as a function of rearing history. Furthermore, Martin et al. ('91) have demonstrated within a group of socially deprived monkeys that a loss of TH expression occurs in the substantia nigra and ventral tegmental area. In accordance, a goal of specific aim 5 was to compare the involvement of the TIDA and mesocortical/mesostriatal dopamine-containing systems in relation to social rearing history. However, the subjects used in the study by Martin et al. ('91) were aged monkeys exposed to total social isolation, a more severe form of deprivation than the partial social isolation used in the present studies (Harlow, '58; Harlow et al., '71). Therefore, the severity of early maternal and peer deprivation may be one of the determining factors whether neuropathological changes are manifested.

In the light of the aberrant stress responses displayed by socially deprived monkeys, a quantitative assessment of CRF-immunoreactive neurons within the PVH was also performed. Corticotropin-releasing factor is a potent secretagogue for ACTH, and the resultant glucocorticoid stress cascade. In addition to the effects on the HPA axis, CRF administration has been reported in a dose- and environment-dependent fashion, to increase arousal, specifically eliciting anorexigenic, anxiety-like, and self-directed responses in rhesus monkeys (Kalin, '85; Glowa and Gold, '91).

Four decades of descriptive psychopathology in socially deprived monkeys has led us to undertake careful and exhaustive neuroanatomical experiments in specific brain regions, targeting several transmitter systems in

order to evaluate how maternal and peer deprivation may permanently effect brain circuitry. The results of these experiments are reported in Chapters Five and Six.

Table Five

Quantitative data on neurotransmitter-identified systems collected for each subject[1]

[1]Note The quantitative assessments of DßH-immunoreactive varicosity density in both PC and MC regions of the PVH, PC and MC TH-immunoreactive neurons within the PVH, PC TH-immunoreactive neurons within the ARC, and CRF-immunoreactive neurons within the PVH are reported in relation to the rearing condition each subject. Socially reared (SR) subjects and socially deprived (SD) subjects are reported.

Monkey	# PC DßH ir varicosities/ 9.27×10^{-3} mm^3	# MC DßH ir varicosities/ 9.27×10^{-3} mm^3	# PC TH ir neurons/9 PVH sections	# MC TH ir neurons/9 PVH sections	# ARC TH ir neurons/9 PVH sections	# CRF ir neurons/9 PVH sections
AP03 (SR)	6,917	4,583	846	27	336	594
AP10 (SR)	15,260	11,749	729	16	291	479
A098 (SR)	11,666	8,765	1,086	24	260	765
AP04 (SR)	8,403	6,636	768	24	360	1,035
A096 (SR)	9,211	7,592	971	16	306	848
A064 (SD)	8,156	6,401	745	25	249	680
A073 (SD)	8,222	4,822	966	19	236	920
A075 (SD)	9,012	8,087	902	22	350	613
A067 (SD)	10,738	9,284	874	27	257	1,090
A065 (SD)	8,603	7,275	920	25	313	778

BIBLIOGRAPHY

Ahima, R., Z. Krozowski and R. Harlan (1991) Type I corticosteroid receptor-like immunoreactivity in the rat CNS: Distribution and regulation by corticosteroids. J. Comp. Neurol. *313*: 522-538.

Ahima, R.S. and R.E. Harlan (1991) Differential corticosteroid regulation of type II glucocorticoid receptor-like immunoreactivity in the rat central nervous system: Topography and implications. Endocrinology *129*: 226-235.

Airaksinen, M.S., S. Alanen, E. Szabat, T.J. Visser and P. Panula (1992) Multiple neurotransmitters in the tuberomammillary nucleus: Comparison of rat, mouse, and guinea pig. J. Comp. Neurol. *323*: 103-116.

Albert, D.J., L.H. Storlien, J.G. Albert and C.J. Mah (1971) Obesity following disturbance of the ventromedial hypothalamus: A comparison of lesions, lateral cuts, and anterior cuts. Physiol. Behav. *7*: 135-141.

Allen, G.V. and D.F. Cechetto (1992) Functional and anatomical organization of cardiovascular pressor and depressor sites in the lateral hypothalamic area: I. Descending projections. J. Comp. Neurol. *315*: 313-332.

Altman, J. and S.A. Bayer (1978) Development of the diencephalon in the rat: I. Autoradiographic study of the time of origin and settling patterns of neurons of the hypothalamus. J. Comp. Neurol. *182*: 945-972.

Amaral, D.G., R.B. Veazey and W.M. Cowan (1982) Some observations on hypothalamo-amygdaloid connections in the monkey. Brain Res. *252*: 13-27.

Andrew, R.D., B.A. MacVicar, F.E. Dudek and G.I. Hatton (1981) Dye transfer through gap junctions between neuroendocrine cells of rat hypothalamus. Science *211*: 1187-1189.

Antoni, F.A., M.C. Holmes and M.T. Jones (1983) Oxytocin as well as vasopressin potentiate ovine CRF *in vitro*. Peptides 4: 411-415.

Antunes, J.L., P.W. Carmel and E.A. Zimmerman (1977) Projections from the paraventricular nucleus to the zona externa of the median eminence of the rhesus monkey: An immunohistochemical study. Brain Res. *137*: 1-10.

Antunes, J.L. and E.A. Zimmerman (1978) The hypothalamic magnocellular system of the rhesus monkey: An immunocytochemical study. J. Comp. Neurol. *181*: 539-566.

Armstrong, W.E., S. Warach, G.I. Hatton and T.H. McNeill (1980) Subnuclei in the rat hypothalamic paraventricular nucleus: A cytoarchitectural, horseradish peroxidase and immunocytochemical analysis. Neuroscience 5: 1931-1958.

Bai, F.L., M. Yamano, Y. Shiotani, P.C. Emson, A.D. Smith, J.F. Powell and M. Tohyama (1985) An arcuato-paraventricular and -dorsomedial hypothalamic neuropeptide Y-containing system which lacks noradrenaline in the rat. Brain Res. *331*: 172-175.

Bargmann, W. and E. Scharrer (1951) The site of origin of the hormones of the posterior pituitary. Am. Sci. *39*: 255-259.

Beauchamp, A. J., J. P. Gluck, H. E. Fouty and M. H. Lewis (1991) Associative processes in differentially reared rhesus monkeys (*Macaca mulatta*): Blocking. Dev. Psychobiol. *24*: 175-189.

Bethea, C.L., W.H. Fahrenbach, S.A. Sprangers and F. Freesh (1992) Immunocytochemical localization of progestin receptors in monkey hypothalamus: Effect of estrogen and progestin. Endocrinology *130*: 895-905.

Bicknell, R.J., S.M. Luckman, K. Inenaga, W.T. Mason and G.I. Hatton (1989) ß-adrenergic and opioid receptors on pituicytes cultured from adult rat neurohypophysis: Regulation of cell morphology. Brain Res. Bull. *22*: 379-388.

Björklund, A., R.Y. Moore, A. Nobin and U. Stenevi (1973) The organization of tubero-hypophysial and reticulo-infundibular catecholamine neuron systems in the rat brain. Brain Res. *51*: 171-191.

Blaustein, J.D. (1992) Cytoplasmic estrogen receptors in rat brain: Immunocytochemical evidence using three antibodies with distinct epitopes. Endocrinology *131*: 1336-1342.

Bleier, R. (1984) The Hypothalamus of the Rhesus Monkey: A Cytoarchitectonic Atlas. Madison: The University of Wisconsin Press.

Blessing, W.W. and J.O. Willoughby (1985) Excitation of neuronal function in rabbit caudal ventrolateral medulla elevates plasma vasopressin. Neurosci. Lett. *58*: 189-194.

Bloch, G.J. and R.A. Gorski (1988) Cytoarchitectonic analysis of the SDN-POA of the intact and gonadectomized rat. J. Comp. Neurol. *275*: 604-612.

Bodian, D. and T.H. Maren (1951) The effect of neuro- and adenohypophysectomy on retrograde degeneration in hypothalamic nuclei of the rat. J. Comp. Neurol. *94*: 485-504.

Boer, G.J., R.M. Buijs, D.F. Swaab and G.J. De Vries (1980) Vasopressin and the developing rat brain. Peptides *1 (Suppl. 1)*: 203-209.

Booth, D.A. (1968) Mechanism of action of norepinephrine in eliciting an eating response on injection into the rat hypothalamus. J. Pharmacol. Exp. Therap. *160*: 336-348.

Bowlby, J. (1969) Attachment and Loss. Volume I: Attachment. New York: Basic Books.

Braak, H. and E. Braak (1987) The hypothalamus of the human adult: Chiasmatic region. Anat. Embryol. *176*: 315-330.

Bridges, T.E., E.W. Hillhouse and M.T. Jones (1976) The effect of dopamine on neurohypophysial hormone release *in vivo* and from the rat neural lobe and hypothalamus *in vitro*. J. Physiol. *260*: 647-666.

Broadwell, R.D. and R. Bleier (1976) A cytoarchitectonic atlas of the mouse hypothalamus. J. Comp. Neurol. *167*: 315-339.

Brooks, D.P., L. Share and J.T. Crofton (1986) Central adrenergic control of vasopressin release. Neuroendocrinology *42*: 416-420.

Buijs, R.M., M. Geffard, C.W. Pool and E.M.D. Hoorneman (1984) The dopaminergic innervation of the supraoptic and paraventricular nucleus. A light and electron microscopical study. Brain Res. *323*: 65-72.

Buijs, R.M., E.M. Van Der Beek, L.P. Renaud and T.A. Day (1990) Oxytocin localization and function in the A1 noradrenergic cell group: Ultrastructural and electrophysiological studies. Neuroscience *39*: 717-725.

Buijs, R.M., E.H.S. van Vulpen and M. Geffard (1987) Ultrastructural localization of GABA in the supraoptic nucleus and neural lobe. Neuroscience *20*: 347-355.

Buijs, R.M., D.N. Velis and D.F. Swaab (1980) Ontogeny of vasopressin and oxytocin in the fetal rat: Early vasopressinergic innervation of fetal rat brain. Peptides *1 (Suppl. 1)*: 315-324.

Caffé, A.R., P.C. Van Ryen, T.P. Vand Der Woude and F.W. Van Leeuwen (1989) Vasopressin and oxytocin systems in the brain and upper spinal cord of *Macaca fascicularis*. J. Comp. Neurol. *287*: 302-325.

Carlsson, A., B. Falck and N.-Å. Hillarp (1962) Cellular localization of brain monoamines. Acta Physiol. Scand. *56 (Suppl. 196)*: 1-28.

Caverson, M.M., J. Ciriello and F. Calaresu (1984) Paraventricular nucleus of the hypothalamus: An electrophysiological investigation of neurons projecting directly to intermediolateral nucleus in the cat. Brain Res. *305*: 380-383.

Cechetto, D.F. and C.B. Saper (1988) Neurochemical organization of the hypothalamic projection to the spinal cord in the rat. J. Comp. Neurol. *272*: 579-604.

Chan-Palay, V., L. Záborszky, C. Köhler, M. Goldstein and S.L. Palay (1984) Distribution of tyrosine hydroxylase-immunoreactive neurons in the hypothalamus of rats. J. Comp. Neurol. *227*: 467-496.

Chang, H.T. (1989) Noradrenergic innervation of the substantia innominata: A light and electron microscopic analysis of dopamine-ß-hydroxylase-immunoreactive elements in the rat. Exp. Neurol. *104*: 101-112.

Christ, J.F. (1969) Derivation and boundaries of the hypothalamus, with atlas of hypothalamic grisea. In W. Haymaker, E. Anderson and W.J.H. Nauta (eds): The Hypothalamus. Springfield: Thomas, pp. 13-60.

Cobbett, P., K.G. Smithson and G.I. Hatton (1986) Immunoreactivity to vasopressin- but not oxytocin-associated neurophysin antiserum in phasic neurons of rat hypothalamic paraventricular nucleus. Brain Res. *362*: 7-16.

Conrad, L.C.A. and D.W. Pfaff (1976) Efferents from the medial basal forebrain and hypothalamus in the rat. II. An autoradiographic study of the anterior hypothalamus. J. Comp. Neurol. *169*: 221-262.

Cross, H.A. and H.F. Harlow (1965) Prolonged and progressive effects of partial isolation on the behavior of macaque monkeys. J. Exp. Res. Pers. *1*: 39-49.

Cummings, S. and V. Seybold (1988) Relationship of alpha-1- and alpha-2-adrenergic-binding sites to regions of the paraventricular nucleus of the hypothalamus containing corticotropin-releasing factor and vasopressin neurons. Neuroendocrinology *47*: 523-532.

Cunningham, Jr., E.T., M.C. Bohn and P.E. Sawchenko (1990) Organization of adrenergic inputs to the paraventricular and supraoptic nuclei of the hypothalamus in the rat. J. Comp. Neurol. *292*: 651-667.

Cunningham, Jr., E.T. and P.E. Sawchenko (1988) Anatomical specificity of noradrenergic inputs to the paraventricular and supraoptic nuclei of the rat hypothalamus. J. Comp. Neurol. *274*: 60-76.

Dahlström, A. and K. Fuxe (1964) Evidence for the existence of monoamine-containing neurons in the central nervous system. I. Demonstration of monoamines in the cell bodies of brain stem neurons. Acta Physiol. Scand. *62*: *(Suppl. 232)* 1-55.

Day, T.A. (1989) Control of neurosecretory vasopressin cells by noradrenergic projections of the caudal ventrolateral medulla. In J. Ciriello, M.M. Caverson and C. Polosa (eds): Progress in Brain Research, Vol. 81. Amsterdam: Elsevier Science, pp. 303-317.

Day, T.A., A.V. Ferguson and L.P. Renaud (1984) Facilitatory influence of noradrenergic afferents on the excitability of rat paraventricular nucleus neurosecretory cells. J. Physiol. *355*: 237-249.

Day, T.A., A.V. Ferguson and L.P. Renaud (1985) Noradrenergic afferents facilitate the activity of tuberoinfundibular neurons of the hypothalamic paraventricular nucleus. Neuroendocrinology *41*: 17-22.

Day, T.A. and L.P. Renaud (1984) Electrophysiological evidence that noradrenergic afferents selectively facilitate the activity of supraoptic vasopressin neurons. Brain Res. *303*: 233-240.

de Goeij, D.C.E., H. Dijkstra and F.J.H. Tilders (1992) Chronic psychosocial stress enhances vasopressin, but not corticotropin-releasing factor, in the external zone of the median eminence of male rats: Relationship to subordinate status. Endocrinology *131*: 847-853.

de Lima, A.D., F.E. Bloom and J.H. Morrison (1988) Synaptic organization of serotonin-immunoreactive fibers in primary visual cortex of the macaque monkey. J. Comp. Neurol. *274*: 280-294.

de Lima, A.D. and J.H. Morrison (1989) Ultrastructural analysis of somatostatin-immunoreactive neurons and synapses in the temporal and occipital cortex of the macaque monkey. J. Comp. Neurol. *283*: 212-227.

de Lima, A.D., T. Voigt and J.H. Morrison (1990) Morphology of the cells within the inferior temporal gyrus that project to the prefrontal cortex in the macaque monkey. J. Comp. Neurol. *296*: 159-172.

Decavel, C., P. Dubourg, B. Leon-Henri, M. Geffard and A. Calas (1989) Simultaneous immunogold labeling of GABAergic terminals and vasopressin-containing neurons in the rat paraventricular nucleus. Cell Tiss. Res. *255*: 77-80.

Decavel, C., M. Geffard and A. Calas (1987) Comparative study of dopamine- and noradrenaline-immunoreactive terminals in the paraventricular and supraoptic nuclei of the rat. Neurosci. Lett. *77*: 149-154.

Decavel, C. and A.N. van den Pol (1992) Converging GABA- and glutamate-immunoreactive axons make synaptic contact with identified hypothalamic neurosecretory neurons. J. Comp. Neurol. *316*: 104-116.

Deitch, J.S., K.L. Smith, C.L. Lee, J.W. Swann and J.N. Turner (1990a) Confocal scanning laser microscope images of hippocampal neurons intracellularly labeled with biocytin. J. Neurosci. Meth. *33*: 61-76.

Deitch, J.S., K.L. Smith, J.W. Swann and J.N. Turner (1990b) Parameters affecting imaging of the horseradish-peroxidase-diaminobenzidine reaction product in the confocal scanning laser microscope. J. Microsc. *160*: 265-278.

Dierickx, K. and F. Vandesande (1977) Immunocytochemical localization of the vasopressinergic and the oxytocinergic neurons in the human hypothalamus. Cell Tiss. Res. *184*: 15-27.

Dierickx, K. and F. Vandesande (1979) Immunocytochemical demonstration of separate vasopressin-neurophysin and oxytocin-neurophysin neurons in the human hypothalamus. Cell Tiss. Res. *196*: 203-212.

Eckenhoff, M.F. and P. Rakic (1988) Nature and fate of proliferative cells in the hippocampal dentate gyrus during the life span of the rhesus monkey. J. Neurosci. *8*: 2729-2747.

Everitt, B.J., T. Hökfelt, L. Terenius, K. Tatemoto, V. Mutt and M. Goldstein (1984a) Differential co-existence of neuropeptide Y (NPY)-like immunoreactivity with catecholamines in the central nervous system of the rat. Neuroscience *11*: 443-462.

Everitt, B.J., T. Hökfelt, J.-Y. Wu and M. Goldstein (1984b) Coexistence of tyrosine hydroxylase-like and gamma-aminobutyric acid-like immunoreactivities in neurons of the arcuate nucleus. Neuroendocrinology *39*: 189-191.

Everitt, B.J., B. Meister, T. Hökfelt, T. Melander, L. Terenius, Å. Rökaeus, E. Theodorsson-Norheim, G. Dockray, J. Edwardson, C. Cuello, R. Elde, et al. (1986) The hypothalamic arcuate nucleus-median eminence complex: Immunohistochemistry of transmitters, peptides, and DARPP-32 with special reference to coexistence in dopamine neurons. Brain Res. Rev. *11*: 97-155.

Fearnley, J.M. and A.J. Lees (1991) Ageing and Parkinson's disease: Substantia nigra regional selectivity. Brain *114*: 2283-2301.

Felten, D.L., C.D. Sladek and J.R. Sladek, Jr. (1985) Noradrenergic innervation of the supraoptic and paraventricular nuclei. In H. Kobayashi, H.A. Bern and A. Urano (eds): Neurosecretion and the Biology of Neuropeptides. Tokyo: Japan Scientific Societies Press/Springer-Verlag, pp. 186-194.

Felten, D.L. and J.R. Sladek, Jr. (1983) Monoamine distribution in primate brain V. Monoaminergic nuclei: Anatomy, pathways and local organization. Brain Res. Bull. *10*: 171-284.

Floeter, M.K. and W.T. Greenough (1979) Cerebellar plasticity: Modification of Purkinje cell structure by differential rearing in monkeys. Science *206*: 227-229.

Foote, S.L. and C.I. Cha (1988) Distribution of corticotropin-releasing-factor-like immunoreactivity in brainstem of two monkey species (*Saimiri sciureus* and *Macaca fascicularis*): An immunohistochemical study. J. Comp. Neurol. *276*: 239-264.

Friedman, E. M., C. L. Coe and W. B. Ershler. (1991) Time-dependent effects of peer separation on lymphocyte proliferation responses in juvenile squirrel monkeys. Dev. Psychobiol. *24*: 159-173.

Frigon, R.P., D.T. O'Connor and G.L. Levine (1981) Human dopamine-ß-hydroxylase. Comparison of the enzyme from plasma, adrenal medulla, and pheochromocytoma by radioimmunoassay. Mol. Pharmacol. *19*: 444-450.

Furutani, Y., Y. Morimoto, S. Shibahara, M. Noda, H. Takahashi, T. Hirose, M. Asai, S. Inayama, H. Hayashida, T. Miyata and S. Numa (1983) Cloning and sequence analysis of cDNA for ovine corticotropin-releasing factor precursor. Nature *310*: 537-540.

Fuxe, K. (1965) Evidence for the existence of monoamine-containing neurons in the central nervous system. IV. The distribution of monoamine terminals in the central nervous system. Acta Physiol. Scand. *64 (Suppl. 247)*: 37-85.

Gainer, H., Y. Sarne and M.J. Brownstein (1977) Biosynthesis and axonal transport of rat neurohypophysial proteins and peptides. J. Cell. Biol. *73*: 366-381.

Gardiner, T.W., J.G. Verbalis and E.M. Stricker (1985) Impaired secretion of vasopressin and oxytocin in rats after lesions of nucleus medianus. Am. J. Physiol. *249*: R681-R688.

Gilbey, M.P., J.H. Coote, S. Fleetwood-Walker and D.F. Peterson (1982) The influence of the paraventriculo-spinal pathway, and oxytocin and vasopressin on sympathetic preganglionic neurones. Brain Res. *251*: 283-290.

Gillies, G.E., E.A. Linton and P.J. Lowry (1982) Corticotropin releasing activity of the new CRF is potentiated several times by vasopressin. Science *299*: 355-357.

Ginsberg, S.D., P.R. Hof, W.T. McKinney and J.H. Morrison (1993a) Quantitative analysis of tuberoinfundibular tyrosine hydroxylase- and corticotropin-releasing factor-immunoreactive neurons in monkeys raised with differential rearing conditions. Exp. Neurol., in press.

Ginsberg, S.D., P.R. Hof, W.T. McKinney, and J.H. Morrison (1993b) The noradrenergic innervation density of the monkey paraventricular nucleus is not altered by early social deprivation. Neurosci. Lett., submitted.

Ginsberg, S.D., P.R. Hof, W.G. Young, G.W. Kraemer, W.T. McKinney and J.H. Morrison (1991) Quantitative analysis of transmitter-identified systems in the monkey paraventricular nucleus: Effects of differential rearing conditions. Proc. Soc. Neurosci. *17*: 895.

Ginsberg, S.D., P.R. Hof, W.G. Young and J.H. Morrison (1992a) Quantification of noradrenergic varicosities in apposition to vasopressin-immunoreactive neurons in the monkey paraventricular nucleus. Proc. Soc. Neurosci. *18*: 1415.

Ginsberg, S.D., P.R. Hof, W.G. Young and J.H. Morrison (1993c) Noradrenergic innervation of the hypothalamus of rhesus monkeys: Distribution of dopamine-ß-hydroxylase-immunoreactive fibers and quantitative analysis of varicosities in the paraventricular nucleus. J. Comp. Neurol., in press.

Ginsberg, S.D., S.J. Siegel, P.R. Hof, W.G. Young, G.W. Kraemer, W.T. McKinney and J.H. Morrison (1992b) Effects of social isolation on specific neuronal populations in the primate hypothalamus and hippocampus. Biol. Psychiatry *31*: 196A.

Ginsberg, S.D., W.G. Young, P.R. Hof and J.H. Morrison (1993d) Noradrenergic innervation of vasopressin- and oxytocin-containing neurons in the hypothalamic paraventricular nucleus of the macaque: Quantitative analysis using double label immunohistochemistry and confocal laser microscopy. J. Comp. Neurol., submitted.

Glowa, J.R. and P.W. Gold (1991) Corticotropin-releasing hormone produces profound anorexigenic effects in the rhesus monkey. Neuropeptides *18*: 55-61.

Go, C.-G., C. Aoki, O. Cartano, H. Kurose and R. Lefkowitz (1992) Immunocytochemical localization of alpha-2A-, alpha-2B-, and alpha-2C-adrenergic receptors in brains of rat and monkey. Proc. Soc. Neurosci. *18*: 457.

Goldsmith, P.C., K.K. Thind, T. Song, E.J. Kim and J.E. Boggan (1990) Location of the neuroendocrine dopamine neurons in the monkey hypothalamus by retrograde tracing and immunostaining. J. Neuroendocrinol. 2: 169-179.

Griffin, G. A. and H. F. Harlow (1966) Effects of three months of total social deprivation on social adjustment and learning in the rhesus monkey. Child Dev. 37: 533-547.

Harlow, H.F. (1958) The nature of love. Am. Psychologist *13*: 673-685.

Harlow, H.F. (1974) Sexual behavior in the rhesus monkey. In F.A. Beach (ed): Sex and Behavior. Huntington: Robert E. Krieger Publishing, pp. 234-265.

Harlow, H.F., M.K. Harlow and S.J. Suomi (1971) From thought to therapy: Lessons from a primate laboratory. Am. Sci. *59*: 538-549.

Harris, G.W. (1948) Neural control of the pituitary gland. Physiol. Rev. *28*: 139-179.

Hatton, G.I., S.M. Luckman and R.J. Bicknell (1991) Adrenaline activation of ß2-adrenoceptors stimulates morphological changes in astrocytes (pituicytes) cultured from adult rat neurohypophyses. Brain Res. Bull. *26*: 765-769.

Hatton, G.I., L.S. Perlmutter, A.K. Salm and C.D. Tweedle (1984) Dynamic neuronal-glial interactions in hypothalamus and pituitary: Implication for control of hormone synthesis and release. Peptides *5 (Suppl. 1)*: 121-138.

Herman, J.P., M.K.-H. Schafer, E.A. Young, R. Thompson, J. Douglass, H. Akil and S.J. Watson (1989) Evidence for hippocampal regulation of neuroendocrine neurons of the hypothalamo-pituitary-adrenocortical axis. J. Neurosci. *9*: 3072-3082.

Hofer, M. A. (1987) Early social relationships: A psychobiologist's view. Child Dev. 58: 633-647.

Hoffman, G.E., D.L. Felten and J.R. Sladek, Jr. (1976) Monoamine distribution in primate brain. III. Catecholamine-containing varicosities in the hypothalamus of *Macaca mulatta*. Am. J. Anat. *147*: 501-514.

Hoffman, N.W., J.G. Tasker and F.E. Dudek (1991) Immunohistochemical differentiation of electrophysiologically defined neuronal populations in the region of the rat hypothalamic paraventricular nucleus. J. Comp. Neurol. *307*: 405-416.

Hornby, P.J. and D.T. Piekut (1987) Catecholamine distribution and relationship to magnocellular neurons in the paraventricular nucleus of the rat. Cell Tiss. Res. *248*: 239-246.

Hosoya, Y. and M. Matsushita (1979) Identification and distribution of the spinal and hypophysial projection neurons in the paraventricular nucleus of the rat. A light and electron microscopic study with the horseradish peroxidase method. Exp. Brain Res. *35*: 315-331.

Hosoya, Y., Y. Sugiura, N. Okado, A.D. Loewy and K. Kohno (1991) Descending input from the hypothalamic paraventricular nucleus to sympathetic preganglionic neurons in the rat. Exp. Brain Res. *85*: 10-20.

Hou-Yu, A., P.H. Ehrlich, G. Valiquette, D.L. Engelhardt, W.H. Sawyer, G. Nilaver and E.A. Zimmerman (1982) A monoclonal antibody to vasopressin: Preparation, characterization, and application in immunocytochemistry. J. Histochem. Cytochem. *30*: 1249-1260.

Hou-Yu, A., A.T. Lamme, E.A. Zimmerman and A.-J. Silverman (1986) Comparative distribution of vasopressin and oxytocin neurons in the rat brain using a double-label procedure. Neuroendocrinology *44*: 235-246.

Huntley, G.W., S.W. Rogers, T. Moran, W. Janssen, N. Archin, J.C. Vickers, K. Cauley, S.F. Heinemann and J.H. Morrison (1993) Selective distribution of kainate receptor subunit immunoreactivity in monkey neocortex revealed by a monoclonal antibody which recognizes glutamate receptor subunits Glu R5/6/7. J. Neurosci., submitted.

Ibata, Y., K. Fukui, H. Okamura, T. Kawakami, M. Tanaka, H.L. Obata, T. Tsuto, H. Terubayashi, C. Yanaihara and N. Yanaihara (1983) Coexistence of dopamine and neurotensin in hypothalamic arcuate and periventricular neurons. Brain Res. *269*: 177-179.

Inagaki, N., A. Yamatodani, M. Ando-Yamamoto, M. Tohyama, T. Watanabe and H. Wada (1988) Organization of histaminergic fibers in the rat brain. J. Comp. Neurol. *273*: 283-300.

Inagaki, S., Y. Shiotani, M. Yamano, S. Shiosaka, H. Takagi, K. Tateishi, E. Hashimura, T. Hamaoka and M. Tohyama (1984) Distribution, origin, and fine structures of cholecystokinin-8-like immunoreactive terminals in the nucleus ventromedialis hypothalami of the rat. J. Neurosci. *4*: 1289-1299.

Ingram, W.R. (1940) Nuclear organization and chief connections of the primate hypothalamus. Assoc. Res. Nerv. Ment. Dis. *20*: 195-244.

Inoué, S. (1990) Foundations of confocal scanned imaging in light microscopy. In J.B. Pawley (ed): Handbook of Biological Confocal Microscopy. New York: Plenum Press, pp. 1-14.

Insausti, R., D.G. Amaral and W.M. Cowan (1987) The entorhinal cortex of the monkey: II. Cortical afferents. J. Comp. Neurol. *264*: 356-395.

Insel, T.R. (1992) Oxytocin- A neuropeptide for affiliation: Evidence from behavioral, receptor autoradiographic, and comparative studies. Psychoneuroendocrinology *17*: 3-35.

Ishikawa, M. and C. Tanaka (1977) Morphological organization of catecholamine terminals in the diencephalon of the rhesus monkey. Brain Res. *119*: 43-55.

Jhamandas, J.H., K.H. Harris, T. Petrov and T.L. Krukoff (1992) Characterization of the parabrachial nucleus input to the hypothalamic paraventricular nucleus in the rat. J. Neuroendocrinol. *4*: 461-471.

Jhamandas, J.H., W. Raby, J. Rogers, R.M. Buijs and L.P. Renaud (1989) Diagonal band projection towards the hypothalamic supraoptic nucleus: Light and electron microscopic observations in the rat. J. Comp. Neurol. *282*: 15-23.

Jhamandas, J.H. and L.P. Renaud (1986a) Diagonal band neurons may mediate arterial baroreceptor input to hypothalamic vasopressin-secreting neurons. Neurosci. Lett. *65*: 214-218.

Jhamandas, J.H. and L.P. Renaud (1986b) A g-aminobutyric-acid-mediated baroreceptor input to supraoptic vasopressin neurones in the rat. J. Physiol. *381*: 595-606.

Joseph, S.A. and D.T. Piekut (1986) Dual immunostaining procedure demonstrating neurotransmitter and neuropeptide codistribution in the same brain section. Am. J. Anat. *175*: 331-342.

Kalin, N.H. (1985) Behavioral effects of ovine corticotropin-releasing factor administered to rhesus monkeys. Fed. Proc. *44*: 249-253.

Kawano, H. and S. Daikoku (1987) Functional topography of the rat hypothalamic dopamine neuron systems: Retrograde tracing and immunohistochemical study. J. Comp. Neurol. *265*: 242-253.

Kawano, H., S. Daikoku and T. Shibasaki (1988) CRF-containing neuron systems in the rat hypothalamus: Retrograde tracing and immunohistochemical studies. J. Comp. Neurol. *272*: 260-268.

Kawata, M. and Y. Sano (1982) Immunohistochemical identification of the oxytocin and vasopressin neurons in the hypothalamus of the monkey (*Macaca fuscata*). Anat. Embryol. *165*: 151-167.

Khachaturian, H. and J.R. Sladek, Jr. (1980) Simultaneous monoamine histofluorescence and neuropeptide immunocytochemistry: III. Ontogeny of catecholamine varicosities and neurophysin neurons in the rat supraoptic and paraventricular nuclei. Peptides *1*: 77-95.

Kiss, J.Z., J. Martos and M. Palkovits (1991) Hypothalamic paraventricular nucleus: A quantitative analysis of cytoarchitectonic subdivisions in the rat. J. Comp. Neurol. *313*: 563-573.

Kiss, J.Z. and E. Mezey (1986) Tyrosine hydroxylase in magnocellular neurosecretory neurons: Response to physiological manipulations. Neuroendocrinology *43*: 519-525.

Kiss, J.Z., M. Palkovits, L. Záborszky, E. Tribollet, D. Szabo and G.B. Makara (1983) Quantitative histological studies on the hypothalamic paraventricular nucleus in rats: I. Number of cells and synaptic boutons. Brain Res. *262*: 217-224.

Kitahama, K., P.-H. Luppi, A. Bérod, M. Goldstein and M. Jouvet (1987) Localization of tyrosine hydroxylase-immunoreactive neurons in the cat hypothalamus, with special reference to fluorescence histochemistry. J. Comp. Neurol. *262*: 578-593.

Kovacs, K.J. and E. Mezey (1987) Dexamethasone inhibits corticotropin-releasing factor gene expression in the rat paraventricular nucleus. Neuroendocrinology *46*: 365-368.

Kraemer, G.W. (1991) Strangers in a strange land: A psychobiological study of rhesus monkey infants before and after separation from their mothers or inanimate mother substitutes. Child Dev. *62*: 548-566.

Kraemer, G.W. (1992) A psychobiological theory of attachment. Behav. Brain Sci. *15*: 493-541.

Kraemer, G.W., M.H. Ebert, C.R. Lake and W.T. McKinney (1984) Cerebrospinal fluid measures of neurotransmitter changes associated with pharmacological alteration of the despair response to social separation in rhesus monkeys. Psychiatry Res. *11*: 303-315.

Kraemer, G.W., M.H. Ebert, D.E. Schmidt and W.T. McKinney (1989) A longitudinal study of the effect of different social rearing conditions on cerebrospinal fluid norepinephrine and biogenic amine metabolites in rhesus monkeys. Neuropsychopharmacology 2: 175-189.

Krettek, J.E. and J.L. Price (1978) Amygdaloid projections to subcortical structures within the basal forebrain and brainstem in the rat and cat. J. Comp. Neurol. *178*: 225-253.

Krieger, M.S., L.C.A. Conrad and D.W. Pfaff (1979) An autoradiographic study of the efferent connections of the ventromedial nucleus of the hypothalamus. J. Comp. Neurol. *183*: 785-816.

Larsen, P.J., M. Møller and J.D. Mikkelsen (1991) Efferent projections from the periventricular and medial parvicellular subnuclei of the hypothalamic paraventricular nucleus to circumventricular organs of the rat: A *Phaseolus vulgarize*-leucoagglutinin (PHA-L) tracing study. J Comp. Neurol. *306*: 462-479.

Lauder, J.M., and F.E. Bloom (1974) Ontogeny of monoamine neurons in the locus coeruleus, raphe nuclei and substantia nigra of the rat. I. Cell differentiation. J. Comp. Neurol. *155*:469-482.

Lauder, J.M., and F.E. Bloom (1975) Ontogeny of monoamine neurons in the locus coeruleus, raphe nuclei and substantia nigra of the rat. II. Synaptogenesis. J. Comp. Neurol. *163*:251-264.

Laurent, F.M., C. Hindelang, M.J. Klein, M.E. Stoeckel and J.M. Felix (1989) Expression of the oxytocin and vasopressin genes in the rat hypothalamus during development: An *in situ* hybridization study. Dev. Brain Res. *46*: 145-154.

Lechan, R.M., J.L. Nestler and S. Jacobson (1982) The tuberoinfundibular system of the rat as demonstrated by immunohistochemical localization of retrogradely transported wheat germ agglutinin (WGA) from the median eminence. Brain Res. *245*: 1-15.

Legendre, P. and D.A. Poulain (1992) Intrinsic mechanisms involved in the electrophysiological properties of the vasopressin-releasing neurons of the hypothalamus. Prog. Neurobiol. *38*: 1-17.

Lehman, M.N. and A.-J. Silverman (1988) Ultrastructure of luteinizing hormone-releasing hormone (LHRH) neurons and their projections in the golden hamster. Brain Res. Bull. *20*: 211-221.

Leibowitz, S.F. (1978) Paraventricular nucleus: A primary site mediating adrenergic stimulation of feeding and drinking. Pharmacol. Biochem. Behav. *8*: 163-175.

Leibowitz, S.F. (1988) Hypothalamic paraventricular nucleus: Interaction between alpha-2 noradrenergic system and circulating hormones and nutrients in relation to energy balance. Neurosci. Biobehav. Rev. *12*: 101-109.

Leibowitz, S.F. (1991) Brain neuropeptide Y: An integrator of endocrine, metabolic, and behavioral processes. Brain Res. Bull. *27*: 333-337.

Leibowitz, S.F., M. Jhanwar-Uniyal, B. Dvorkin and M.H. Makman (1982) Distribution of alpha-adrenergic and beta-adrenergic and dopaminergic receptors in discrete hypothalamic areas of rat. Brain Res. *233*: 97-114.

Leranth, C., N.J. MacLusky, T.J. Brown, E.C. Chen, D.E. Redmond, Jr. and F. Naftolin (1992) Transmitter content and afferent connections of estrogen-sensitive progestin receptor-containing neurons in the primate hypothalamus. Neuroendocrinology *55*: 667-682.

Leranth, C., L. Záborszky, J. Marton and M. Palkovits (1975) Quantitative studies on the supraoptic nucleus in the rat. I. Synaptic organization. Exp. Brain Res. *22*: 509-523.

Lerea, L.S. and K.D. McCarthy (1989) Astroglial cells *in vitro* are heterogeneous with respect to expression of the alpha-1-adrenergic receptor. Glia *2*: 135-147.

LeVay, S. (1991) A difference in hypothalamic structure between heterosexual and homosexual men. Science *253*: 1034-1037.

Lewis, D.A., M.J. Campbell, S.L. Foote, M. Goldstein and J.H. Morrison (1987) The distribution of tyrosine hydroxylase-immunoreactive fibers in primate neocortex is widespread but regionally specific. J. Neurosci. *7*: 279-290.

Lewis, D.A., S.L. Foote, M. Goldstein and J.H. Morrison (1988) The dopaminergic innervation of monkey prefrontal cortex: A tyrosine hydroxylase immunohistochemical study. Brain Res. *449*: 225-243.

Li, Y.-W., Z.J. Gieroba and W.W. Blessing (1992) Chemoreceptor and baroreceptor responses of A1 area neurons projecting to supraoptic nucleus. Am. J. Physiol. *263*: R310-R317.

Li, Y.W., G.M. Halliday, T.H. Joh, L.B. Geffen and W.W. Blessing (1988) Tyrosine hydroxylase-containing neurons in the supraoptic and paraventricular nuclei of the adult human. Brain Res. *461*: 75-86.

Lincoln, D.W. and J.B. Wakerley (1975) Factors governing the periodic activation of supraoptic and paraventricular neurosecretory cells during suckling in the rat. J. Physiol. *250*: 443-461.

Lind, R.W. (1988) Angiotensin and the lamina terminalis: Illustrations of a complex unity. Clin. Exp. Hyperten. *A10 (Suppl. 1)*: 79-105.

Lindvall, O., A. Björklund and G. Skagerberg (1984) Selective histochemical demonstration of dopamine terminal systems in rat di- and telencephalon: New evidence for dopaminergic innervation of hypothalamic neurosecretory nuclei. Brain Res. *306*: 19-30.

Liposits, Z. and W.K. Paull (1989) Association of dopaminergic fibers with corticotropin-releasing hormone (CRH)-synthesizing neurons in the paraventricular nucleus of the rat hypothalamus. Histochemistry *93*: 119-127.

Liposits, Z., C. Phelix and W.K. Paull (1986a) Adrenergic innervation of corticotropin-releasing factor (CRF)-synthesizing neurons in the hypothalamic paraventricular nucleus of the rat. A combined light and electron microscopic immunocytochemical study. Histochemistry *84*: 201-205.

Liposits, Z., C. Phelix and W.K. Paull (1986b) Electron microscopic analysis of tyrosine hydroxylase, dopamine-ß-hydroxylase, and phenylethanolamine-N-methyltransferase immunoreactive innervation of the hypothalamic paraventricular nucleus in the rat. Histochemistry *84*: 105-120.

Liposits, Z., D. Sherman, C. Phelix and W.K. Paull (1986c) A combined light and electron microscopic immunocytochemical method for the simultaneous localization of multiple tissue antigens: Tyrosine hydroxylase-immunoreactive innervation of corticotropin-releasing factor synthesizing neurons in the paraventricular nucleus of the rat. Histochemistry *85*: 95-106.

Liposits, Z., L. Sievers and W.K. Paull (1988) Neuropeptide-Y and ACTH-immunoreactive innervation of corticotropin releasing factor (CRF)-synthesizing neurons in the hypothalamus of the rat. Histochemistry *88*: 227-234.

Liposits, Z., R.M. Uht, R.W. Harrison, F.P. Gibbs, W.K. Paull and M.C. Bohn (1987) Ultrastructural localization of glucocorticoid receptor (GR) in hypothalamic paraventricular neurons synthesizing corticotropin-releasing factor (CRF). Histochemistry *87*: 407-412.

Luiten, P.G.M., G.J. Ter Horst and A.B. Steffens (1987) The hypothalamus, intrinsic connections and outflow pathways to the endocrine system in relation to the control of feeding and metabolism. Prog. Neurobiol. *28*: 1-54.

Markey, K.A., S. Kondo, L. Shenkman and M. Goldstein (1980) Purification and characterization of tyrosine hydroxylase from a clonal pheochromocytoma cell line. Mol. Pharmacol. *17*: 79-85.

Martin, G.E. and R.D. Myers (1975) Evoked release of [^{14}C]norepinephrine from the rat hypothalamus during feeding. Am. J. Physiol. *229*: 1547-1555.

Martin, L.J., D.M. Spicer, M.H. Lewis, J.P. Gluck and L.C. Cork (1991) Social deprivation of infant rhesus monkeys alters the chemoarchitecture of the brain: I. Subcortical regions. J. Neurosci. *11*: 3344-3358.

Mason, P., S.A. Back and H.L. Fields (1992) A confocal laser microscopic study of enkephalin-immunoreactive appositions onto physiologically identified neurons in the rostral ventromedial medulla. J. Neurosci. *12*: 4023-4036.

Mason, W.T. (1983) Excitation by dopamine of putative oxytocinergic neurones in the rat supraoptic nucleus *in vitro*: Evidence for two classes of continuously firing neurones. Brain Res. *267*: 113-121.

Mason, W.T., Y.W. Ho, F. Eckenstein and G.I. Hatton (1983) Mapping of cholinergic neurons associated with rat supraoptic nucleus: Combined immunocytochemical and histochemical identification. Brain Res. Bull. *11*: 617-626.

Mason, W.T., Y.W. Ho and G.I. Hatton (1984) Axon collaterals of supraoptic neurones: Anatomical and electrophysiological evidence for their existence in the lateral hypothalamus. Neuroscience *11*: 169-182.

McBride, R.L. and J. Sutin (1977) Amygdaloid and pontine projections to the ventromedial nucleus of the hypothalamus. J. Comp. Neurol. *174*: 377-396.

McEwen, B.S., E.R. De Kloet and W. Rostene (1986) Adrenal steroid receptors and actions in the nervous system. Physiol. Rev. *66*: 1121-1188.

McKinley, M.J., R.M. McAllen, F.A.O. Mendelsohn, A.M. Allen, S.Y. Chai and B.J. Oldfield (1990) Circumventricular organs: Neuroendocrine interfaces between the brain and the hemal milieu. In W.F. Ganong and L. Martini (eds): Frontiers in Neuroendocrinology. New York: Raven Press, pp. 91-127.

McNeill, T.H. and J.R. Sladek, Jr. (1980) Simultaneous monoamine histofluorescence and neuropeptide immunocytochemistry: II. Correlative distribution of catecholamine varicosities and magnocellular neurosecretory neurons in the rat supraoptic and paraventricular nuclei. J. Comp. Neurol. *193*: 1023-1033.

Meeker, R.B., D.J. Swanson and J.N. Hayward (1988) Local synaptic organization of cholinergic neurons in the basolateral hypothalamus. J. Comp. Neurol. *276*: 157-168.

Meister, B., M.J. Villar, S. Ceccatelli and T. Hökfelt (1990) Localization of chemical messengers in magnocellular neurons of the hypothalamic supraoptic and paraventricular nuclei: An immunohistochemical study using experimental manipulations. Neuroscience *37*: 603-633.

Miller, R.E., W.F. Caul and I.A. Mirsky (1971) Patterns of eating and drinking in socially-isolated rhesus monkeys. Physiol. Behav. *7*: 127-134.

Miller, R.E., I.A. Mirsky, W.F. Caul and T. Sakata (1969) Hyperphagia and polydipsia in socially isolated rhesus monkeys. Science *165*: 1027-1028.

Mitchell, G.D., E.J. Raymond, G.C. Ruppenthal and H.F. Harlow (1966) Long-term effects of total social isolation upon behavior of rhesus monkeys. Psychol. Rep. *18*: 567-580.

Moore, K.E., K.T. Demarest and K.J. Lookingland (1987) Stress, prolactin and hypothalamic dopaminergic neurons. Neuropharmacology *26*: 801-808.

Moore, R.Y. (1989) The geniculohypothalamic tract in monkey and man. Brain Res. *486*: 190-194.

Moore, R.Y. and N.J. Lenn (1972) Retinohypothalamic projection in the rat. J. Comp. Neurol. *146*: 1-14.

Moos, R. and P. Richard (1982) Excitatory effect of dopamine on oxytocin and vasopressin reflex releases in the rat. Brain Res. *221*: 249-260.

Morrison, J.H., S.L. Foote, D. O'Connor and F.E. Bloom (1982) Laminar, tangential and regional organization of the noradrenergic innervation of monkey cortex: Dopamine-ß-hydroxylase immunohistochemistry. Brain Res. Bull. *9*: 309-319.

Morrison, J.H., P.R. Hof, W. Janssen, J.L. Bassett, S.L. Foote, G.W. Kraemer and W.T. McKinney (1990) Quantitative neuroanatomic analyses of cerebral cortex in rhesus monkeys from different rearing conditions. Proc. Soc. Neurosci. *16*: 789.

Morrison, J.H., M.E. Molliver, R. Grzanna and J.T. Coyle (1981) The intracortical trajectory of the coeruleo-cortical projection in the rat: A tangentially organized cortical afferent. Neuroscience *6*: 139-158.

Moss, R.L., R.E.J. Dyball and B.A. Cross (1971) Responses of antidromically identified supraoptic and paraventricular units to acetylcholine, noradrenaline and glutamate applied iontophoretically. Brain Res. *35*: 573-575.

Moss, R.L., I. Urban and B.A. Cross (1972) Microelectrophoresis of cholinergic and aminergic drugs of paraventricular neurons. Am. J. Physiol. *232*: 310-318.

Mossberg, K., U. Arvidsson and B. Ulfhake (1990) Computerized quantification of immunofluorescence-labeled axon terminals and analysis of co-localization of neurochemicals in axon terminals with a confocal scanning laser microscope. J. Histochem. Cytochem. *38*: 179-190.

Mossberg, K. and M. Ericsson (1990) Detection of doubly stained fluorescent specimens using confocal microscopy. J. Microsc. *158*: 215-224.

Nakada, H. and Y. Nakai (1985) Electron microscope examination of the catecholaminergic innervation of neurophysin- or vasopressin-containing neurons in the rat hypothalamus. Brain Res. *361*: 247-257.

Nakai, Y., S. Shioda, H. Ochiai and K. Kozasa (1986) Catecholamine-peptide interactions in the hypothalamus. In D. Ganten and D. Pfaff (eds): Current Topics in Neuroendocrinology, Vol. 7. Morphology of Hypothalamus and Its Connections. Berlin, Heidelberg: Springer-Verlag, pp. 135-160.

Negro-Vilar, A., C. Johnston, E. Spinedi, M. Valenca and F. Lopez (1987) Physiological role of peptides and amines on the regulation of ACTH secretion. Ann. N.Y. Acad. Sci. *512*: 218-236.

Neill, J.D., S. Frawley, P.M. Plotsky and G.T. Tindall (1981) Dopamine in hypophysial stalk blood of the rhesus monkey and its role in regulating prolactin secretion. Endocrinology *108*: 489-494.

Niimi, K. and E. Kuwahara (1973) The dorsal thalamus of the cat and comparison with monkey and man. J. Hirnforsch. *14*: 303-325.

Norgren, R. (1977) Taste pathways to hypothalamus and amygdala. J. Comp. Neurol. *166*: 17-30.

O'Connor, D.T., R.P. Frigon and R.A. Stone (1979) Human pheochromocytoma dopamine-beta-hydroxylase: Purification and molecular parameters of the tetramer. Mol. Pharmacol. *16*: 529-538.

Ochiai, H., C. Iwai and Y. Nakai (1988) Ultrastructural demonstration of the catecholaminergic innervation of vasopressin neurons in the paraventricular nucleus of the rat by double-labeling immunocytochemistry. Neurosci. Lett. *85*: 14-18.

Ochiai, H. and Y. Nakai (1990) Ultrastructural demonstration of dopamine-ß-hydroxylase-immunoreactive nerve terminals on vasopressin neurons in the paraventricular nucleus of the rat by double-labeling immunocytochemistry. Neurosci. Lett. *120*: 87-90.

Okamura, H., S. Murakami, K. Chihara, I. Nagatsu and Y. Ibata (1985) Coexistence of growth hormone-releasing factor-like and tyrosine hydroxylase-like immunoreactivities in neurons of the rat arcuate nucleus. Neuroendocrinology *41*: 177-179.

Oldfield, B.J., A. Hou-Yu and A.-J. Silverman (1985) A combined electron microscopic HRP and immunocytochemical study of the limbic projections to rat hypothalamic nuclei containing vasopressin and oxytocin neurons. J. Comp. Neurol. *231*: 221-231.

Oldfield, B.J. and A.-J. Silverman (1985) A light microscopic HRP study of limbic projections to the vasopressin-containing nuclear groups of the hypothalamus. Brain Res. Bull. *14*: 143-157.

Olschowka, J.A., M.E. Molliver, R. Grzanna, F.L. Rice and J.T. Coyle (1981) Ultrastructural demonstration of noradrenergic synapses in the rat central nervous system by dopamine-ß-hydroxylase immunocytochemistry. J. Histochem. Cytochem. *29*: 271-280.

Palkovits, M., M. Brownstein, J.M. Saavedra and J. Axelrod (1974) Norepinephrine and dopamine content of hypothalamic nuclei of the rat. Brain Res. *77*: 137-149.

Papadopoulos, G.C., J.G. Parnavelas and R.M. Buijs (1987) Monoaminergic fibers form conventional synapses in the cerebral cortex. Neurosci. Lett. *76*: 275-279.

Papadopoulos, G.C., J.G. Parnavelas and R.M. Buijs (1989) Light and electron microscopic immunocytochemical analysis of the noradrenaline innervation of the rat visual cortex. J. Neurocytol. *18*: 1-10.

Papez, J.W. (1937) A proposed mechanism of emotion. Arch. Neurol. Psychiat. 725-743.

Papez, J.W. and L.R. Aronson (1934) Thalamic nuclei of Pithecus (*Macacus*) rhesus. I. Ventral thalamus. Arch. Neurol. Psychiat. *32*: 1-26.

Paull, W.K., C.F. Phelix, M. Copeland, P. Palmiter, F.P. Gibbs and C. Middleton (1984) Immunohistochemical localization of corticotropin-releasing factor (CRF) in the hypothalamus of the squirrel monkey, *Saimiri sciureus*. Peptides *5*: 45-51.

Pfaff, D. and M. Keiner (1973) Atlas of estradiol-concentrating cells in the central nervous system of the female rat. J. Comp. Neurol. *151*: 121-157.

Pfaff, D.W., J.L. Gerlach, B.S. McEwen, M. Ferin, P. Carmel and E.A. Zimmerman (1976) Autoradiographic localization of hormone-concentrating cells in the brain of the female rhesus monkey. J. Comp. Neurol. *170*: 279-293.

Piekut, D.T. (1983) Immunocytochemical localization of luteinizing hormone-releasing hormone (LHRH) and LHRH-like material in brain. Influence of fixation solution at various pH values. J. Histochem. Cytochem. *31*: 1329-1332.

Plant, T.M., L.C. Krey, J. Moossy, J.T. McCormack, D.L. Hess and E. Knobil (1978) The arcuate nucleus and the control of gonadotropin and prolactin secretion in the female rhesus monkey (*Macaca mulatta*). Endocrinology *102*: 52-62.

Plotsky, P.M. (1985) Hypophyseotropic regulation of adenohypophysial adrenocorticotropin secretion. Fed. Proc. *44*: 207-213.

Plotsky, P.M. (1987) Facilitation of immunoreactive corticotropin-releasing factor secretion into the hypophysial-portal circulation after activation of catecholaminergic pathways or central norepinephrine injection. Endocrinology *121*: 924-930.

Plotsky, P.M., E.T. Cunningham, Jr. and E.P. Widmaier (1989) Catecholaminergic modulation of corticotropin-releasing factor and adrenocorticotropin secretion. Endocr. Rev. *10*: 437-458.

Poitras, D. and A. Parent (1975) Fluorescence microscopic study of the distribution of monoamines in the hypothalamus of the cat. J. Morphol. *145*: 387-408.

Poulain, P., L. Martin-Bouyer, J.C. Beauvillain and G. Tramu (1984) Study of the efferent connections of the enkephalinergic magnocellular dorsal nucleus in the guinea pig hypothalamus using lesions, retrograde tracing and immunohistochemistry: Evidence for a projection to the lateral septum. Neuroscience *11*: 331-343.

Rafols, J.A., N. Aronin and M. Difiglia (1987) A Golgi study of the monkey paraventricular nucleus: Neuronal types, afferent and efferent fibers. J. Comp. Neurol. *257*: 595-613.

Randle, J.C.R., C.W. Bourque and L.P. Renaud (1986a) Serial reconstruction of lucifer yellow-labeled supraoptic nucleus neurons in perfused rat hypothalamic explants. Neuroscience *17*: 453-467.

Randle, J.C.R., M. Mazurek, D. Kneifel, J. Dufresne and L.P. Renaud (1986b) Alpha-1 adrenergic receptor activation releases vasopressin and oxytocin from perfused rat hypothalamic explants. Neurosci. Lett. *65*: 219-223.

Ranson, S.W. (1940) Regulation of body temperature. Assoc. Res. Nerv. Ment. Dis. *20*: 342-399.

Renaud, L.P. (1987) Magnocellular neuroendocrine neurons: Update on intrinsic properties, synaptic inputs and neuropharmacology. Trends Neurosci. *10*: 498-502.

Renaud, L.P. and C.W. Bourque (1991) Neurophysiology and neuropharmacology of hypothalamic magnocellular neurons secreting vasopressin and oxytocin. Prog. Neurobiol. *36*: 131-169.

Rhodes, C.H., J.I. Morrell and D.W. Pfaff (1981) Immunohistochemical analysis of magnocellular elements in rat hypothalamus: Distribution and numbers of cells containing neurophysin, oxytocin, and vasopressin. J. Comp. Neurol. *198*: 45-64.

Ricardo, J.A. and E.T. Koh (1978) Anatomical evidence of direct projections from the nucleus of the solitary tract to the hypothalamus, amygdala, and other forebrain structures in the rat. Brain Res. *153*: 1-26.

Rioch, D.M., G.B. Wislocki and J.L. O'Leary (1940) A précis of preoptic, hypothalamic and hypophysial terminology with atlas. Assoc. Res. Nerv. Ment. Dis. *20*: 3-30.

Rivier, C. and W. Vale (1983) Modulation of stress-induced ACTH release by corticotropin-releasing factor, catecholamines, and vasopressin. Nature *305*: 325-327.

Rivier, C.L. and P.M. Plotsky (1986) Mediation by corticotropin-releasing factor (CRF) of adenohypophysial hormone secretion. Annu. Rev. Physiol. *48*: 475-494.

Ruggiero, D.A., H. Baker, T.H. Joh and D.J. Reis (1984) Distribution of catecholamine neurons in the hypothalamus and preoptic region of mouse. J. Comp. Neurol. *223*: 556-582.

Salm, A.K. and K.D. McCarthy (1989) Expression of beta-adrenergic receptors by astrocytes isolated from adult rat cortex. Glia *2*: 346-352.

Saper, C.B., A.D. Loewy, L.W. Swanson and W.M. Cowan (1976a) Direct hypothalamo-autonomic connections. Brain Res. *117*: 305-312.

Saper, C.B., L.W. Swanson and W.M. Cowan (1976b) The efferent connections of the ventromedial nucleus of the hypothalamus of the rat. J. Comp. Neurol. *169*: 409-442.

Saphier, D. (1989) Catecholaminergic projections to tuberoinfundibular neurones of the paraventricular nucleus: I. Effects of stimulation of A1, A2, A6 and C2 cell groups. Brain Res. Bull. *23*: 389-395.

Saphier, D. and S. Feldman (1989) Catecholaminergic projections to tuberoinfundibular neurones of the paraventricular nucleus: II. Effects of stimulation of the ventral noradrenergic bundle: evidence for cotransmission. Brain Res. Bull. *23*: 397-404.

Saphier, D. and S. Feldman (1991) Catecholaminergic projections to tuberoinfundibular neurones of the paraventricular nucleus: III. Effects of adrenoceptor agonists and antagonists. Brain Res. Bull. 26: 863-870.

Sapolsky, R., L. Krey and B. McEwen (1984) Glucocorticoid-sensitive hippocampal neurons are involved in terminating the adrenocortical stress response. Proc. Natl. Acad. Sci. USA *81*: 6174-6178.

Sapolsky, R.M., S. Zola-Morgan and L.R. Squire (1991) Inhibition of glucocorticoid secretion by the hippocampal formation in the primate. J. Neurosci. *11*: 3695-3704.

Sawchenko, P.E. (1987) Adrenalectomy-induced enhancement of CRF and vasopressin immunoreactivity in parvicellular neurosecretory neurons: Anatomic, peptide, and steroid specificity. J. Neurosci. 7: 1093-1106.

Sawchenko, P.E., C. Arias and J.C. Bittencourt (1990) Inhibin ß, somatostatin, and enkephalin immunoreactivities coexist in caudal medullary neurons that project to the paraventricular nucleus of the hypothalamus. J. Comp. Neurol. *291*: 269-280.

Sawchenko, P.E. and S.W. Pfeiffer (1988) Ultrastructural localization of neuropeptide Y and galanin immunoreactivity in the paraventricular nucleus of the hypothalamus in the rat. Brain Res. *474*: 231-245.

Sawchenko, P.E. and L.W. Swanson (1981a) Central noradrenergic pathways for the integration of hypothalamic neuroendocrine and autonomic responses. Science *214*: 685-687.

Sawchenko, P.E. and L.W. Swanson (1981b) A method for tracing biochemically defined pathways in the central nervous system using combined fluorescence retrograde transport and immunohistochemical techniques. Brain Res. *210*: 31-51.

Sawchenko, P.E. and L.W. Swanson (1982) Immunohistochemical identification of neurons in the paraventricular nucleus of the hypothalamus that project to the medulla or to the spinal cord in the rat. J. Comp. Neurol. *205*: 260-272.

Sawchenko, P.E. and L.W. Swanson (1983a) The organization and biochemical specificity of afferent projections to the paraventricular and supraoptic nuclei. In B.A. Cross and G. Leng (eds): The Neurohypophysis: Structure, Function and Control. Progress in Brain Research, Vol. 60. Amsterdam: Elsevier Science, pp. 19-29.

Sawchenko, P.E. and L.W. Swanson (1983b) The organization of forebrain afferents to the paraventricular and supraoptic nuclei of the rat. J. Comp. Neurol. *218*: 121-144.

Sawchenko, P.E. and L.W. Swanson (1990) Organization of CRF immunoreactive cells and fibers in the rat brain: Immunohistochemical studies. In E.B. DeSouza and C.B. Nemeroff (eds): Corticotropin-releasing factor: Basic and clinical studies of a neuropeptide. Boca Raton: CRC Press, pp. 29-51.

Sawchenko, P.E., L.W. Swanson, R. Grzanna, P.R.C. Howe, S.R. Bloom and J.M. Polak (1985) Colocalization of neuropeptide Y immunoreactivity in brainstem catecholaminergic neurons that project to the paraventricular nucleus of the hypothalamus. J. Comp. Neurol. *241*: 138-153.

Sawchenko, P.E., L.W. Swanson and S.A. Joseph (1982) The distribution and cells of origin of ACTH (1-39)-stained varicosities in the paraventricular and supraoptic nuclei. Brain Res. *232*: 365-374.

Sawchenko, P.E., L.W. Swanson, H.W.M. Steinbusch and A.A.J. Verhofstad (1983) The distribution and cells of origin of serotonergic inputs to the paraventricular and supraoptic nuclei of the rat. Brain Res. *277*: 355-360.

Schimchowitsch, S., M.E. Stoeckel, A. Vigny and A. Porte (1983) Oxytocinergic neurons with tyrosine hydroxylase-like immunoreactivity in the paraventricular nucleus of the rabbit hypothalamus. Neurosci. Lett. *43*: 55-59.

Schimchowitsch, S., P. Vuillez, M.L. Tappaz, M.J. Klein and M.E. Stoeckel (1991) Systematic presence of GABA-immunoreactivity in the tubero-infundibular and tubero-hypophysial dopaminergic axonal systems: An ultrastructural immunogold study on several mammals. Exp. Brain Res. *83*: 575-586.

Schofield, S.P.M. and B.J. Everitt (1981) The organization of catecholamine-containing neurons in the brain of the rhesus monkey *(Macaca mulatta)*. J. Anat. *132*: 391-418.

Schmale, H., and D. Richter (1984) Single base deletion in the vasopressin gene is the cause of diabetes insipidus in Brattleboro rats. Nature *308*:705-709.

Schöler, J., and J.R. Sladek, Jr. (1981) Supraoptic nucleus of the Brattleboro rat has an altered afferent noradrenergic input. Science *214*:347-349.

Schöler, J., and J.R. Sladek, Jr. (1982) An altered noradrenergic innervation of the Brattleboro rat supraoptic nucleus. Ann. N.Y. Acad. Sci. *394*:718-729.

Semenenko, F.M. and B.M. Lumb (1992) Projections of anterior hypothalamic neurons to the dorsal and ventral periaqueductal grey in the rat. Brain Res. *582*: 237-245.

Shibahara, S., Y. Morimoto, Y. Furutani, M. Notake, H. Takahashi, S. Shimizu, S. Horikawa and S. Numa (1983) Isolation and sequence analysis of the human corticotropin-releasing factor precursor gene. EMBO *2*: 775-779.

Shioda, S. and Y. Nakai (1992) Noradrenergic innervation of vasopressin-containing neurons in the rat hypothalamic supraoptic nucleus. Neurosci. Lett. *140*: 215-218.

Shioda, S., Y. Nakai, A. Sato, S. Sunayama and Y. Shimoda (1986) Electron-microscopic cytochemistry of the catecholaminergic innervation of TRH neurons in the rat hypothalamus. Cell Tiss. Res. *245*: 247-252.

Siegel, S.J., S.D. Ginsberg, P.R. Hof, S.L. Foote, W.G. Young, G.W. Kraemer, W.T. McKinney and J.H. Morrison (1992) Effects of social deprivation in prepubescent rhesus monkeys: Immunohistochemical analysis of the neurofilament protein triplet in the hippocampal formation. Brain Res., submitted.

Silverman, A.-J., R. Goldstein and C.A. Gadde (1980) The ontogenesis of neurophysin-containing neurons in the mouse hypothalamus. Peptides *1 (Suppl. 1)*: 27-44.

Silverman, A.-J., A. Hou-Yu and B.J. Oldfield (1983) Ultrastructural identification of noradrenergic nerve terminals and vasopressin-containing neurons of the paraventricular nucleus in the same thin section. J. Histochem. Cytochem. *31*: 1151-1156.

Silverman, A.-J., B. Oldfield, A. Hou-Yu and E.A. Zimmerman (1985) The noradrenergic innervation of vasopressin neurons in the paraventricular nucleus of the hypothalamus: An ultrastructural study using radiography and immunocytochemistry. Brain Res. *325*: 215-229.

Simerly, R.B., R.A. Gorski and L.W. Swanson (1986) Neurotransmitter specificity of cells and fibers in the medial preoptic nucleus: An immunohistochemical study in the rat. J. Comp. Neurol. *246*: 343-363.

Skagerberg, G. and O. Lindvall (1985) Organization of diencephalic dopamine neurones projecting to the spinal cord in the rat. Brain Res. *342*: 340-351.

Sladek, Jr., J.R. and C.D. Sladek (1983) Anatomical reciprocity between magnocellular peptides and noradrenaline in putative cardiovascular pathways. In B.A. Cross and G. Leng (eds): The Neurohypophysis: Structure, Function and Control. Progress in Brain Research, Vol. 60. Amsterdam: Elsevier Science, pp. 437-443.

Sladek, Jr., J.R. and E.A. Zimmerman (1982) Simultaneous monoamine histofluorescence and neuropeptide immunocytochemistry: VI. Catecholamine innervation of vasopressin and oxytocin neurons in the rhesus monkey hypothalamus. Brain Res. Bull. *9*: 431-440.

Sofroniew, M.V. and A. Weindl (1978) Projections from the parvicellular vasopressin- and neurophysin-containing neurons of the suprachiasmatic nucleus. Am. J. Anat. *153*: 391-430.

Sofroniew, M.V. and A. Weindl (1980) Identification of parvicellular vasopressin and neurophysin neurons in the suprachiasmatic nucleus of a variety of mammals including primates. J. Comp. Neurol. *193*: 659-675.

Sofroniew, M.V., A. Weindl, U. Schrell and R. Wetzstein (1981) Immunohistochemistry of vasopressin, oxytocin, and neurophysin in the hypothalamus and extrahypothalamic regions of the human and primate brain. Acta Histochem. Suppl. *24*: 79-95.

Stanley, B.G. and S.F. Leibowitz (1985) Neuropeptide Y injected in the paraventricular hypothalamus: A powerful stimulant of feeding behavior. Proc. Natl. Acad. Sci. USA *82*: 3940-3943.

Stellar, E. (1954) The physiology of motivation. Psychol. Rev. *61*: 5-22.

Stephan, F.K., K.J. Berkley and R.L. Moss (1981) Efferent connections of the rat suprachiasmatic nucleus. Neuroscience *6*: 2625-2641.

Sternberger, L.A. (1986) Immunocytochemistry. Third Edition. New York: John Wiley and Sons.

Stewart, W.W. (1978) Functional connections between cells as revealed by dye-coupling with a highly fluorescent naphthalimide tracer. Cell *14*: 741-759.

Struble, R.G. and A.H. Riesen (1978) Changes in cortical dendritic branching subsequent to partial social isolation in stumptailed monkeys. Dev. Psychobiol. *11*: 479-486.

Swaab, D.F. and E. Fliers (1985) A sexually dimorphic nucleus in the human brain. Science *228*: 1112-1115.

Swaab, D.F., F. Nijveldt and C.W. Pool (1975a) Distribution of oxytocin and vasopressin in the rat supraoptic and paraventricular nucleus. J. Endocr. *67*: 461-462.

Swaab, D.F., C.W. Pool and F. Nijveldt (1975b) Immunofluorescence of vasopressin and oxytocin in the rat hypothalamo-neurohypophysial system. J. Neural. Trans. *36*: 195-215.

Swanson, L.W. (1987) The hypothalamus. In A. Björklund, T. Hökfelt and L.W. Swanson (eds): Handbook of Chemical Neuroanatomy, Vol. I. Integrated Systems of the CNS. Amsterdam: Elsevier, pp. 1-124.

Swanson, L.W., M.A. Connelly and B.K. Hartman (1977) Ultrastructural evidence for central monoaminergic innervation of blood vessels in the paraventricular nucleus of the hypothalamus. Brain Res. *136*: 166-173.

Swanson, L.W. and B.K. Hartman (1975) The central adrenergic system. An immunofluorescence study of the location of cell bodies and their efferent connections in the rat utilizing dopamine-ß-hydroxylase as a marker. J. Comp. Neurol. *163*: 467-506.

Swanson, L.W. and H.G.J.M. Kuypers (1980) The paraventricular nucleus of the hypothalamus: Cytoarchitectonic subdivisions and organization of projections to the pituitary, dorsal vagal complex, and spinal cord as demonstrated by retrograde fluorescence double-labeling methods. J. Comp. Neurol. *194*: 555-570.

Swanson, L.W. and S. McKellar (1979) The distribution of oxytocin- and neurophysin- stained fibers in the spinal cord of the rat and monkey. J. Comp. Neurol. *188*: 87-106.

Swanson, L.W. and P.E. Sawchenko (1983) Hypothalamic integration: Organization of the paraventricular and supraoptic nuclei. Annu. Rev. Neurosci. *6*: 269-324.

Swanson, L.W., P.E. Sawchenko, A. Bérod, B.K. Hartman, K.B. Helle and D.E. Van Orden (1981) An immunohistochemical study of the organization of catecholaminergic cells and terminal fields in the paraventricular and supraoptic nuclei of the hypothalamus. J. Comp. Neurol. *196*: 271-285.

Swanson, L.W., P.E. Sawchenko, J. Rivier and W.W. Vale (1983) Organization of ovine corticotropin-releasing factor-immunoreactive cells and fibers in the rat brain: An immunohistochemical study. Neuroendocrinology *36*: 165-186.

Swanson, L.W. and D.M. Simmons (1989) Differential steroid hormone and neural influences on peptide mRNA levels in CRH cells of the paraventricular nucleus: A hybridization histochemistry study in the rat. J. Comp. Neurol. *285*: 413-435.

Szafarczyk, A., F. Malaval, A. Laurent, R. Gibaud and I. Assenmacher (1987) Further evidence for a central stimulatory action of catecholamines on adrenocorticotropin release in the rat. Endocrinology *121*: 883-892.

Tanaka, C., M. Ishikawa and S. Shimada (1982) Histochemical mapping of catecholaminergic neurons and their ascending fiber pathways in the rhesus monkey brain. Brain Res. Bull. *9*: 255-270.

Tasker, J.G. and F.E. Dudek (1991) Electrophysiological properties of neurons in the region of the paraventricular nucleus in slices of rat hypothalamus. J. Physiol. *434*: 271-293.

Ter Horst, G.J., P. de Boer, P.G.M. Luiten and J.D. van Willigen (1989) Ascending projections from the solitary tract nucleus to the hypothalamus. A *Phaseolus vulgaris* lectin tracing study in the rat. Neuroscience *31*: 785-797.

Ter Horst, G.J. and P.G.M. Luiten (1986) The projections of the dorsomedial hypothalamic nucleus in the rat. Brain Res. Bull. *16*: 231-248.

Ter Horst, G.J. and P.G.M. Luiten (1987) *Phaseolus vulgaris* leuco-agglutinin tracing of intrahypothalamic connections of the lateral, ventromedial, dorsomedial, and paraventricular hypothalamic nuclei in the rat. Brain Res. Bull. *18*: 191-203.

Terasawa, E., C. Krook, D.L. Hei, M. Gearing, N.J. Schultz and G.A. Davis (1988) Norepinephrine is a possible neurotransmitter stimulating pulsatile release of luteinizing hormone-releasing hormone in the rhesus monkey. Endocrinology *123*: 1808-1816.

Thind, K.K. and P.C. Goldsmith (1989) Corticotropin-releasing factor neurons innervate dopamine neurons in the periventricular hypothalamus of juvenile macaques. Synaptic evidence for a possible companion neurotransmitter. Neuroendocrinology *50*: 351-358.

Thompson, R.H., N.S. Canteras and L.W. Swanson (1992) The efferent connections of the dorsomedial nucleus of the hypothalamus: A PHA-L study in the rat. Proc. Soc. Neurosci. *18*: 1415.

Turek, F.W. and E. Van Cauter (1988) Rhythms in reproduction. In E. Knobil and J.D. Neill (eds): The Physiology of Reproduction, Vol. 2. New York: Raven Press, pp. 1789-1830.

Ungerstedt, U. (1971) Stereotaxic mapping of the monoamine pathways in the rat brain. Acta Physiol. Scand. *Suppl. 367*: 1-48.

Vale, W., J. Spiess, C. Rivier and J. Rivier (1981) Characterization of a 41-residue ovine hypothalamic peptide that stimulates secretion of corticotropin and ß-endorphin. Science *213*: 1394-1397.

Vale, W., J. Vaughan, G. Yamamoto, T. Bruhn, C. Douglas, D. Dalton, C. Rivier and J. Rivier (1983) Assay of corticotropin-releasing factor. Methods Enzymol. *103*: 565-577.

van den Pol, A.N. (1982) The magnocellular and parvicellular paraventricular nucleus of rat: Intrinsic organization. J. Comp. Neurol. *206*: 317-345.

van den Pol, A.N. (1985) Dual ultrastructural localization of two neurotransmitter-related antigens: Colloidal gold-labeled neurophysin-immunoreactive supraoptic neurons receive peroxidase-labeled glutamate decarboxylase- or gold-labeled GABA-immunoreactive synapses. J. Neurosci. *5*: 2940-2954.

van den Pol, A.N. (1991) Glutamate and aspartate immunoreactivity in hypothalamic presynaptic axons. J. Neurosci. *11*: 2087-2101.

van den Pol, A.N., R.S. Herbst and J.F. Powell (1984) Tyrosine hydroxylase-immunoreactive neurons of the hypothalamus: A light and electron microscopic study. Neuroscience *13*: 1117-1156.

van der Gugten, J., M. Palkovits, H.L.J.M. Winjen and D.H.G. Versteeg (1976) Regional distribution of adrenaline in rat brain. Brain Res. *107*: 171-175.

Veazey, R.B., D.G. Amaral and W.M. Cowan (1982) The morphology and connections of the posterior hypothalamus in the cynomolgus monkey (*Macaca fascicularis*). I. Cytoarchitectonic organization. J. Comp. Neurol. *207*: 114-134.

Versteeg, D.H.G., M. Tanaka, and E.R. De Kloet (1978) Catecholamine concentration and turnover in discrete regions of the brain of the homozygous Brattleboro rat deficient in vasopressin. Endocrinology *103*:1654-1661.

Versteeg, D.H.G., J. van der Gugten, W. De Jong and M. Palkovits (1976) Regional concentrations of noradrenaline and dopamine in rat brain. Brain Res. *113*: 563-574.

Vickers, J.C., G.W. Huntley, A.M. Edwards, T. Moran, S.W. Rogers, S.F. Heinemann and J.H. Morrison (1993) Quantitative localization of AMPA/kainate and kainate glutamate receptor subunit immunoreactivity in neurochemically-identified subpopulations of neurons in the prefrontal cortex of the macaque monkey. J. Neurosci., submitted.

Wallén, P., K. Carlsson, A. Liljeborg and S. Grillner (1988) Three-dimensional reconstruction of neurons in the lamprey spinal cord in whole-mount, using a confocal laser scanning microscope. J. Neurosci. Meth. *24*: 91-100.

Watts, A.G. (1992) Disturbance of fluid homeostasis leads to temporally and anatomically distinct responses in neuropeptide and tyrosine hydroxylase mRNA levels in the paraventricular and supraoptic nuclei of the rat. Neuroscience *46*: 859-879.

Weigand, S.J. and J.L. Price (1980) Cells of origin of the afferent fibers to the median eminence in the rat. J. Comp. Neurol. *192*: 1-19.

Whitnall, M.H. (1988) Distributions of pro-vasopressin expressing and pro-vasopressin deficient CRH neurons in the paraventricular hypothalamic nucleus of colchicine-treated normal and adrenalectomized rats. J. Comp. Neurol. *275*: 13-28.

Whitnall, M.H., S. Key, Y. Ben-Barak, K. Ozato and H. Gainer (1985a) Neurophysin in the hypothalamo-neurohypophysial system. II. Immunocytochemical studies of the ontogeny of oxytocinergic and vasopressinergic neurons. J. Neurosci. 5: 98-109.

Whitnall, M.H., E. Mezey and H. Gainer (1985b) Co-localization of corticotropin-releasing factor and vasopressin in median eminence neurosecretory vesicles. Nature *317*: 248-250.

Willoughby, J.O., P.M. Jervois, M.F. Menadue and W.W. Blessing (1987) Noradrenaline, by activation of alpha-1-adrenoreceptors in the region of the supraoptic nucleus, causes secretion of vasopressin in the unanaesthetized rat. Neuroendocrinology *45*: 219-226.

Yamatodani, A., N. Inagaki, P. Panula, N. Itowi, T. Watanabe and H. Wada (1991) Structure and functions of the histaminergic neuron system. In B. Uvnäs (ed): Handbook of Experimental Pharmacology, Vol. 97. Histamine and Histamine Antagonists. Berlin Heidelberg: Springer-Verlag, pp. 243-283.

Young, III, W.S., M. Warden and E. Mezey (1987) Tyrosine hydroxylase mRNA is increased by hyperosmotic stimuli in the paraventricular and supraoptic nuclei. Neuroendocrinology *46*: 439-444.

Záborszky, L., M.C. Beinfeld, M. Palkovits and L. Heimer (1984) Brainstem projection to the hypothalamic ventromedial nucleus in the rat: A CCK-containing long ascending pathway. Brain Research *303*: 225-231.